KfK 2674
EUR 5755e
EIR-Bericht Nr. 349
Oktober 1978

EIR, KfK joint heat transfer experiment on a single rod, roughened with trapezoidal rounded ribs and cooled by various gases

M. Dalle Donne, M. Hudina, M. Huggenberger,
L. Meyer, K. Rehme

Institut für Neutronenphysik und Reaktortechnik
Projekt Schneller Brüter
Eidgenössisches Institut für Reaktorforschung

Kernforschungszentrum Karlsruhe

KERNFORSCHUNGSZENTRUM KARLSRUHE GMBH
ISSN 0303-4003

KERNFORSCHUNGSZENTRUM KARLSRUHE

Institut für Neutronenphysik und Reaktortechnik
Projekt Schneller Brüter

KfK 2674
EUR 5755e
EIR-Bericht Nr. 349

EIR, KfK joint heat transfer experiment on a single rod, roughened with trapezoidal rounded ribs and cooled by various gases

by

M. Dalle Donne, M. Hudina*, M. Huggenberger*,
L. Meyer and K. Rehme

Kernforschungszentrum Karlsruhe GmbH, Karlsruhe

* Eidgenössisches Institut für Reaktorforschung, Würenlingen

Abstract

Heat transfer and pressure drop experiments with an identical fuel rod simulator have been performed at the two Research Establishments in Würenlingen and in Karlsruhe. The rod was artificially roughened with "two-dimensional" ribs of trapezoidal shape and with rounded edges. The experiments at EIR were performed with CO_2 and the rough rod was contained in a smooth tube and centered by special spacers. The experiments at KfK were performed using helium and nitrogen in the same test section (rod and outer smooth tube with spacers) and air with the rod mounted in another outer smooth tube and with spacers located farther away from the measuring positions. The global measured friction factors and Stanton numbers for different gases agree reasonably well. The differences between the roughness parameters R and G are larger. The possible reasons for the uncertainties in the reduction of these parameters are discussed. It is recommended to perform further experiments with helium in a test section with spacers far apart, to investigate the effect of the temperature ratio on heat transfer and to check if the unfavourable data obtained by the experiment with air are too pessimistic for GCFR application.

Gemeinsames EIR, KfK Wärmeübergangsexperiment an einem Einzelstab mit trapezförmigen abgerundeten Rauhigkeitsrippen und Kühlung durch verschiedene Gase

Zusammenfassung

Wärmeübergangs- und Druckverlustuntersuchungen an einem identischen Brennstabsimulator wurden von den zwei Forschungsinstituten in Würenlingen und Karlsruhe durchgeführt. Der Stab war mit künstlichen "zweidimensionalen" trapezförmigen Rauhigkeiten mit abgerundeten Ecken versehen. Die Untersuchungen beim EIR wurden mit CO_2 in einem glatten Außenrohr mit Abstandshaltern durchgeführt. Beim KfK wurden Versuche mit Helium und Stickstoff in der gleichen Teststrecke (Stab und Außenrohr mit Abstandshaltern) sowie mit Luft in einem zweiten Außenrohr, bei dem die Abstandshalter weiter von der Meßstelle entfernt waren, durchgeführt.

Die global gemessenen Reibungsbeiwerte und Stanton Zahlen für verschiedene Gase stimmen recht gut überein. Die Unterschiede in den Rauhigkeitsparametern R und G sind größer. Die möglichen Gründe für die Unsicherheit bei der Auswertung dieser Parameter werden diskutiert. Es wird vorgeschlagen, weitere Untersuchungen mit Helium in einer Teststrecke mit vergrößerter Distanz zwischen den Abstandshaltern durchzuführen, um den Effekt des Temperaturverhältnisses auf den Wärmeübergang zu untersuchen. Es soll weiter überprüft werden ob die ungünstigen, aus dem Luftexperiment gewonnenen Daten, für die Anwendung bei GSB zu pessimistisch sind.

1. Introduction

The original data source for the roughness form choosen for the GCFR application was provided by the Swiss Federal Institute for Reactor Research (EIR). The choice was made /1/ on the basis of single rod experiments performed with air in annular test sections with different diameter ratios /2/. The aim of this simple experiment was to test different rough surfaces (different dimensions and different roughness shapes) in order to obtain the relative values of their thermohydraulic performances.

During the recent years, the Nuclear Research Center Karlsruhe (KfK) has carried out several experiments with rough rods and has become the main source of the thermohydraulic performances for rectangular ribs /3,4/. For the BR-2 calibration experiment trapezoidal ribs, similar to those suggested by EIR were also tested in an electrically heated 12-rod bundle /5/. Based on these measurements, KfK reported some results which were significantly different from those given by EIR. Whereas the agreement in the transformed friction factors was quite good, the transformed Stanton numbers differed considerably.

An extensive review of the existing experimental information and the data reduction techniques has been conducted at General Atomic (GA), San Diego /6/. In this investigation significant differences between the results of different experiments were found. To obtain more accurate data for the present reference GCFR design roughness some common activities were agreed between GA, EIR and KfK on the Thermal-Hydraulic Review Meeting in San Diego (November 23-24, 1976 /7/ /8/). It was decided to:

- conduct a series of additional single rod experiments at EIR and KfK with the identical equipment (rod and test section) but different coolants (BENCHMARK EXPERIMENT)
- perform a series of computer code calculations (between GA, KfK and EIR) predicting the pressure and temperature distributions in rod bundles. If possible, the calculation task should be based on the current bundle experiments, so that the results can be compared with the available measured information (BENCHMARK CALCULATIONS).

In this report the description and the results of the BENCHMARK EXPERIMENT are given.

2. Purpose of the experiment

The main purpose, indicated in the introduction can be further described in more detail as follows:

- reevaluate the experimental techniques
- test the roughness under equal geometric conditions but with different coolants in order to establish the effect of properties change (T_W/T_B effect mainly)
- obtain some relative information about the Biot number effects if possible (use of different coolants would probably allow some comparative evaluation of this effect)
- obtain data for high Reynolds numbers to avoid the uncertainties of the extrapolation of ROHAN /2/ experimental results
- improve the accuracy of the experimental results obtained in simple channels in order to establish the basic performances of rough surfaces for the analytical predictions of pressure and temperature distributions in complex bundle geometries.

3. Description of the experiment

3.1 General conditions

The parts of the equipment described in this chapter were chosen to be commonly used in the tests at KfK and EIR. They were integrated in the existing operational experimental loops.

Different rough rods, designed for the AGATHE HEX bundle experiment /9/ were already available for these single pin tests. The roughness of these rods of 8.4 mm outer diameter is of trapezoidal profile with roundings at the top and root of the ribs (see Fig.1). The rods are normally instrumented with 4 thermocouples (see Fig.2) distributed each 90°C around the circumference at one of the 5 different axial measuring levels.

One rough rod with thermocouples at the axial level IV (550 mm from the start of heated length) was chosen for the measurements (for identification: rod No 215).

The test section consists of an outer tube, of 16 mm diameter, in which the rod was mounted. The dimensions of the test section with all important positions of spacers, pressure taps and temperature measuring points are given in Fig.3. The rod is electrically heated over a length of 1150 mm. To reduce as much as possible the effect of the spacers on wall temperatures and pressure drop, these are especially designed to reduce the blocked area as much as feasible (approx. 10 times lower pressure drop as for the standard GCFR spacer design). The form and the dimensions of spacers can be seen from the Fig. 4. Some special tests were carried out to measure the pressure drop over these spacers. The scatter of the obtained results is quite large but this is not surprising because of the very small pressure drops. The equation given in Fig.4 is of the general form

$$\xi = c_1 \, Re^{-0.5} + c_2 \qquad (1)$$

obtained by the analytical considerations of spacer pressure drop at EIR /10/.

The test section is not designed for high pressure therefore it is thermally insulated and mounted in an outer housing. The heat losses of the test section were determined by separate tests.

The tests carried out in Karlsruhe with helium and nitrogen were performed with the same geometrical arrangement (outer tube, spacers) used at EIR and described above. With the air tests however the rough rod was placed in a different outer smooth tube of 16 mm I.D. No spacers were used during these tests in the rough portion of the rod. This was done to check if the spacers present in the EIR set-up would have still a certain influence on the temperature of the rough rod wall and on the pressure drop, and to be sure to achieve fully established flow conditions. Fig.5 shows schematically the test section with the dimensions of the EIR rough rod in the KfK outer smooth tube. The Figure shows the number and arrangement of the pressure tappings and of the thermocouples.

3.2 Tests with CO_2 (EIR)

The tests at EIR were carried out in the high pressure, high temperature CO_2 loop AGATHE (Fig.6). The main characteristics of this loop are given in Table 1.

From the circuit diagram (Fig.6), it can be seen that after the gas goes through the blower, it can be led through one of the two built in Venturi tubes for the measurement of mass flow. After going through the venturi tube the gas flow can be directed to one of three parallel test sections. Two of these three test sections were used for testing single heater rods in annuli. After going through the test section, the gas flows through the cooler, or if desired, a part of it can be by-passed back to the blower. The blower has a by-pass circuit with a sintered metal gas filter. Because of the high thermal capacitance of the loop, it had to be built for automatic operation for 24h service.

In addition to the Rod No. 215, at EIR, 2 smooth rods (No.13 and No.111) and one other roughened rod (No 251) were tested. The program of the measurement together with the inlet temperatures and the pressure levels used is given in Fig.7.

3.3 Tests with Helium (KfK)

The investigations with helium were performed in the high pressure helium loop of the heat transfer laboratory of the INR. Helium is circulated in a closed circuit by a centrifugal blower. The main characteristics of the loop are:

- maximum helium flow rate 1.2 kgs^{-1}
- maximum helium pressure 50 bar
- maximum helium temperature 800 K
- maximum heat exchanger capability 600 KW.

It was not suitable to use the complete test section inside the pressure tank. Therefore, the test section was mounted parallel to the tank and connected to the helium circuit by flanges (Fig.8).

3.4 Tests with Nitrogen (KfK)

The same setup was used for the N_2-tests. In this case the helium blower was operated at half the normal speed, which is normally 17800 rpm. The N_2 system pressure was p=12 bar. By operating the helium loop with nitrogen higher Reynolds numbers can be achieved.

3.5 Tests with air (KfK)

Fig.9 shows schematically the experimental setup used for the tests with air. Air is circulated by means of a compressor. The flow oscillations caused by the compressor are dampened by a large vessel. The air is subsequently depurated by the vapor content in a drier and goes to one of various orifice plates for the measurement of the mass flow. These orifice plates are placed in parallel and have been calibrated in the laboratory for the optimum application range. The air flows then through the annular test section, and finally to the atmosphere. By means of a valve placed downstream the test section it is possible to apply a certain back pressure, to increase the air density and therefore the maximum obtainable Reynolds number in the test section. The main characteristics of the air loop are the following:

Coolant max pressure:	5 bar
Coolant temperature:	20 ÷ 250°C
Coolant flow:	0.6 ÷ 90 g /sec
Heating power during experiments:	0 ÷ 13 KW
Rough rod wall temperature:	20 ÷ 400°C

4. Evaluation of results

The results of the investigations with CO_2, He and N_2 were evaluated by the computer code SINGRO, developed at EIR. In this code the following most important measuring results are evaluated:

- heat losses from the test section;
- heat balances;
- power distribution in the rod;
- mass flow (total) and Reynolds number;

- pressure drop of spacers, acceleration and friction pressure drop for the different axial sections;
- mean friction factors of the entire annulus for different smooth and rough axial sections;
- surface temperatures corrected for heat conduction through the cladding;
- convective heat flux (total heat flux corrected for radiation);
- Stanton and Nusselt numbers for the entire annulus.

The results of the investigations with air were evaluated with the code AURIS developed at KfK by L. Meyer (the rationale and the equations used in this code are given in references /3/ and /4/). With the code AURIS all the above mentioned operations performed by SINGRO are performed as well, down to the evaluation of Stanton numbers and friction factors for the entire annulus with the exception of the subtraction of the pressure drop due to the spacers, because no spacers were used in the air tests in the test section region. Furthermore AURIS calculates the functions R and G and the reduced values of these functions according to references /3/ and /4/.

4.1 Data acquisition at EIR

All information from the experiments is recorded by the central data acquisition system of the thermal-hydraulic laboratory (Fig.10).

The measured data are digitized by the ADC system and consequently transformed into engineering quantities. In the next step, further reduction of the data and plausibility checks are performed and a test record is printed. If the measured point is accepted, the processed data will be recorded on the magnetic tape for further evaluation on the large computer with the evaluation code SINGRO.

4.2 Data acquisition at KfK

The thermovoltages are recorded by a data logger. The pressure measurements are performed by means of pressure transducers which had been calibrated against a water column. The helium and nitrogen mass flow rates were measured by means of Venturi

tubes, standard orifice plates, and quarter-circle orifices. All data are punched on tape by Teletype or Facit data logger respectively and translated into BCD-code by computer programms for input into the evaluation programms and storage on magnetic tape and cards.

5. Results of the entire annulus

The results of the entire annulus as a function of the Reynolds number are taken as the basic experimental information. These results are to be used as a starting point for the different methods of transformation to the uniform boundary conditions.

5.1 Friction factors

5.1.1 CO_2 friction factor measurements at EIR

The friction factors measured with CO_2 are presented in Fig.11. These results were analysed against the different T_W/T_B ratios (Fig.12). No appreciable effect was evident for the smooth surface, but an important effect on the friction factor of the rough surface was found. The effect can be well described with a power function of T_W/T_B ($n = -0.2$). After correcting the friction factors with this function $(T_W/T_B)^{-0.2}$, one can see from Fig.13 that the systematic T_W/T_B effect has been eliminated.

5.1.2 He friction factor measurements at KfK

Fig.14 shows the friction factors measured with He. To evaluate the dependence of the friction factors on the T_W/T_B ratio the data are plotted in Fig.15 for the smooth and in Fig.16 for the roughened part of the test rod. As already noticed for the CO_2-data the friction factors of the smooth surface show a very weak (and positive) dependence on the T_W/T_B ratio, but this dependence is strong and negative for the roughened surface. The T_W/T_B-effect can be described by a power function $(T_W/T_B)^n$. For the smooth surface we get

$$n = 0.085 \quad Re > 2 \cdot 10^4 \qquad (2)$$
$$n = 0.132 \quad Re < 2 \cdot 10^4$$

and for the roughened surface

$$n = -0.281 \qquad Re > 10^4$$
$$n = -0.131 \qquad Re < 10^4 \ . \qquad (3)$$

Applying these power functions to the experimental results the scatter of the data is considerably reduced (Fig.17).

5.1.3 N_2 friction factor measurements at KfK

The results of the measurements with N_2 are plotted in Fig.18. Again, the friction factors of the roughened surface show a strong dependence on the T_W/T_B-ratio. The friction factors of the smooth surface are plotted versus the temperature ratio in Fig.19. The temperature effect is practically zero. It was determined to n = 0.048.

For the rough surface the exponent of the temperature ratio was determined to n = -0.128 (Fig.20). Thus, the temperature effect on the friction factor is less for N_2 than for He, both for the smooth and rough surfaces, respectively.

Applying the functions determined to the experimental data the scatter is definitely reduced (Fig. 21).

5.1.4 Air friction factor measurements at KfK

The results of the measurements with air at KfK in the test section with two spacers only are plotted in Fig.22. As in the previous cases a T_W/T_B effect is evident for Reynolds numbers above 6000. This effect disappears for lower Reynolds numbers (transition between turbulent and laminar flow). Fig.23 shows the friction factor corrected for the T_W/T_B effect, where n was taken equal to - 0.128 (the same as for nitrogen). The T_W/T_B is practically eliminated for Reynolds numbers above 6000. For lower Reynolds numbers there is of course an over-correction.

5.1.5 Comparison of friction factors

A comparison of the measured friction factors with the different coolants (CO_2, He, N_2) in the same test section shows that the data are in fairly good agreement. A comparison of the measured rough friction factor corrected for the T_W/T_B effect, in the EIR test section with many spacers (CO_2,He,N_2) with the air data obtained at KfK in the test section with two spacers only (distance of the spacers $\frac{l}{D}$ = 105, against $\frac{l}{D}$ = 32 for EIR test section) indicate that the friction factors with the EIR test section are lower(see Fig.55).

5.2 Stanton numbers

5.2.1 CO_2 Stanton number measurements at EIR

The measured Stanton numbers obtained in CO_2 are presented in Fig.24. The analysis of the T_W/T_B effect shows a similar behaviour as for the friction factor (Fig.25); no clear effect for the smooth surface, whereas for the rough surface the best fit is obtained with a power function (n = - 0.15). After correction with this power function the scatter of the Stanton number results is somewhat smaller (see Fig.26).

5.2.2 He Stanton number measurements at KfK

The measured Stanton numbers obtained with He as coolant are shown in Fig.27. The effect of the temperature ratio T_W/T_B is demonstrated in Fig.28. Only two different ratios were measured ($\sim$1.3 and $\sim$1.5). The exponent of the power function is highly uncertain, however the most likely value appears to be n = - 0.368. Assuming this value the data for the different temperature ratios agree quite well (Fig. 29).

5.2.3 N_2 Stanton number measurements at KfK

In case of N_2 as coolant only one temperature ratio ($\sim$1.5) was investigated. Fig.30 shows the results obtained. Since the effect of the temperature ratio could not be evaluated an exponent of n = - 0.2 was assumed to reduce the Stanton numbers. In Fig. 31 the reduced results are plotted.

5.2.4 Air Stanton number measurements at KfK

The results of the measurements with air at KfK in the test section with two spacers only are plotted in Fig.32. As in the previous cases a T_W/T_B is evident, although considerably more pronounced at lower Reynolds numbers (transition flow regime). Fig.33 shows the Stanton numbers corrected for the T_W/T_B effect, where n was taken equal to - 0.2 (the same as for nitrogen). The T_W/T_B effect has been eliminated only for $Re \geq 30000$, for lower Reynolds numbers the correction $(T_W/T_B)^{-0.2}$ is too weak.

5.2.5 Comparison of Stanton numbers

Comparing the results of the Stanton numbers, corrected for the T_W/T_B-effect for the four gases investigated (Fig.26, 29, 31 and 33), one can observe a reasonable agreement of all the data for higher Reynolds numbers. The dependence of the He-Stanton data on the Reynolds number is less than for the N_2 data. This may be an effect of different Biot numbers. For the comparison of the Stanton numbers, curves representing an approximate fit of the measured data are presented in Fig.56. The agreement of all data seems to be within the experimental scatter. However, comparison of the air data (without spacers, Fig.33) and helium data (with spacers Fig.29) would indicate that spacers have an effect on the Stanton number for $Re \leq 15000$, the Stanton numbers being higher in presence of spacers (decrease of rough rod wall temperature).This explanation would be than in agreement with Hassan and Rehme /11/ which found experimentally that the effect of spacers on rough rods is greater at lower Reynolds numbers.

6. Transformation procedure

The basic results (f and St) for the entire annulus were transformed with the different transformation methods typically applied at KfK and EIR.

6.1 CO_2 data at EIR

The calculation can be performed adding a transformation subroutine to the SINGRO basic code or using the special punch output of SINGRO as an input for a particular transformation code.

The transformation principle described in Ref./12/ was applied at EIR to obtain the transformed friction factors and Stanton numbers. The performances can also be presented in form of multipliers but the aim of the methods is to obtain the basic roughness functions R and G. The EIR transformation code TRANS was added to SINGRO as a subroutine.

The values of the roughness functions R and G are presented in Fig. 34 to 36. The results for the R function show a considerable T_W/T_B effect (Fig.34), as in the case of the friction factors. It was found that the results can be well correlated with the following equation:

$$R = R(T_W/T_B=1) + \frac{3}{5\times10^{-3}h^+ + 1}\left(\frac{T_W}{T_B} - 1\right)^2 . \qquad (4)$$

Fig.35 shows the $R(T_W/T_B = 1)$ values plotted versus h^+. The scatter of the points has been considerably decreased and the T_W/T_B-effect practically eliminated. The values of R, achieved for $h^+ \gtrsim 40$, are approximately constant and equal to 5.4.

The measured G values are plotted in Fig.36 versus h^+. The scatter of the points is relatively low, so that no clear effect of the T_W/T_B ratio was found. Additional systematic investigation is needed to be sure about the amount of this effect with CO_2. The points for T_W/T_B between 1.3 and 1.4 were used to obtain the following equation, which could be considered as an approximation for all the measured G-values ($25 < h^+ < 300$):

$$G = 4.5\ h^{+0.24}\ Pr^{0.44} \quad . \qquad (5)$$

6.2 Helium, nitrogen and air data (KfK) and CO_2 data (EIR) evaluated with KfK method

All the helium and nitrogen data measured at KfK were transformed with the code AUTØG. AUTØG is the same as the code AURIS mentioned in Section 4, but it takes account of the pressure drop in the test section, caused by the spacers with equation (1) suggested by EIR. Also the EIR-CO_2 data were transformed by this code at KfK.

As a result we obtain the roughness parameter of the velocity profile $R(h_W^+)$, the reduced roughness parameter $R(h_W^+)_{01}$, the roughness parameter of the temperature profile $G(h_W^+)$ and reduced roughness parameter $G(h_W^+)_{01}$ (for the definition and explanation of the correction factors which take account of the temperature effect and of the length of the velocity and temperature profile see references /3/ and/or /4/).

6.2.1 Friction data

The roughness parameters $R(h_W^+)$ evaluated from the measurements are shown in Fig.37 for helium, in Fig.38 for N_2 and in Fig.39 for CO_2. The $R(h_W^+)$ are plotted versus h_W^+ as suggested in reference /3/ and /4/. There is some scatter of the data measured, especially for the non-isothermal helium case and high h_W^+ values. These were the first measurements taken with the test section in the helium loop. These non-isothermal data which are lower than the isothermal ones are felt not to be reliable. The measurements of the mass flow rate and of the pressure gradient along the outer tube were substantially improved after these first results. Omitting these data (non-isothermal, $h_W^+ > 35$), the coincidence between the helium and N_2 results is fair for the isothermal and non-isothermal runs ($T_W/T_B \sim 1.6$) indicating that the T_W/T_B-effect on the roughness parameter $R(h_W^+)$ is nearly the same for both fluids. The CO_2 data are lower than the results for He and N_2 of about 0.8 point in $R(h_W^+)$. The quasi-constant value of $R(h_W^+)$ for CO_2 (see Fig.39) for high h_W^+ values is about the same as that obtained by EIR for CO_2

$(R(h_W^+)_\infty = 5.8)$ indicating that the two transformation methods lead to about the same values of R. The reduced parameter $R(h_W^+)$ corrected for the temperature effect

$$\Delta R(h_W^+)_{Temp.} = - \frac{5}{\sqrt{h_W^+}} \left(\frac{T_W}{T_1} - 1\right)^2 \qquad (6)$$

and for the length-of-velocity-profile-effect:

$$\Delta R(h_W^+)_{vel.length} = - 0.4 \ln \left(\frac{h}{0.01\hat{y}}\right) \qquad (7)$$

suggested in references /3,4/ are plotted for helium, N_2 and CO_2 in Figures 40, 41 and 42 respectively. Looking at the results, we find that the temperature effect on the roughness parameter has not completely disappeared indicating a stronger dependence than assumed in the transformation code AUTØG which is based on the air results for two-dimensional rectangular roughnesses /3-4/. The $R(h_W^+)_{01}$-values for high h_W^+'s are almost constant; $R(h_W^+)_{01\infty}$ being 5.8 for helium and N_2 but 4.9 for CO_2, considering mainly the isothermal point (and this may be too little to characterize the CO_2 data).

Figure 43 shows the roughness parameter $R(h_W^+)$ obtained with the experiments with air at KfK in the test section with long distance between the spacers. The temperature effect is evident. Figure 44 shows the same friction data plotted in the diagram $R(h_W^+)_{01}$ versus h_W^+, where $R(h_W^+)_{01}$ has been reduced according to the equation (6) and (7). The T_W/T_B effect is decreased in respect of the previous plot, however the data with heat transfer are slightly higher than the isothermal ones in the region $15 \leq h_W^+ \leq 90$. In the transition region to hydraulically smooth flow regime, the isothermal points are considerably higher than the thermal. The transition to fully smooth flow regime is with heat transfer much more gradual. This fact has been observed already before both with two-dimensional /3/ and three-dimensional roughness ribs /13/. The quasi-static value of $R(h_W^+)_{01}$ for high h_W^+ is equal to about 4.7, i.e. smaller than the values obtained with the other experiments (CO_2:4.9; He,N_2:5.8). The $R(h_W^+)_{01}$ values with heat transfer can be correlated in the range $3.5 \leq h_W^+ \leq 150$ by the equation:

$$R(h_W^+)_{01} = 4 + \frac{2.75}{h_W^+ \; 0.256} \qquad (8)$$

6.2.2 Heat transfer data

The $G(h_W^+)$ values evaluated from the measurements by the KfK transformation method are shown plotted versus h_W^+ in the Figures 45, 46 and 47 for the three gases helium, nitrogen and CO_2 respectively.

The helium data show a strong effect of the temperature ratio. The ratios during the measurements were $T_W/T_B \approx 1.35$ for the lower values of $G(h_W^+)$ at higher h_W^+ and $T_W/T_B \approx 1.53$ for the higher values of $G(h_W^+)$ at lower h_W^+. The N_2 data are lower than the helium data at the same temperature ratio (1.53). The CO_2 data and N_2 data are almost coincident for $h_W^+ < 30$, but for $h_W^+ > 30$ the CO_2 data are increasingly lower than the N_2 data with increasing h_W^+.

The calculated $G(h_W^+)$ values were reduced for the Prandtl, temperature and length-of-temperature-profile effects with the relationship:

$$G(h_W^+)_{01} = \frac{G(h_W^+)}{Pr^{0.44}} \left(\frac{T_W}{T_B}\right)^n \left(\frac{h}{0.01(r_2-r_1)}\right)^{-0.053} \qquad (9)$$

suggested in references /3,4/.

The exponents of the temperature ratio for helium and CO_2 were from the experimental data. For the experiment with N_2, the air value /3,4/ was chosen:

$$\begin{aligned} &He: && n = -1 \\ &CO_2: && n = -0.29 \\ &N_2: && n = -0.5 \end{aligned} \qquad (10)$$

The results are plotted in the form $G(h_W^+)_{01}$ versus h_W^+ in the Figures 48, 49 and 50 for helium, N_2 and CO_2 respectively. Considering the uncertainty in the helium data for high values of h_W^+ as discussed in Section 6.2.1 above, the results with helium and nitrogen agree quite well. The data can be correlated by the equation:

$$G(h_W^+)_{01} = 4.6\ h_W^{+\,0.215} \qquad (11)$$

in the range $8 \leq h_W^+ \leq 73$.

The CO_2 data are higher than the helium and nitrogen data for lower h_W^+ values. All data agree for higher h_W^+ . The difference between CO_2 and He, N_2 data is increasing with decreasing h_W^+. The CO_2 data can be correlated by the equation:

$$G(h_W^+)_{01} = 6.0 \; h_W^{+\,0.16} \qquad (12)$$

in the range $10 \leq h_W^+ \leq 250$.

Fig.51 shows the CO_2 data plotted versus h^+. Comparing these results, corrected for the T_w/T_b effect, with the plot of $G(h_w^+)_{01}$ versus h_w^+, a similar scatter of the data can be found. The same tendency was observed for the CO_2 G-values obtained by the EIR transformation method (Fig.36). Fig.51 shows that the CO_2 heat transfer data, transformed with the KfK method can be correlated by the equation:

$$G = 7 \cdot h^{+\,0.14} \; Pr^{0.44} \qquad (13)$$

In the Figure also the correlation obtained by EIR is shown (eqn.(5)). The comparison of the two lines of Fig.51 shows the differences due to the transformation methods of KfK and EIR in the heat transfer data: the same CO_2 experimental data lead to about the same Stanton numbers, but the transformed G-values differ of about 11% at h^+=20 and 12% at h^+=290, whereby the KfK-transformation produces higher G-values at low h^+'s and lower at higher values of h^+. A difference of

12% in G means a difference of about 8% in heat transfer coefficient. However, for the typical nominal GCFR conditions ($h^+ \approx 100$), the differences are considerably smaller (about 3% in G and about 2% in heat transfer coefficient).

Fig. 52 shows the roughness temperature parameter $G(h_W^+)$ obtained with the experiments with air at KfK in the test section with the spacers far apart. The temperature effect is evident and similar to that already found by Dalle Donne and Meyer for roughness with rectangular ribs /4/. For $h_W^+ > 20$ the $G(h_W^+)$ values increase with h_W^+ while for $h_W^+ < 20$ the $G(h_W^+)$'s are more or less constant. This qualitive behaviour was already observed by Dipprey and Sabersky for sand-roughness /15/ and by Dalle Donne and Meyer for roughness with two-dimensional rectangular ribs /4/. Fig. 53 shows the same heat transfer data plotted in the diagramm $G(h_W^+)_{01}$ versus h_W^+, where the $G(h_W^+)_{01}$ values have been reduced according to equation (9) (n=-0.5). The temperature effect is practically eliminated. All the experimental data can be correlated by the relationship:

$$G(h_W^+)_{01} = 4.45\ h_W^{+\,0.24} + \frac{10.3}{h_W^{+\,0.7}} \qquad (14)$$

in the range $3.5 \leq h_W^+ \leq 150$; the first term on the right side of the equation being the prevalent in the fully rough flow regime region (high values of h_W^+), the second being prevalent in the transition region to hydraulically smooth flow.

7. Discussion of results

A convenient way to present the data is to show them in form of the reduced roughness parameters $R(h_W^+)_{01}$ and $G(h_W^+)_{01}$. This implies that the temperature, Prandtl and velocity or tempera-

ture profile length effects are known. Here it is assumed that the Prandtl effect is that found by Dipprey and Sabersky /15/ and the temperature and profile length effects are those found by Dalle Donne and Meyer /4/. The Prandtl and profile length effects are not very strong, thus these assumption do not affect the results very much. The temperature effect (T_W/T_B) is more important and can be quite different from gas to gas being dependent upon the variation of viscosity, thermal conductivity and specific heat with temperature (for all the gases considered the density is inverse proportional to the temperature in the range of interest). For air and nitrogen the property variations with temperature are very similar. These variations are also similar between air and helium /16,17/, so that the temperature effects are approximately the same for air and helium for smooth surfaces /18/. This should be the case for rough surfaces as well, however we can see from equation (10) that the present experimental results would indicate a stronger negative (T_W/T_B)-effect on the heat transfer data for helium than for air or nitrogen. This discrepancy could be real (that is really given by the slightly different property variations with temperature for helium and air: for instance the specific heat of helium is constant , while the specific heat of air varies proportionally to $T^{0.12}$ /16/) or simply given by the uncertainty of the experimental results. Indeed, since the exponent n is evaluated from small differences between various experimental results, it is subjected to quite a large experimental uncertainty.

The exponent n for the CO_2 heat transfer data has the lowest absolute value of all the gases considered here. The dependence of the CO_2 properties on temperature is quite different from the other gases. This fact was already observed by Walker and White /14/. Probably also the Biot number effect which is different for the different gases affects the heat transfer results. However, it is impossible to correct the data for this effect on the basis of the present results. As far as the roughness friction data are concerned the temperature correction factor suggested in reference /4/ seems to be too small for gases other than air.

This can simply be explained by the uncertainty in the experimental results. Contrary to heat transfer data, for the friction data there should be no great difference between temperature effects for helium, air, nitrogen and carbon dioxide, because density and viscosity (the only two gas physical properties which affect the friction data) vary with temperature for these gases more or less all in the same way /19/.

The friction data can be compared easily by comparing the different values of the reduced roughness parameter $R(h_W^+)_{O1\infty}$, the quasi-constant value in the region of fully established rough flow regime. The following values have been obtained in the present experiments:

$$R(h_W^+)_{O1\infty} = 5.8 \quad \text{(helium, nitrogen)}$$

$$R(h_W^+)_{O1\infty} = 4.9 \quad (CO_2) \qquad (15)$$

$$R(h_W^+)_{O1\infty} = 4.7 \quad \text{(air)}$$

Since the main difference between the test sections for the air and CO_2, He and N_2 experiments is the fact that the spacers are far apart in the air test section, the higher $R(h_W^+)_{O1\infty}$ values could stem from an overestimation of the pressure drop due to the spacers, which is substracted from the measured pressure drop. However, this cannot explain the main part of the difference because

a) the correction for the spacer pressure drop is small,
b) the data of the air and CO_2 test agree quite well, and
c) the main difference is between the He, N_2 and CO_2 data, which were measured with the same test section and evaluated by the same code (SINGRO).

The difference between the highest value of $R(h_W^+)_{O1\infty}$ (5.8) and the lowest value (4.7) means roughly a difference of 11 % in friction factor for typical GCFR fuel element conditions. This discrepancy seems not to come from the difference in transformation methods between EIR and KfK (the transformation of the same CO_2 friction data both with the EIR and KfK methods produces the same $R(h_W^+)$ values).

Fig. 54 shows, in the plot $G(h_W^+)_{01}$ versus h_W^+, the equations obtained from the different experiments of the report. All the data have been transformed with the KfK transformation method, thus the differences are not given by differences in the transformation method. Of course these lines are the averages among experimental points which scatter considerably, however a systematic difference between the data of the experiments with air, CO_2 and the data with nitrogen and helium is evident from the figure. This difference could stem from experimental errors. Other possible effects couldbe given by the highly uncertain T_W/T_B correction, by the different Biot numbers, and by modifications in boundary conditions: especially the adiabatic condition at the wall of outer smooth tube is important for the heat transfer data. For h_W^+=100 the He, N_2 and CO_2 values of $G(h_W^+)_{01}$ agree reasonable well but the air data are about 12% higher, which means for a fixed R value a difference of about 8% in the heat transfer coefficient for typical GCFR fuel element conditions. However, if the corresponding roughness parameters R and G are consistently used for all gases, as done in their evaluation, the differences between the heat transfer coefficients calculated for N_2 (lowest G value) and air (highest G value) are about 2.8% only. The standard deviation of heat transfer coefficient from the mean value of all gases is about ±3.5%.

8. Conclusions and recommendations

a) Experiments at EIR and KfK on the same rod artificially roughened with two-dimensional ribs of trapezoidal shape and with rounded edges lead to some differences in the results. As far as the global values of friction factors and Stanton numbers of the annulus are concerned the agreement between the results with different gases is reasonable indicating that the experimental techniques used are not producing large experimental errors.

b) A comparison of the same experimental CO_2 data transformed with the different methods used at the two laboratories shows that the differences due to the transformation methods are not large for the h^+ range 20÷300. The values of the friction parameter R agree rather well, while the maximum difference in the heat transfer parameter G is about 12% (8% in the heat transfer coefficient for GCFR fuel element conditions).

c) The difference between the $R(h_W^+)_{01\infty}$ values are large (about 23 %, which means about 11% in the friction factor for GCFR fuel element conditions). Comparing the results for air and CO_2 the differences reduces to 4% (about 2% difference in friction factors) and can be certainly explained by experimental uncertainties. The value $R(h_W^+)_{01\infty}=5.8$ for helium and nitrogen appears to be too high.

d) The differences in the heat transfer data are also large. Whereas the $G(h_W^+)_{01}$ of measurements with He, N_2 and CO_2 at h_W^+ higher than 70 agree reasonably well, the air values are considerably higher. For $h_W^+=100$ (approx. nominal GCFR conditions) this difference is about 12% which means for a fixed R value about 8% in the heat transfer coefficient. However, if the corresponding roughness parameters R and G are consistently used, the standard deviation of heat transfer coefficient from the main value of all gases is about ±3.5%. This discrepancy does not stem from differences in the experimental techniques used in the two Research Establishments. This differences could arise from experimental error and from not ideal boundary conditions ($q \neq 0$ at smooth tube wall). To some extent these discrepancies could be given by the uncertainty in the exponent n of the T_W/T_B-effect and/or in the Biot number correction for the various gases, which would produce uncertainty in the reduction of the $G(h_W^+)$ values.

e) It is recommended to perform further experiments with helium and a test section with spacers far apart to investigate the (T_W/T_B) effect especially on heat transfer and to check if the unfavourable data obtained with air are too pessimistic for GCFR application.

References

/1/ Hudina M.: Roughening characteristics and choices for the gas-cooled fast breeder reactor.
Nuclear Engng. and Design. Volume 40, No.1, 1977. pp. 133-142.

/2/ Hudina M., ROHAN experiment (Final Report) Part 1.
EIR internal report TM-IN-694, Würenlingen, Switzerland, 1977, unpublished.

/3/ Dalle Donne M.: Wärmeübergang von rauhen Oberflächen,
Kernforschungszentrum Report KfK 2397, EUR 5506d,
Januar 1977

/4/ Dalle Donne M., Meyer L.: Turbulent convective heat transfer from rough surfaces with two-dimensional rectangular ribs,
Int. J. Heat Mass Transfer, Vol.20 pp.583-620, 1977.

/5/ Dalle Donne M., Marek J., Martelli A., Rehme K.:
BR2 bundle mockup heat transfer experiments,
Nuclear Engineering and Design, Vol.40, No.1, 1977,
pp 143-156.

/6/ Schlueter G., Lund K.O., Thompson W.I., (1976) , unpublished.

/7/ Schlueter G., (1976), unpublished.

/8/ Hudina M.: Bericht über Besprechungen in USA vom 18.-29. Nov.1976, EIR internal memo AN-IN-597, Würenlingen, Switzerland, 1976, unpublished

/9/ Hudina M., Markoczy G.: The hexagonal bundle heat transfer and fluid flow experiment AGATHE HEX.
Nuclear Engineering and Design Vol.40, No.1, 1977, pp.121-132.

/10/ Büttiker P.; A method to calculate spacer pressure drop coefficients.
EIR internal report TM-IN-466, Würenlingen, Switzerland, 1971, unpublished.

/11/ Hassan M.A. and Rehme K.: Heat transfer near spacer grids in gas-cooled rod bundles for small Reynolds numbers,
NEA Coord. Group on Gas-cooled Fast Reactor Development, 4th Specialist Meeting on GCFR Heat Transfer, Karlsruhe 18-20 October 1977.

/12/ Hudina M.: Evaluation of heat transfer performances of rough surfaces from experimental investigation in annular channels,
NEA Coord. Group on Gas-cooled Fast Reactor Development, 4th Spec. Meeting on GCFR Heat Transfer, Karlsruhe 18-20 October 1977, EIR report SL-R/21.

/13/ Dalle Donne M. and Meyer L.: Experimental heat transfer and pressure drop of Rods with three-dimensional roughness in annuli,
NEA Coord. Group on Gas-cooled Fast Reactor Development, 3rd Spec. Meeting on GCFR Heat Transfer, Petten 17-19 September 1975.

/14/ Walker V. and White L.: The effect of physical property variations on heat transfer roughened surfaces,
Heat Transfer Conf. 1970, Paris, Paper FC 5.4, Vol.2.

/15/ Dipprey D.F. and Sabersky D.H.: Heat and momentum transfer in smooth and rough tubes at various Prandtl number,
Int. J. Heat Mass Transfer 6, 329-353, (1963)

/16/ Dalle Donne M. and Bowditch F.H.: Local heat transfer and average friction coefficients for subsonic laminar, transitional and turbulent flow of air in a tube at high temperature,
Dragon Project Report D.P. 88, U.K.A.E.A. Winfrith, Dorchester, England, 1962.

/17/ Pfriem H.J.: Der turbulente Wärmeübergang an Helium und Wasserstoff in beheizten Rohren bei großen axial steigenden Temperaturdifferenzen und das sich daraus ergebende Temperaturprofil.
Kernforschungszentrum Karlsruhe Report KfK 1860.

/18/ Dalle Donne M. and Bowditch F.H.: Experimental local heat transfer and friction coefficients for subsonic laminar transitional and turbulent flow of air or helium in a tube at high temperatures,
Dragon Project Report DP 184, U.K.A.E.A. Winfrith, Dorchester, England, 1963.

/19/ Barnes J.F.: An experimental investigation of heat transfer from the inside surface of a hot smooth tube to air, helium and carbon dioxide, National Gas Turbine Establishment, Pyestock, Hants, England, N.G.T.E. R.241, 1960

Nomenclature

c_1, c_2	constants in the equation for the pressure drop of the spacer (-)
D	hydraulic diameter of the test channel (m)
G	roughness parameter of the temperature profile, as a function of h^+ (-)
$G(h_W^+)$	roughness parameter of the temperature profile, as a function of h_W^+ (-)
$G(h_W^+)_{O1}$	roughness parameter of the temperature profile, corrected for $h/\hat{y}$ and T_W/T_B
h	height of roughness (m)
h^+	dimensionless height of roughness, evaluated at T_B (-)
h_W^+	dimensionless height of roughness, evaluated at T_W (-)
ℓ	distance between the spacers (m)
n	exponent of the temperature ratio (-)
p	pressure (bar)
Pr	Prandtl number (-)
R	roughness parameter of the velocity profile, as a function of h^+ (-)
$R(h_W^+)$	roughness parameter of the velocity profile, as a function of h_W^+ (-)
$R(h_W^+)_{O1}$	the same as before, but corrected for $h/\hat{y}$ and T_W/T_B (-)
$R(h_W^+)_{O1\infty}$	the same as before, but for fully rough flow (-) (quasi-constant)

ΔR	correction of the roughness parameter of the velocity profile (-)
Re	Reynolds number (-)
r_2	radius of outer smooth surface (m)
r_1	volumetric radius of rough rod (m)
r_o	radius of the zero-shear stress position (m)
T	temperature (K)
T_B	gas bulk temperature (K)
T_W	wall temperature (K)
T_1	gas bulk temperature of the inner (rough) region of the annulus (K)
$\hat{y}$	$= r_o - r_1$ (m)
ξ	drag coefficient of the spacer

Table 1: AGATHE loop

Performance characteristics

Coolant	CO_2
Coolant pressure	1 - 60 bar
Coolant temperature	30 - 500°C
Maximum coolant mass flow	4.5 kg/sec
Number of possible test sections	3
Heating power	0 to 1000 kW

Explanation of the labelling of the figures

RE	Reynolds number
FR	friction factor rough
FS	friction factor smooth
TW	wall temperature
TB	gas bulk temperature
F(TW/TB=1)	friction factor, corrected for TW/TB
ST/PR**(-.6)	Stanton number, reduced for Prandtl number
ST/PR**(-.6) (TW/TB=1)	as before, corrected for TW/TB
HW+	h_W^+
R(HW+)	$R(h_W^+)$
GPR	$G/Pr^{0.44}$
G(H+)	$G(h_W^+)$
GPR01	$G(h_W^+)_{01}$
H+W	h_W^+
H+	h^+

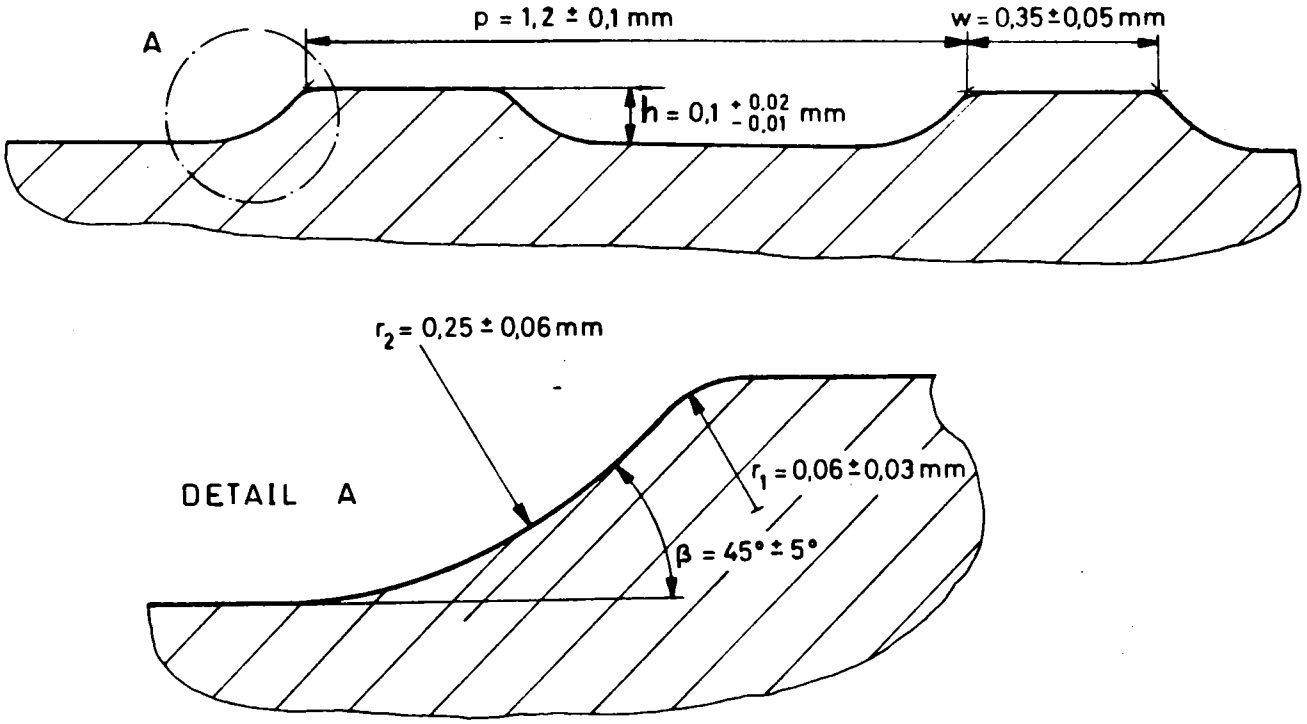

Fig.1: Roughness form of the rod surface

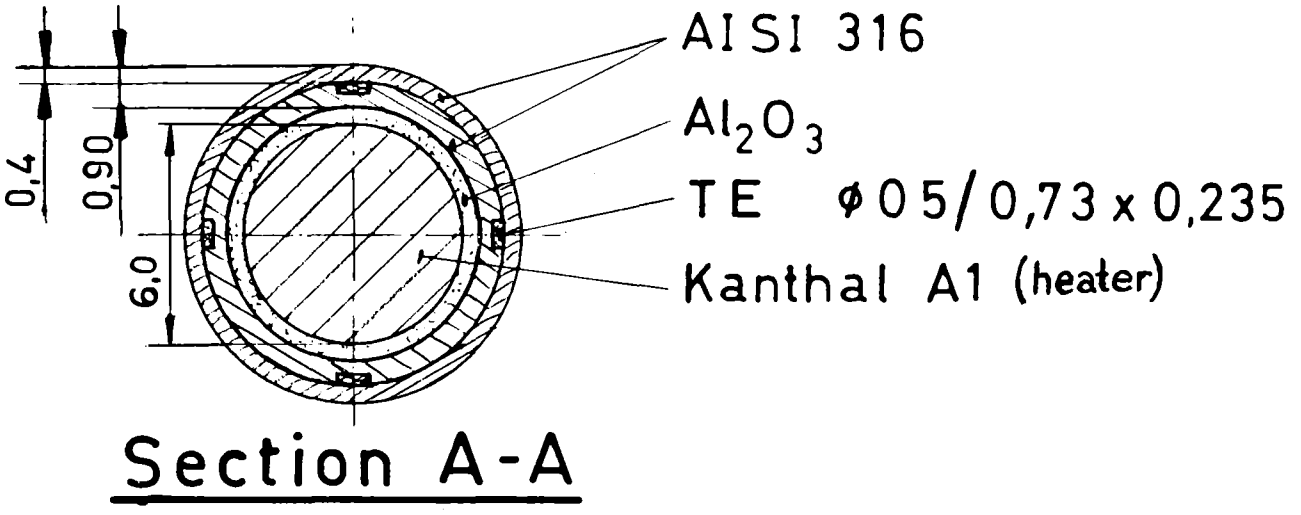

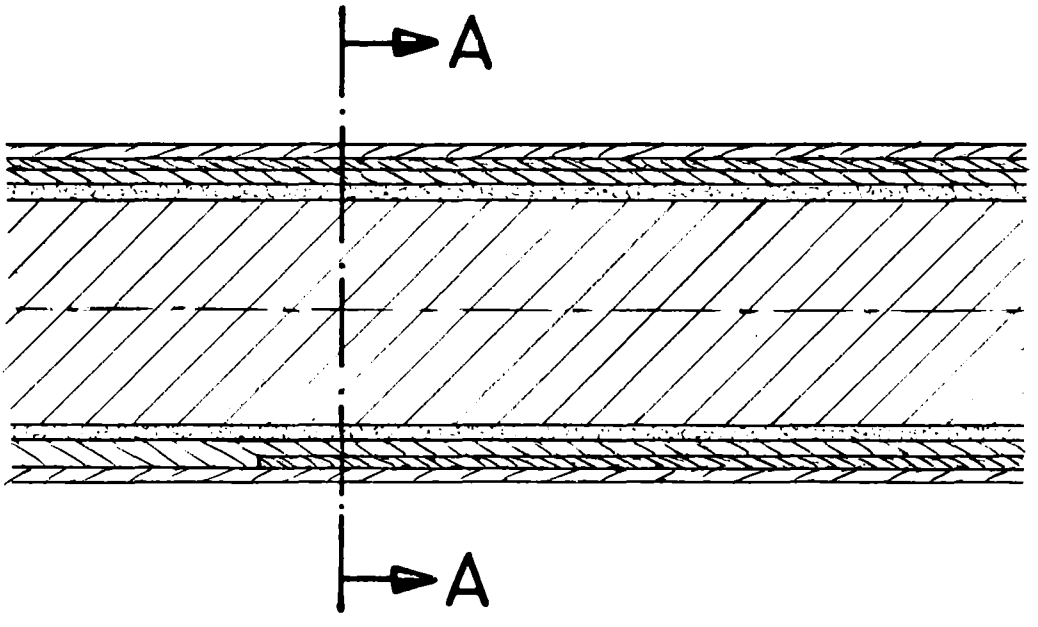

Fig.2: Rod cross section

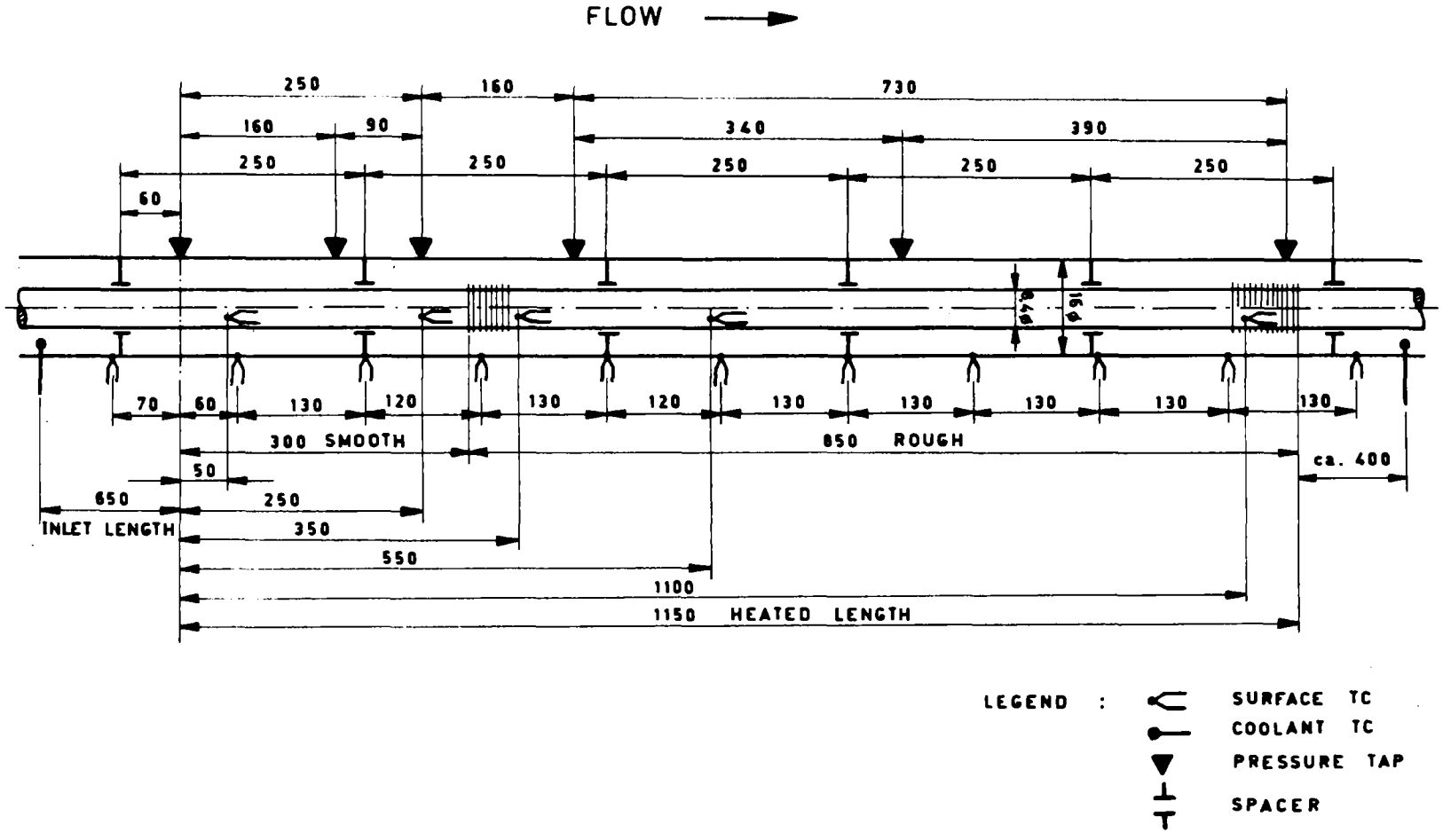

Fig.3: Single pin test section, diam. 16/8.4 (mm)

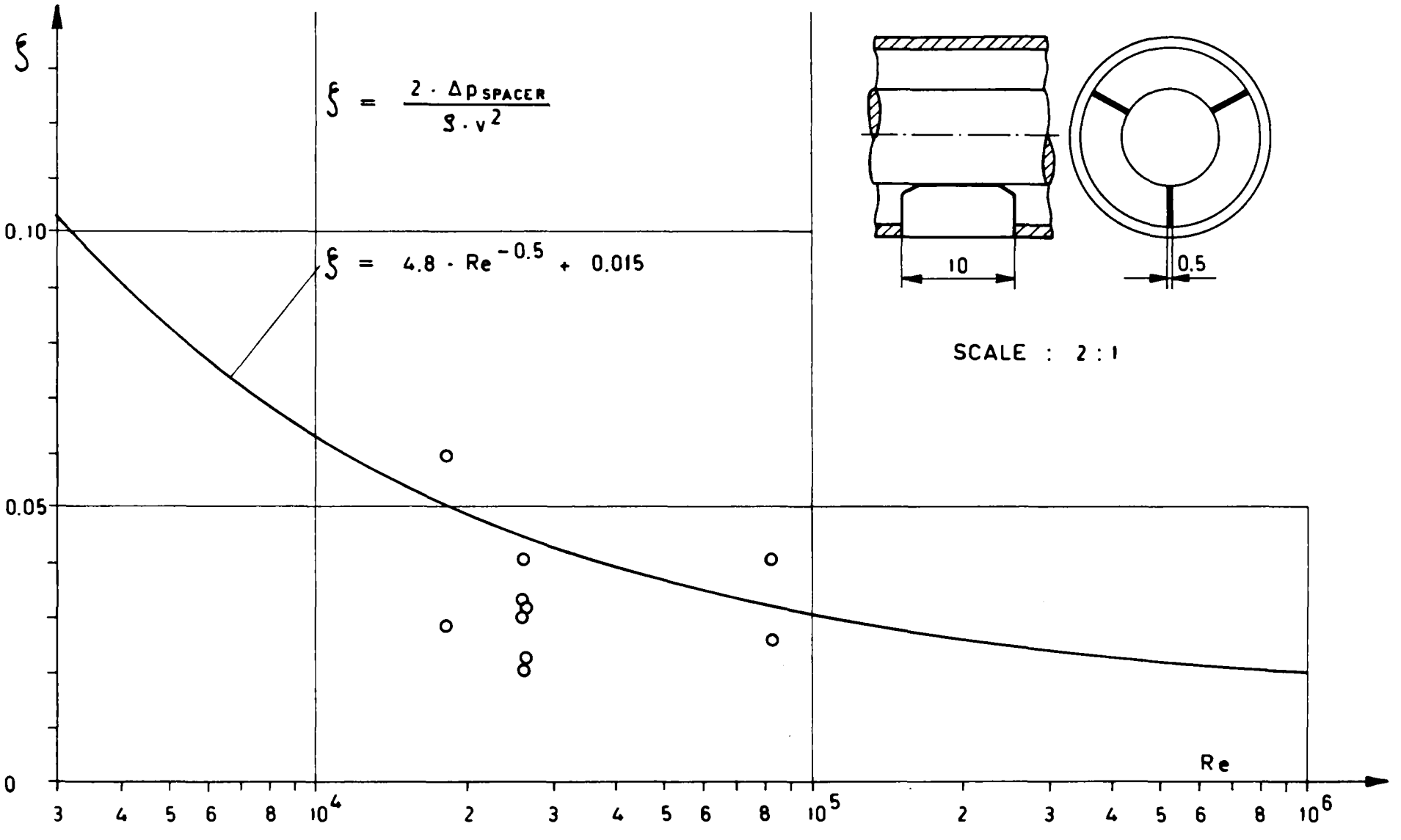

Fig.4: Spacer pressure drop coefficient

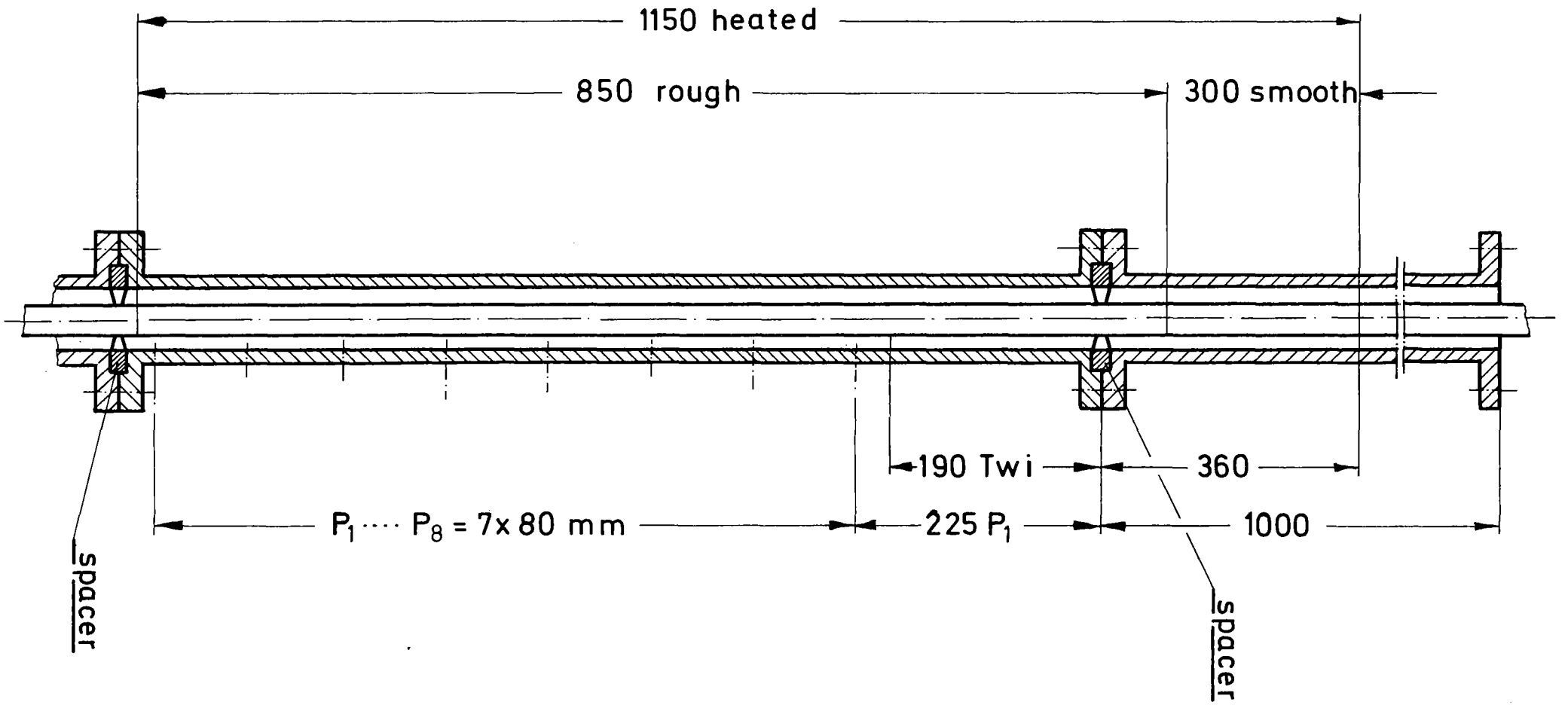

Fig.5: Arrangement of EIR rough rod in KfK outer smooth tube for air tests

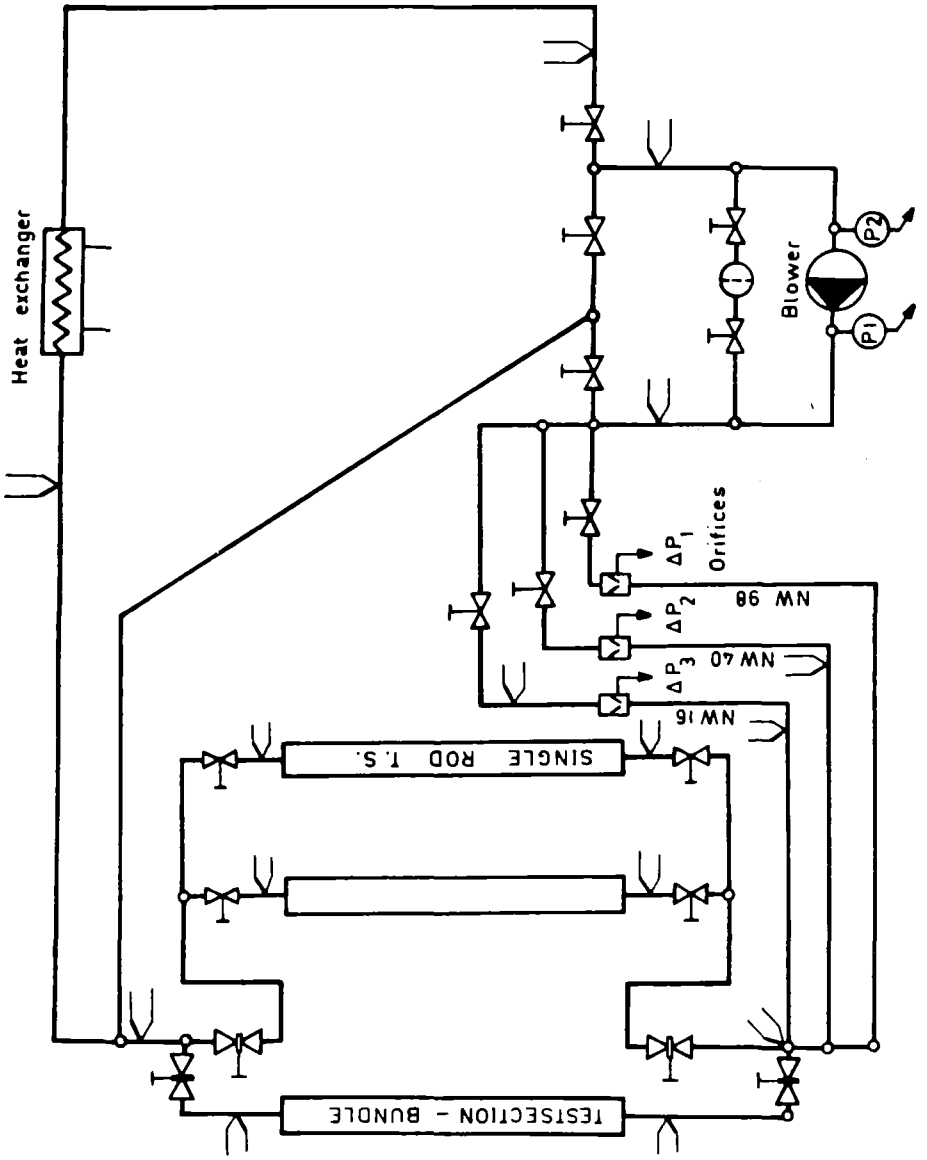

Fig.6: AGATHE circuit diagram

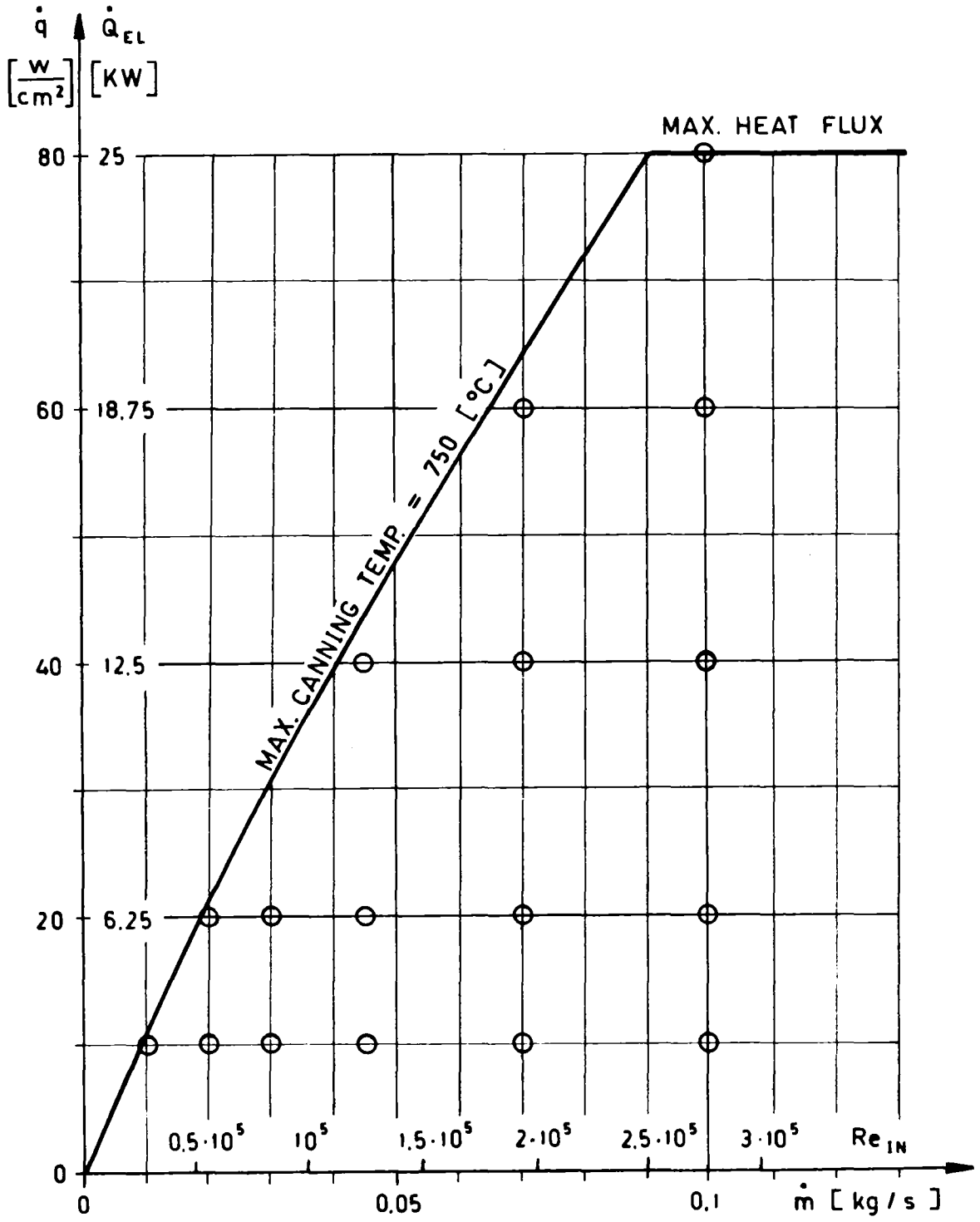

COOLANT CO_2 ○ MEASURING POINT

$T_{IN\ GAS}$ = 100 [°C] P_{TEST} = 20 [b]

Fig.7: Measurement program

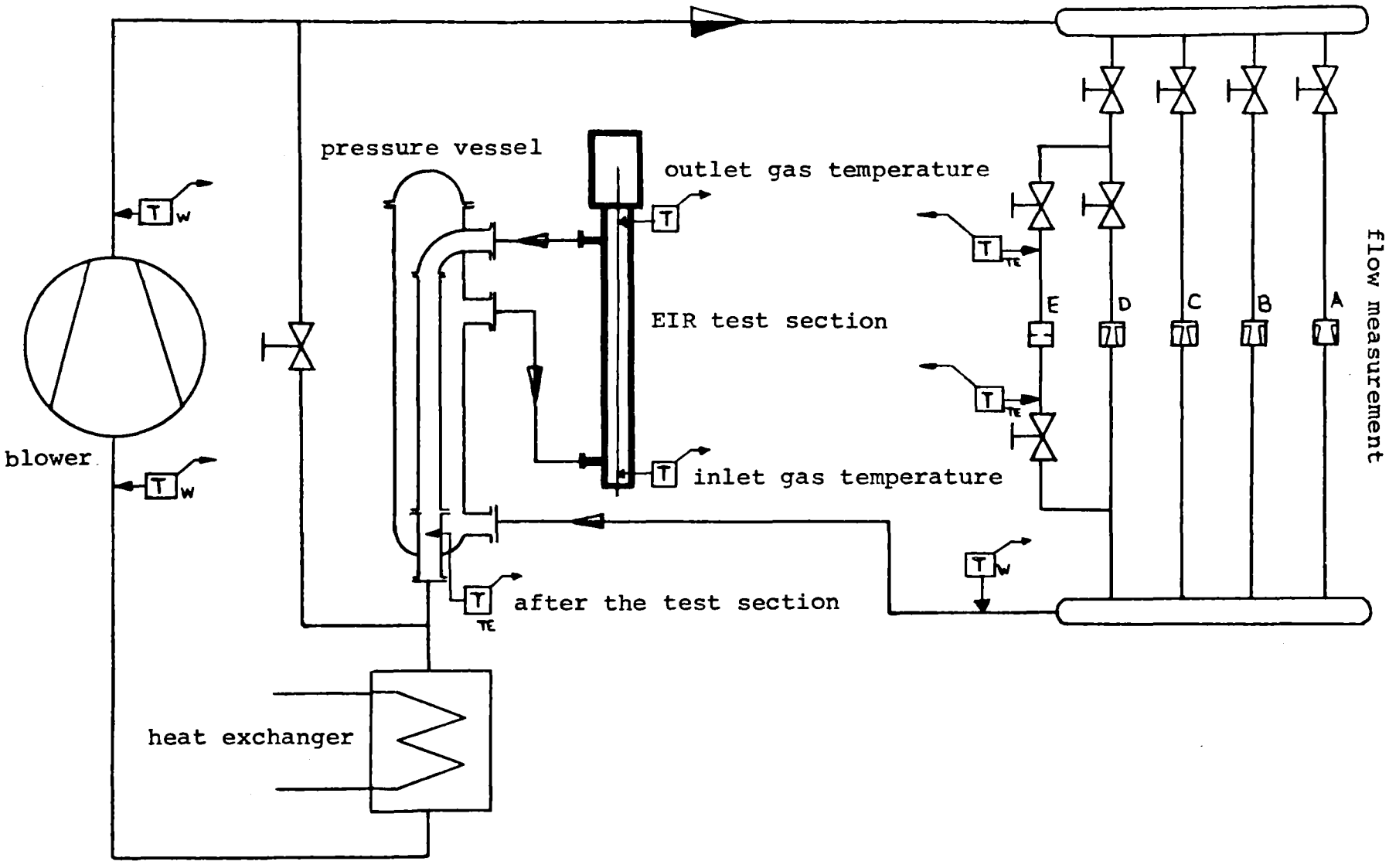

Fig.8: Schematic circuit diagram of KfK high pressure loop for the measurements with the EIR test section

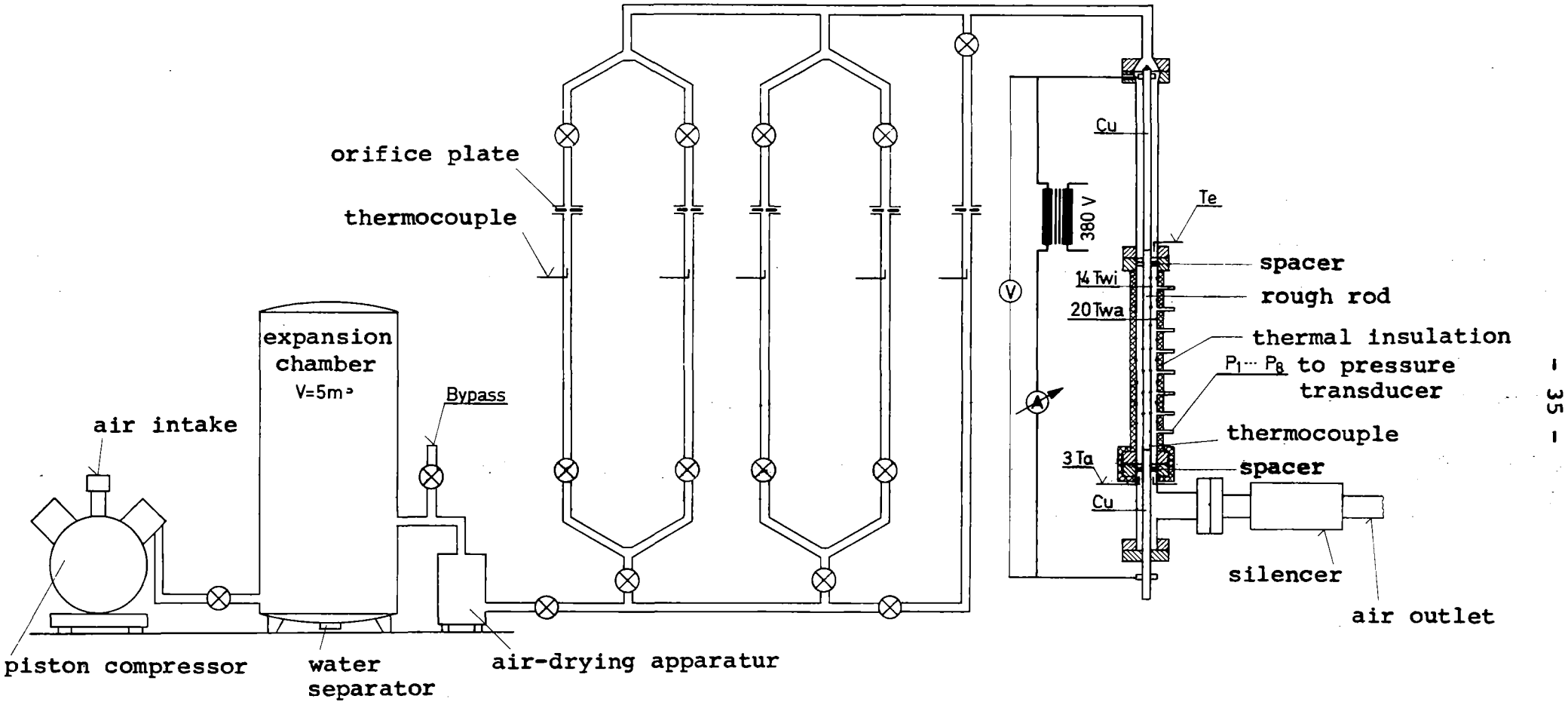

Fig.9: Experimental setup used for the KfK air tests

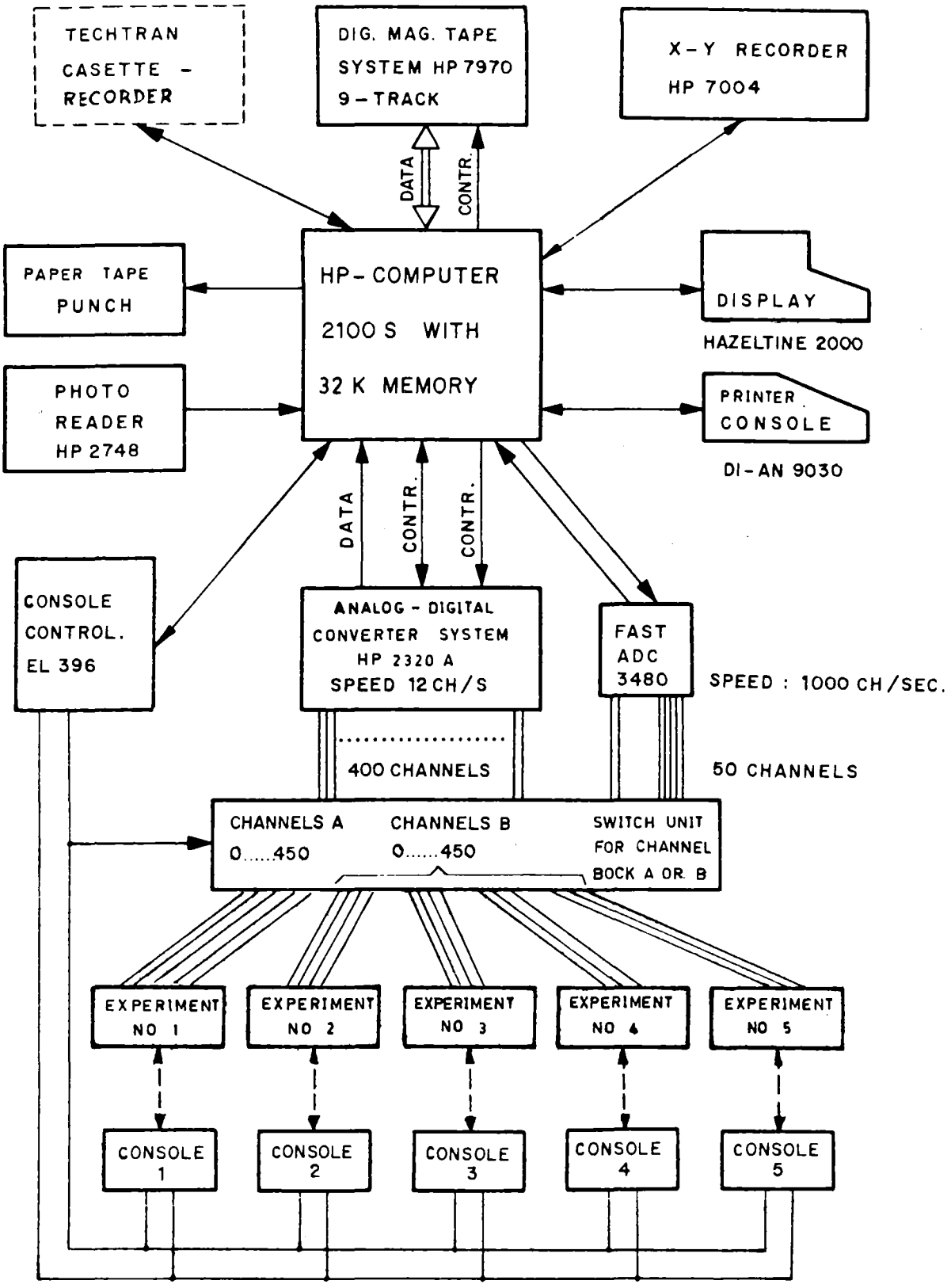

Fig.10: Central data aquisition system HP 9600 A

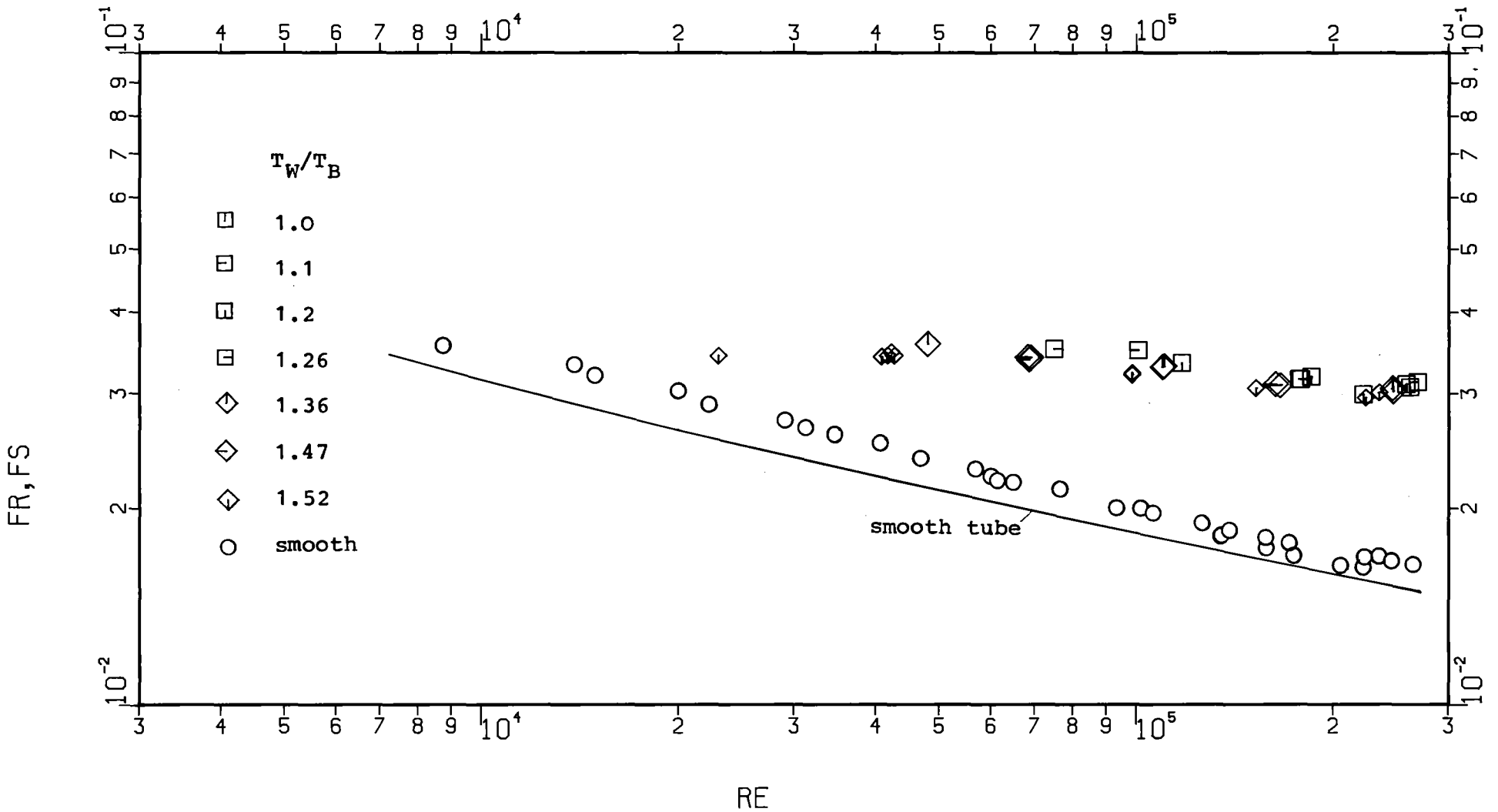

Fig.11: Measured friction factors with CO_2 at EIR

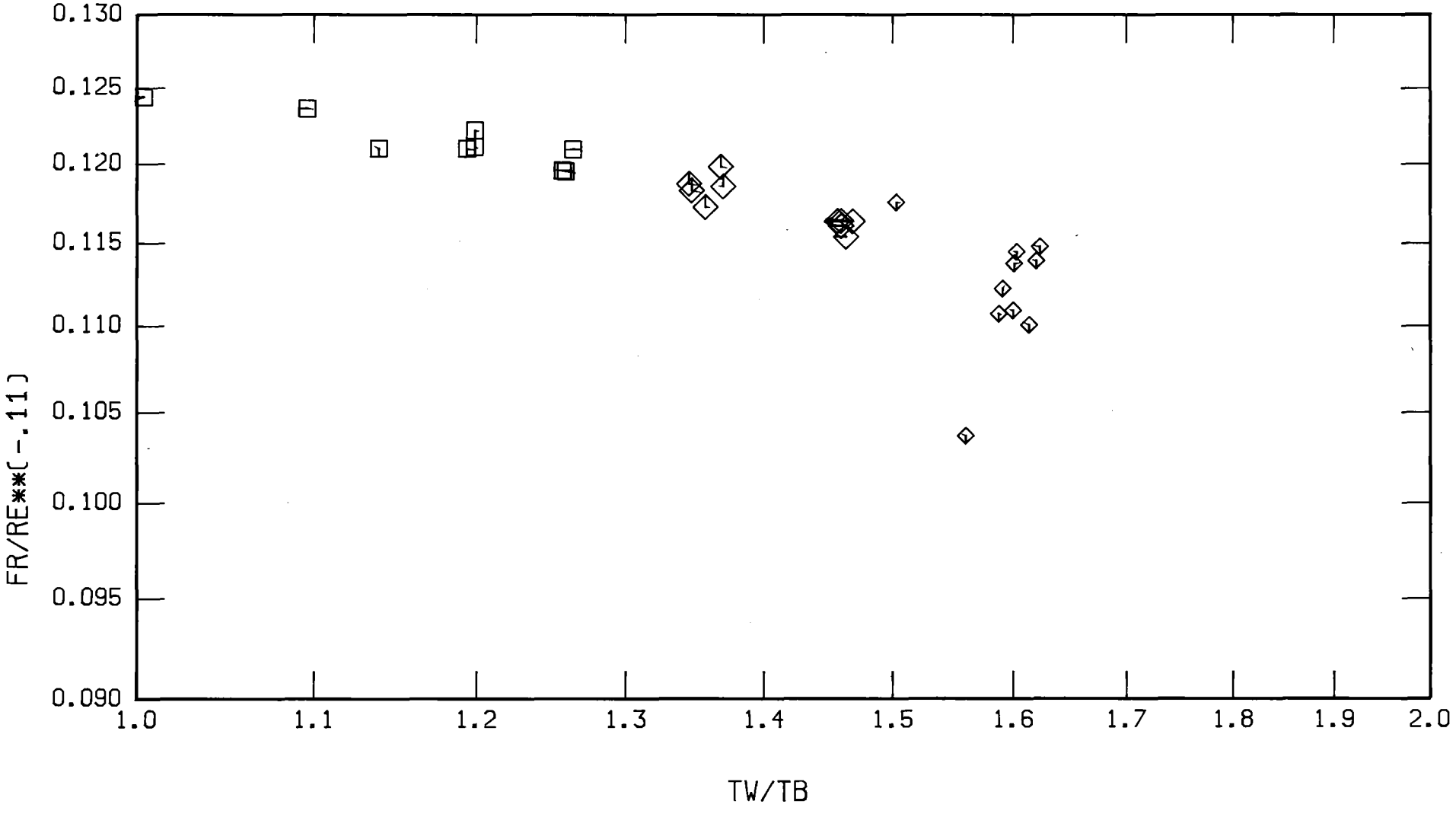

Fig.12: T_W/T_B-effect on friction factor (CO_2, EIR)

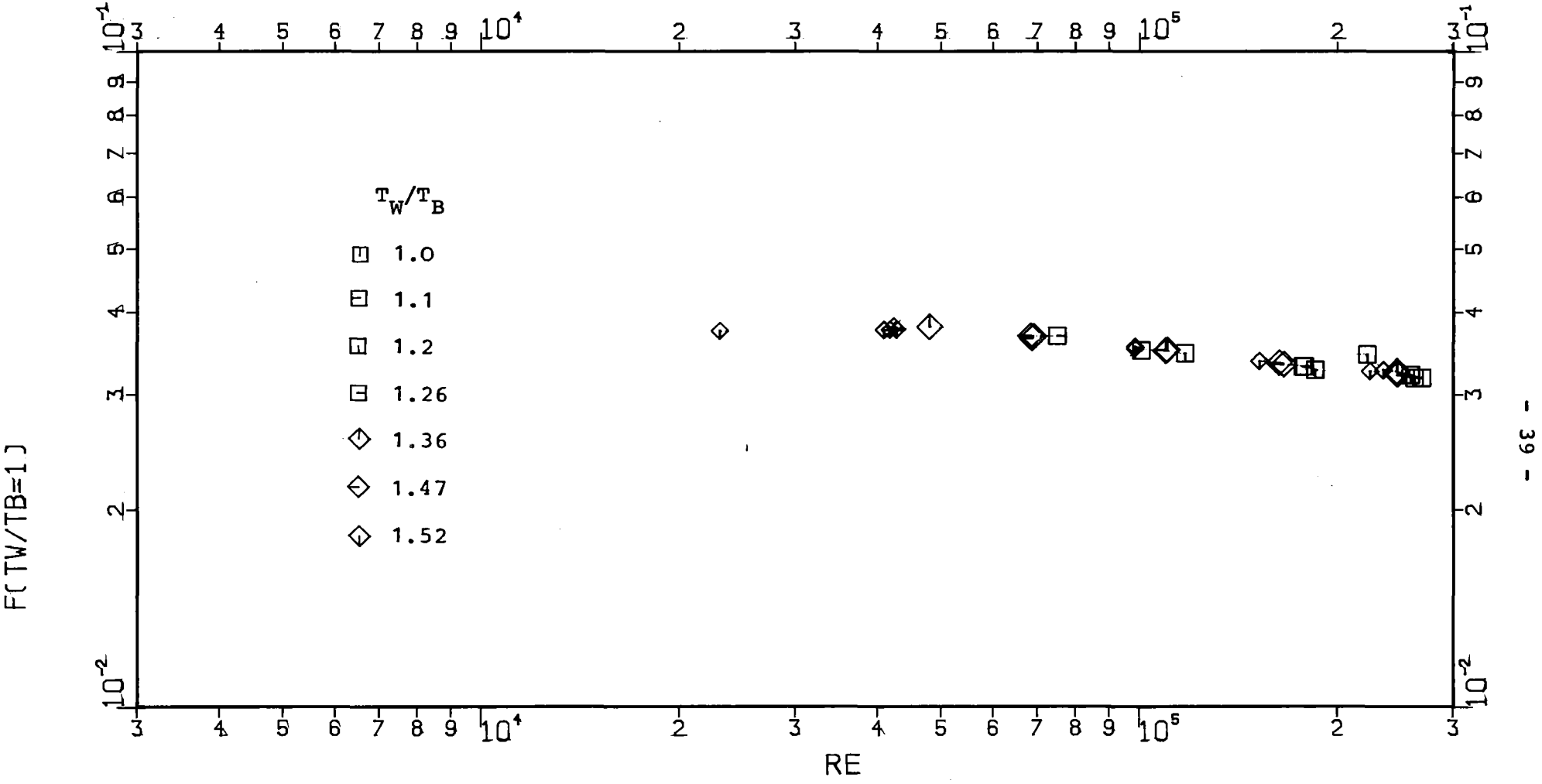

Fig.13: Measured friction factors corrected for the wall to bulk temperature ratio (CO_2, EIR)

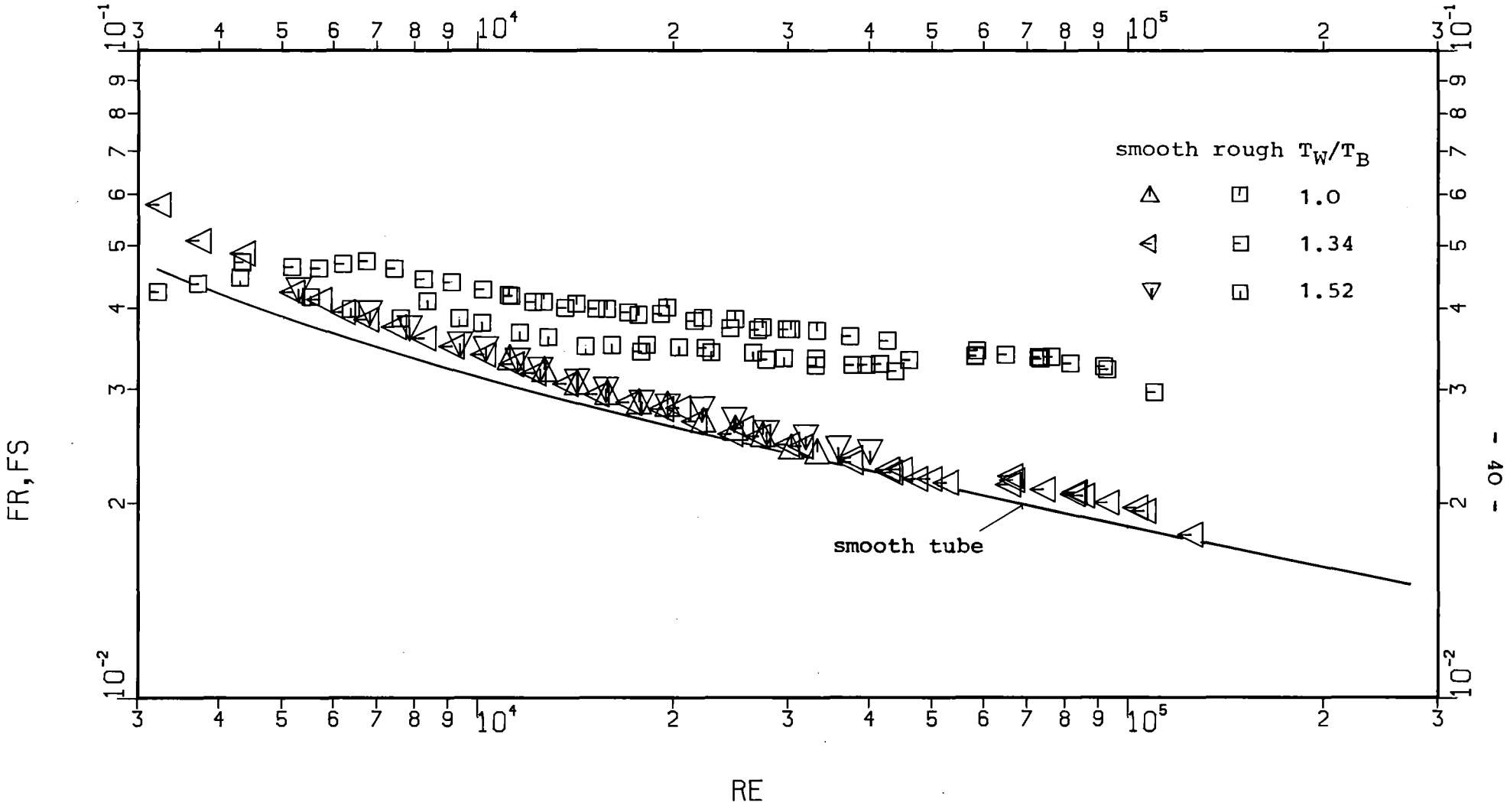

Fig.14: Measured friction factors with He at KfK

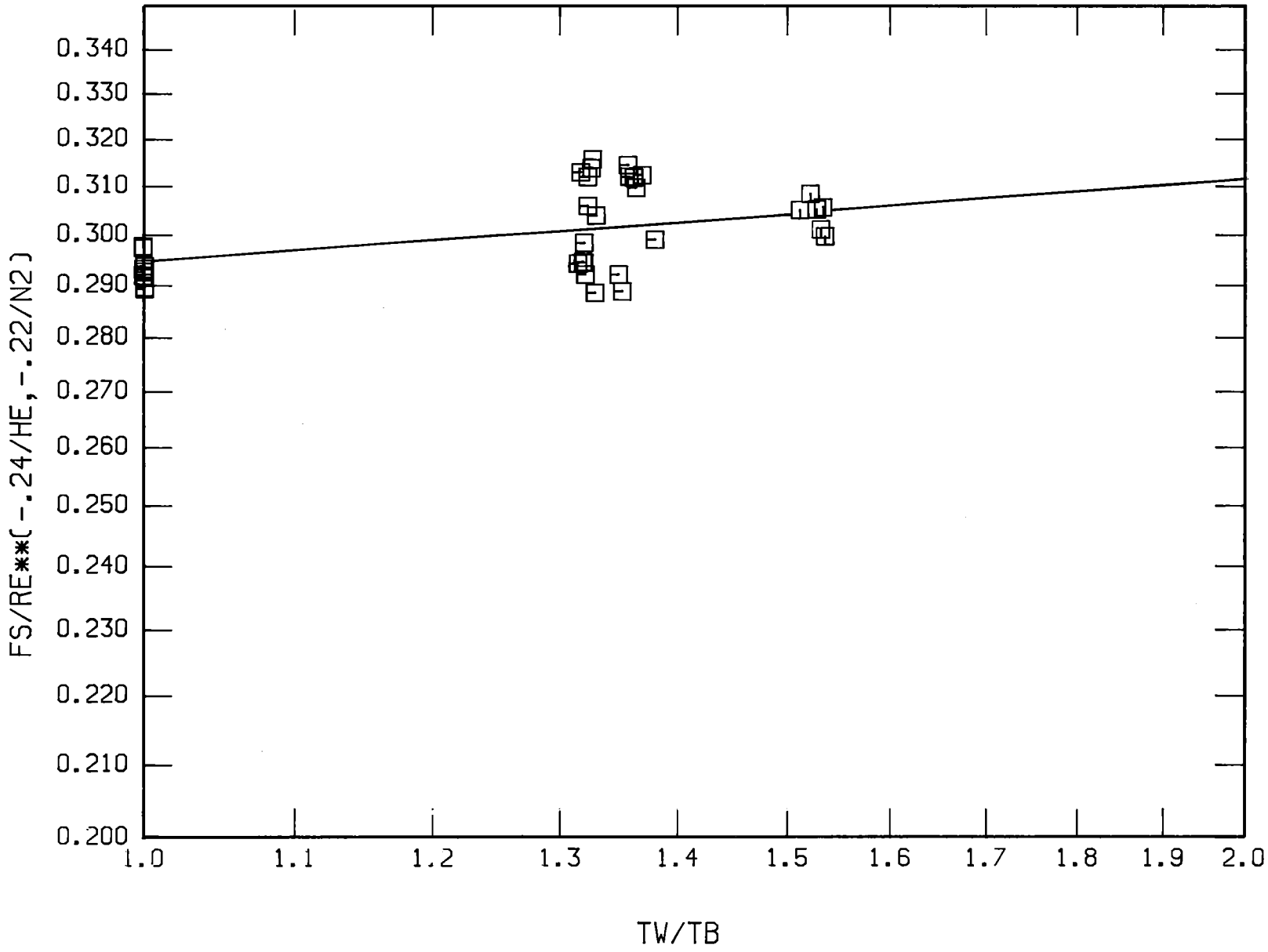

Fig.15: T_W/T_B-effect on smooth friction factor (He, KfK)

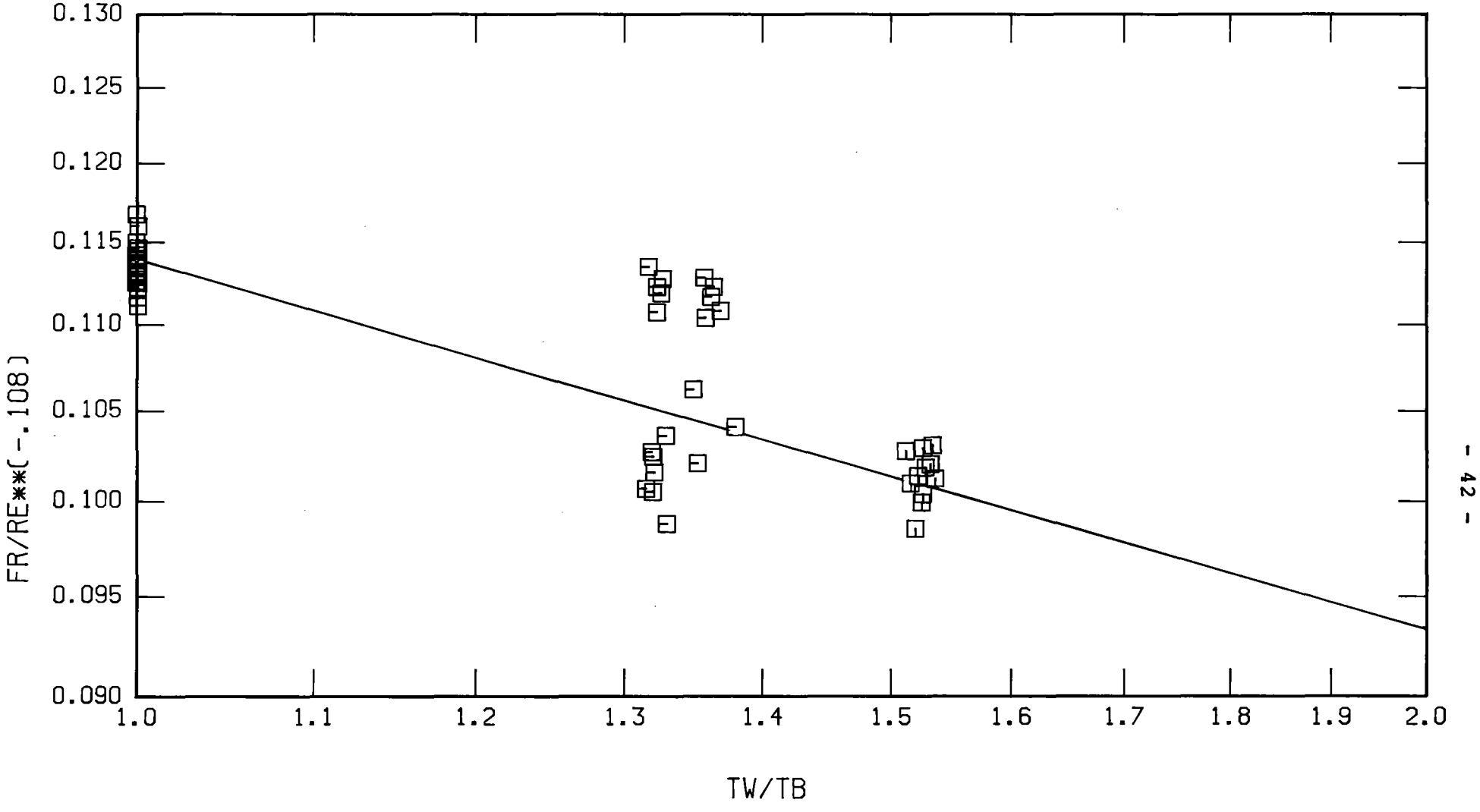

Fig.16: T_W/T_B-effect on rough friction factor (He, KfK)

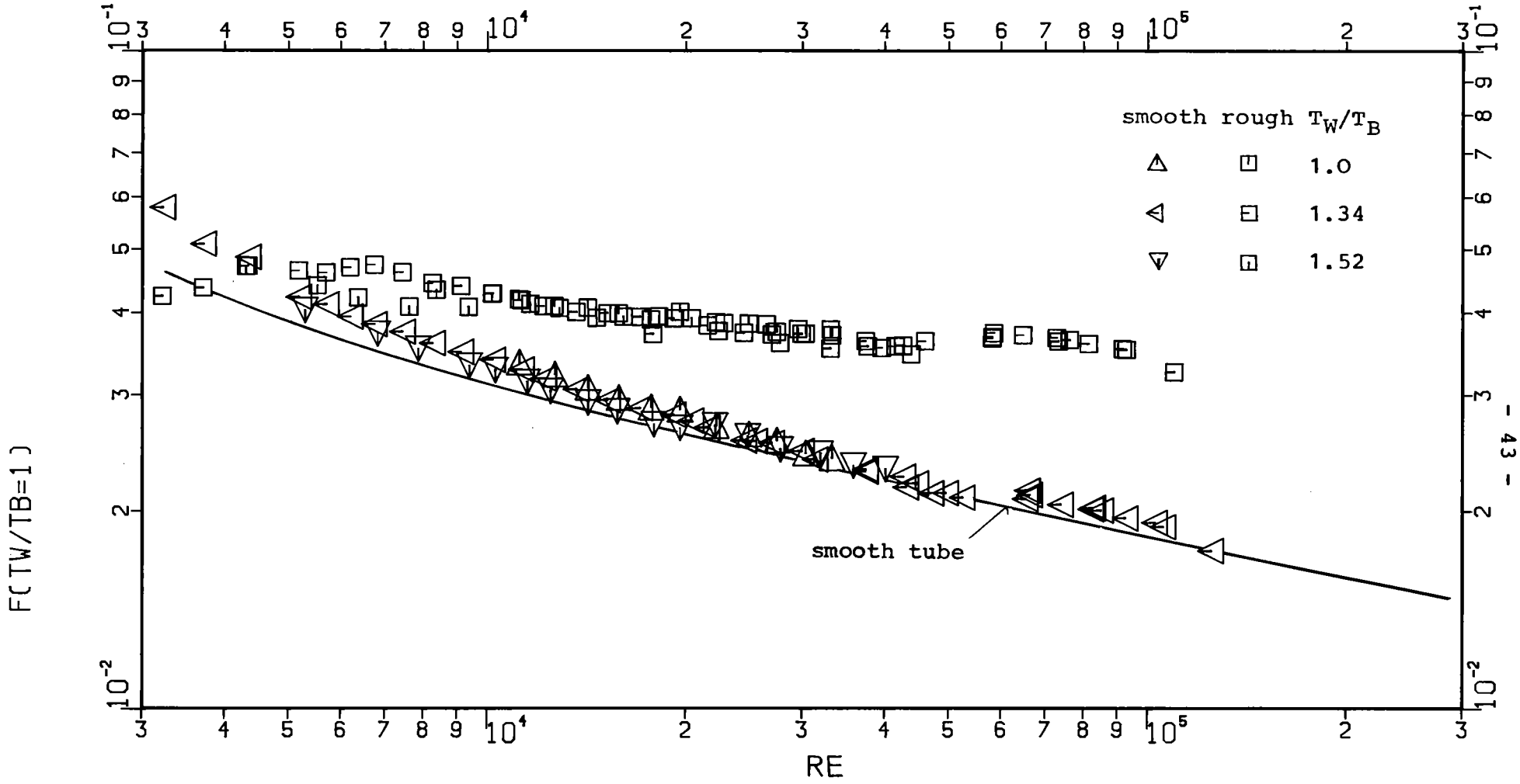

Fig.17: Measured friction factors corrected for the wall to bulk temperature ratio (He, KfK)

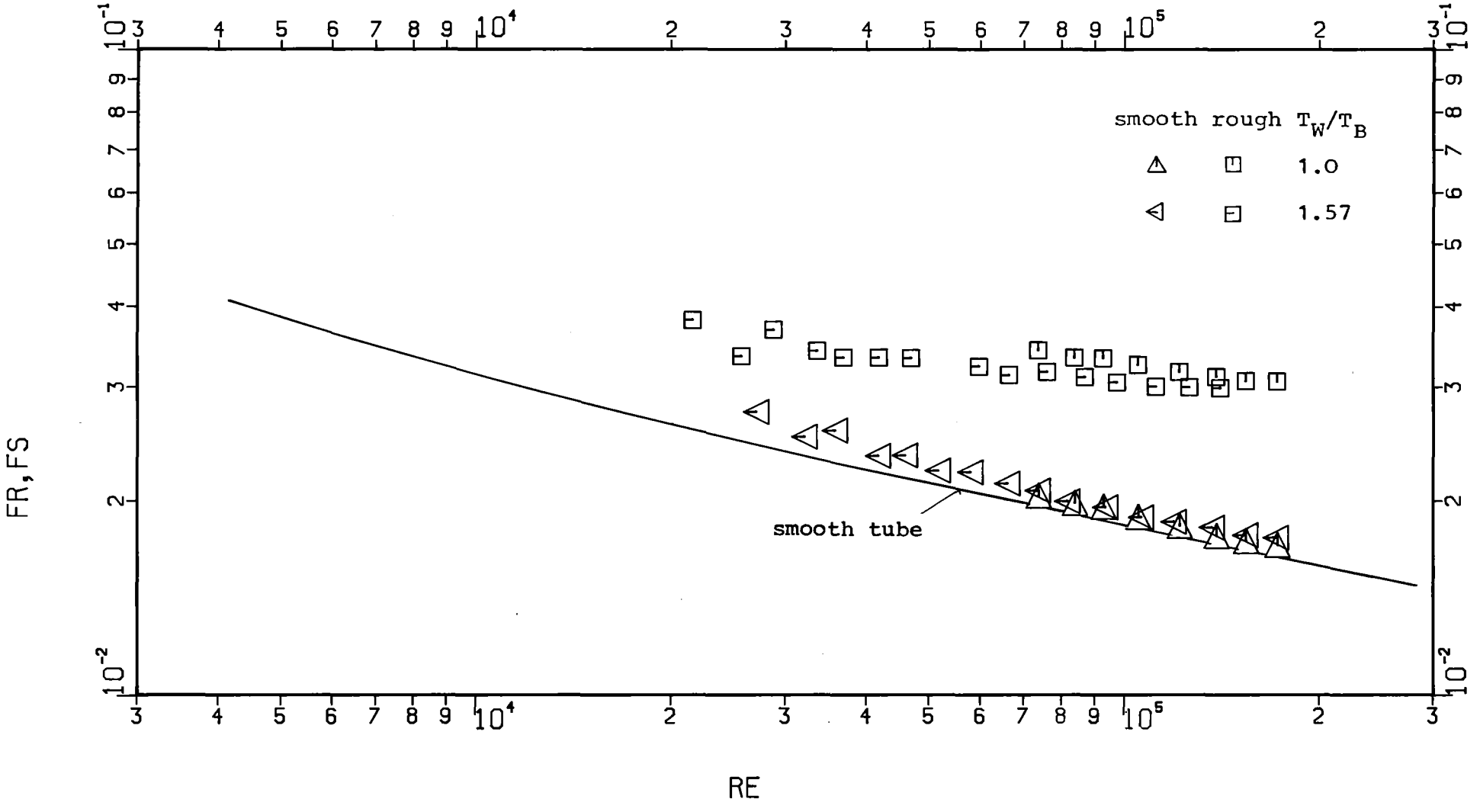

Fig.18: Measured friction factors with N_2 at KfK

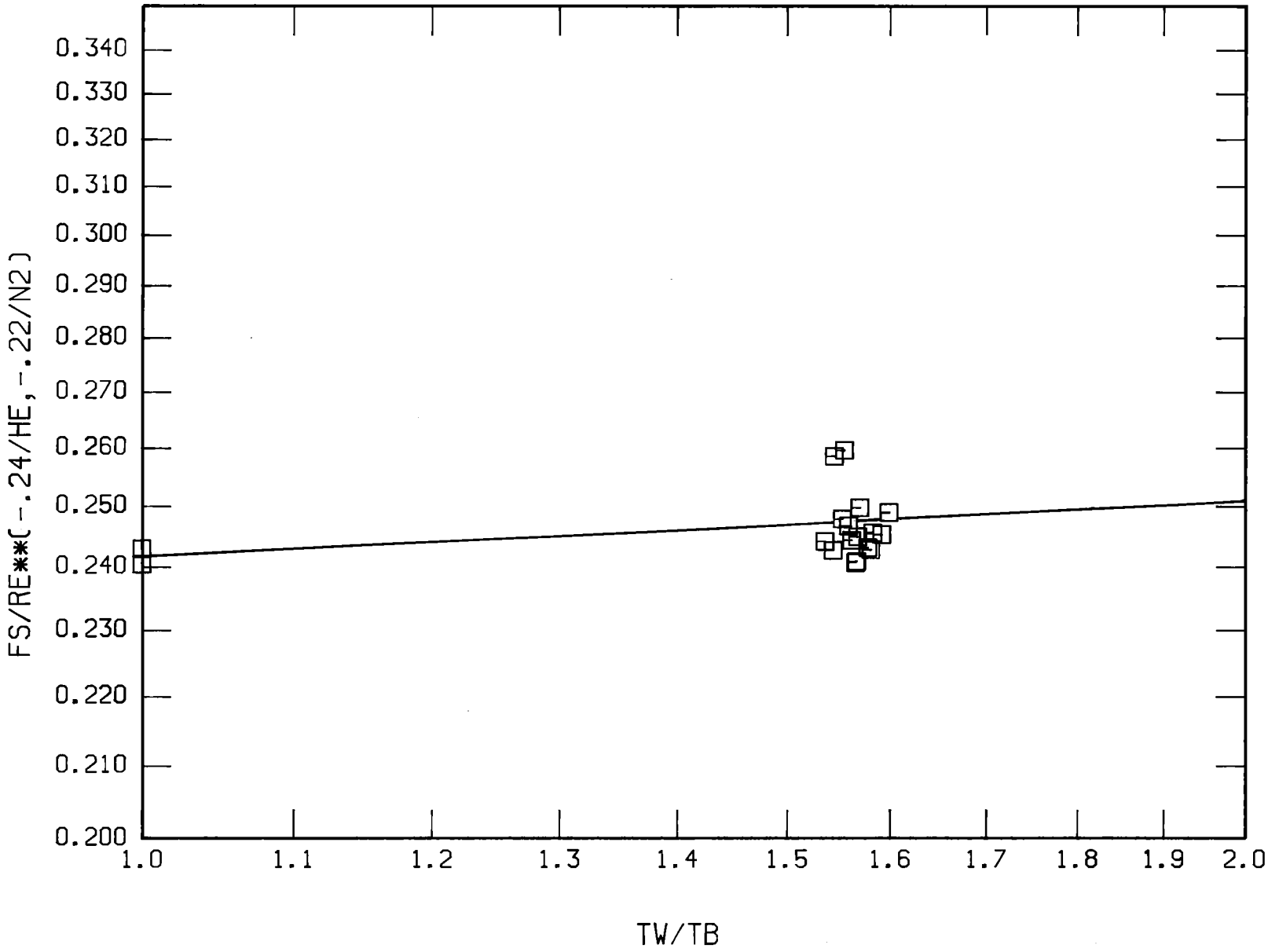

Fig.19: T_W/T_B-effect on smooth friction factor (N_2, KfK)

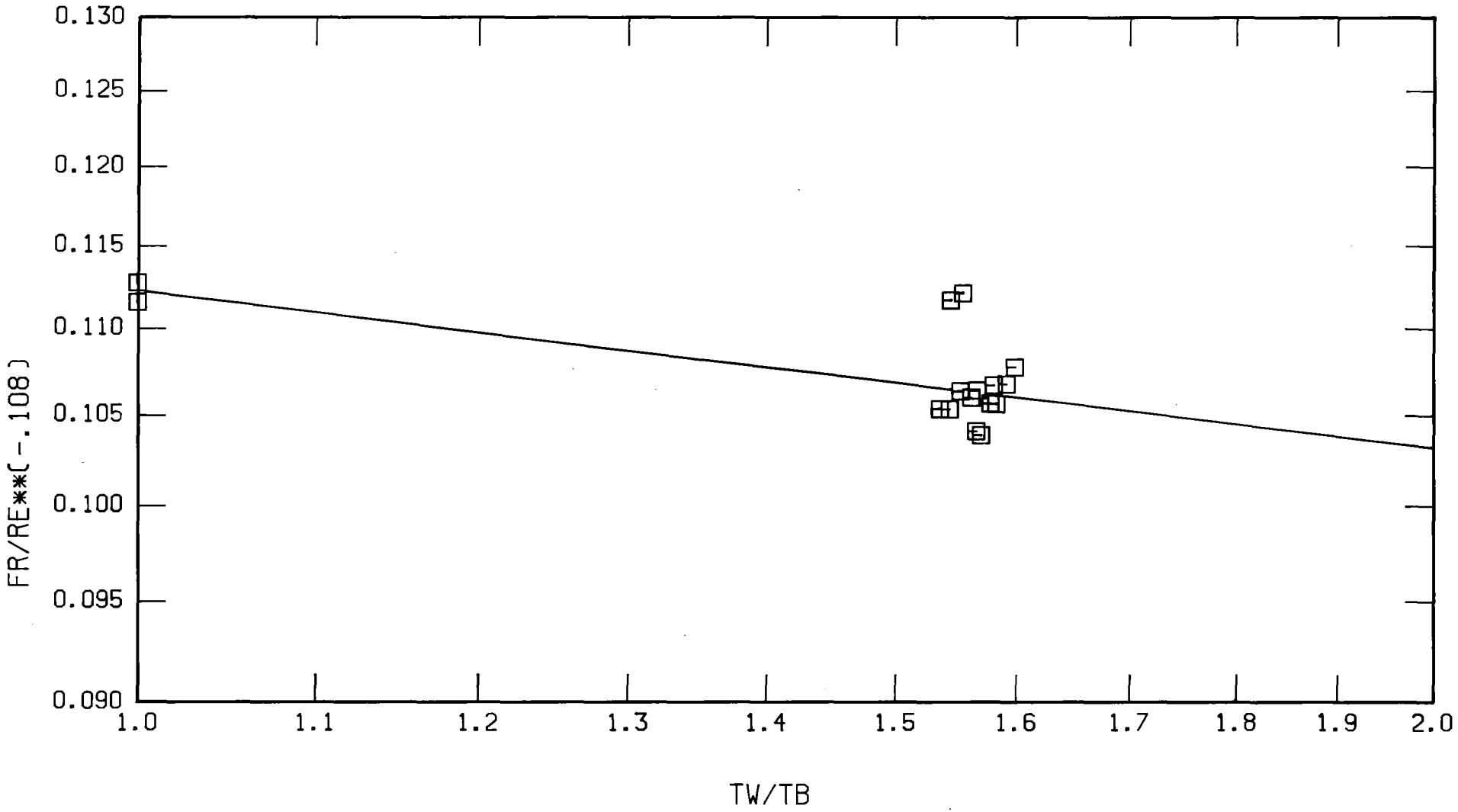

Fig.20: T_W/T_B-effect on rough friction factor (N_2, KfK)

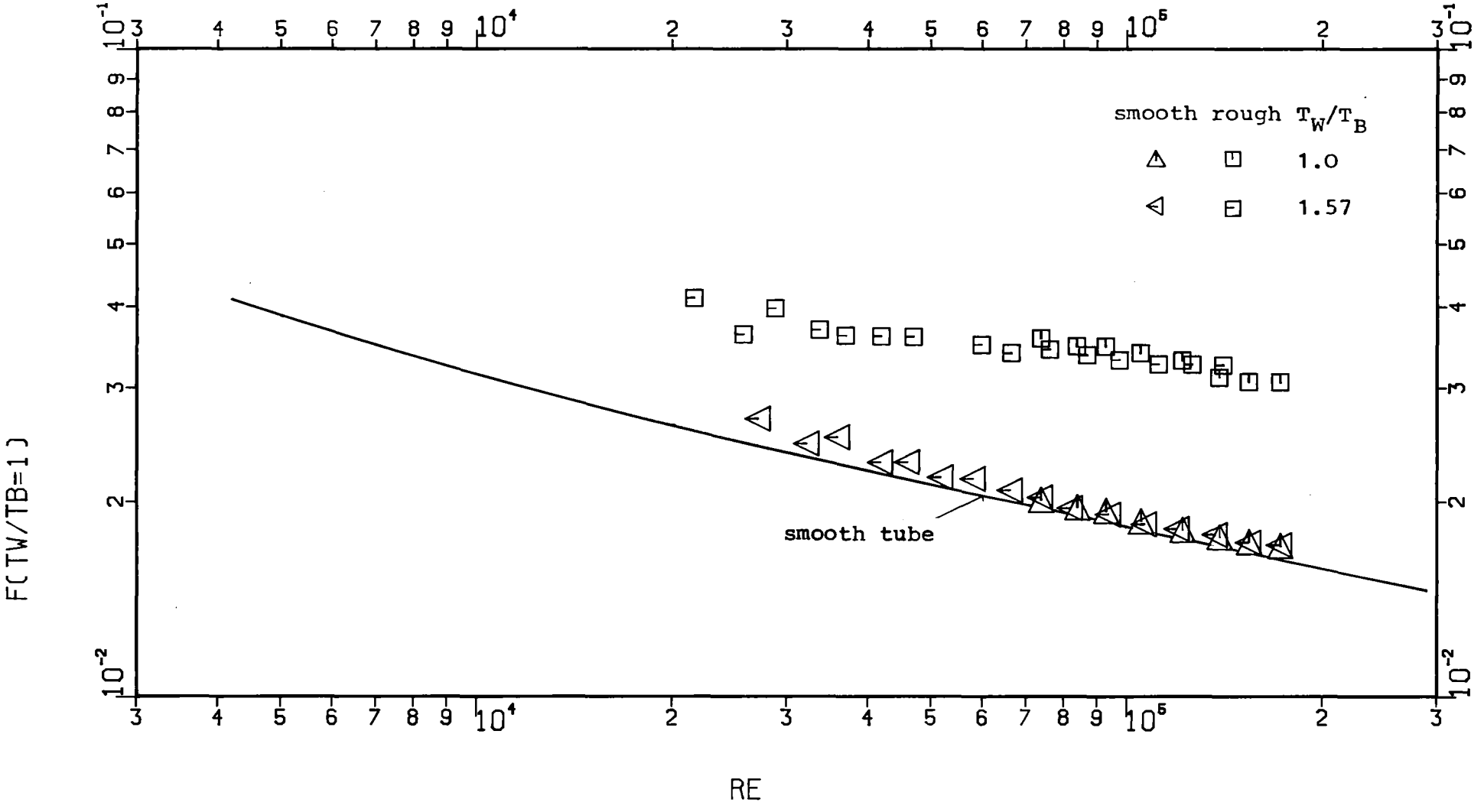

Fig.21: Measured friction factors corrected for the wall to bulk temperature ratio (N_2, KfK)

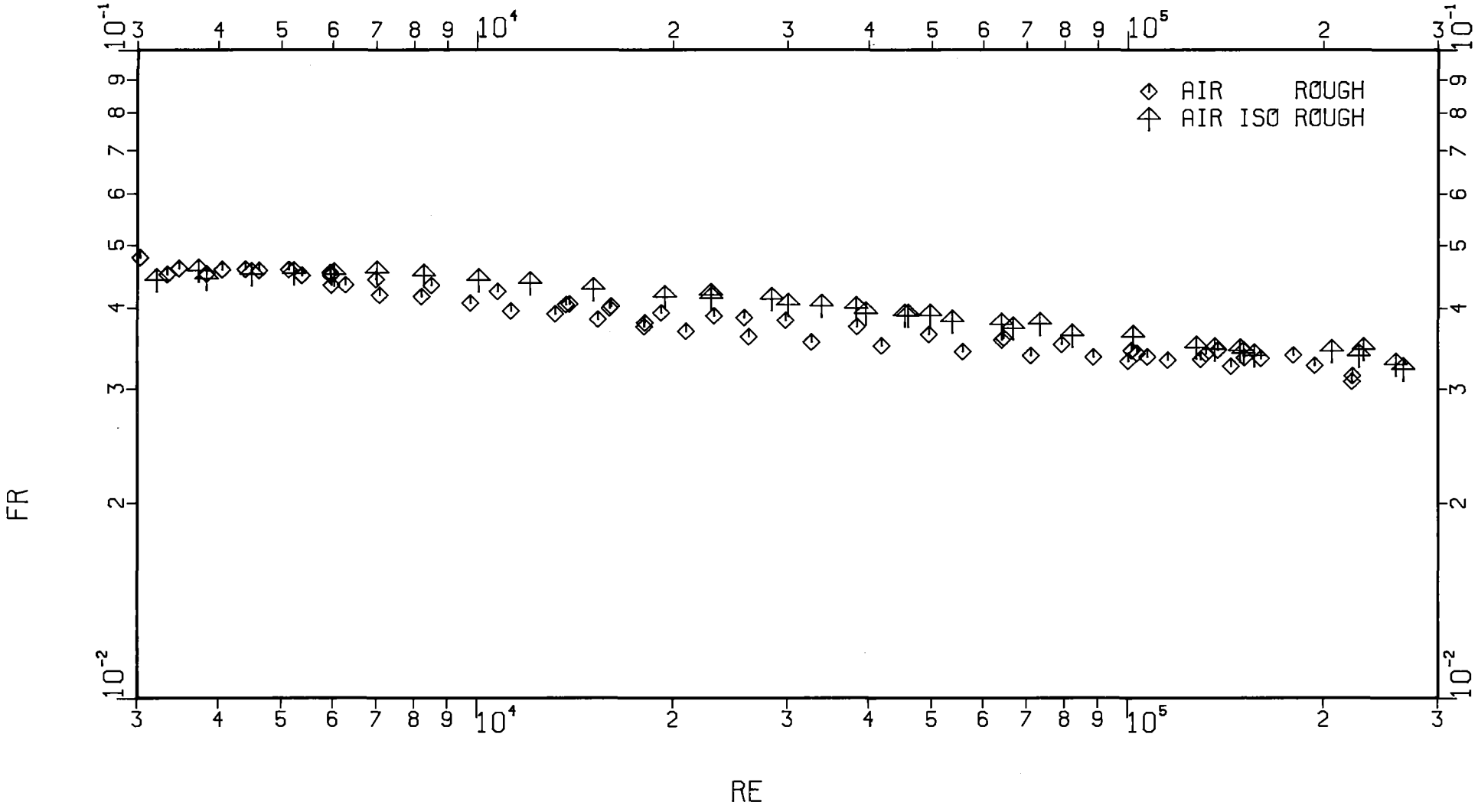

Fig.22: Measured friction factors (air, KfK)

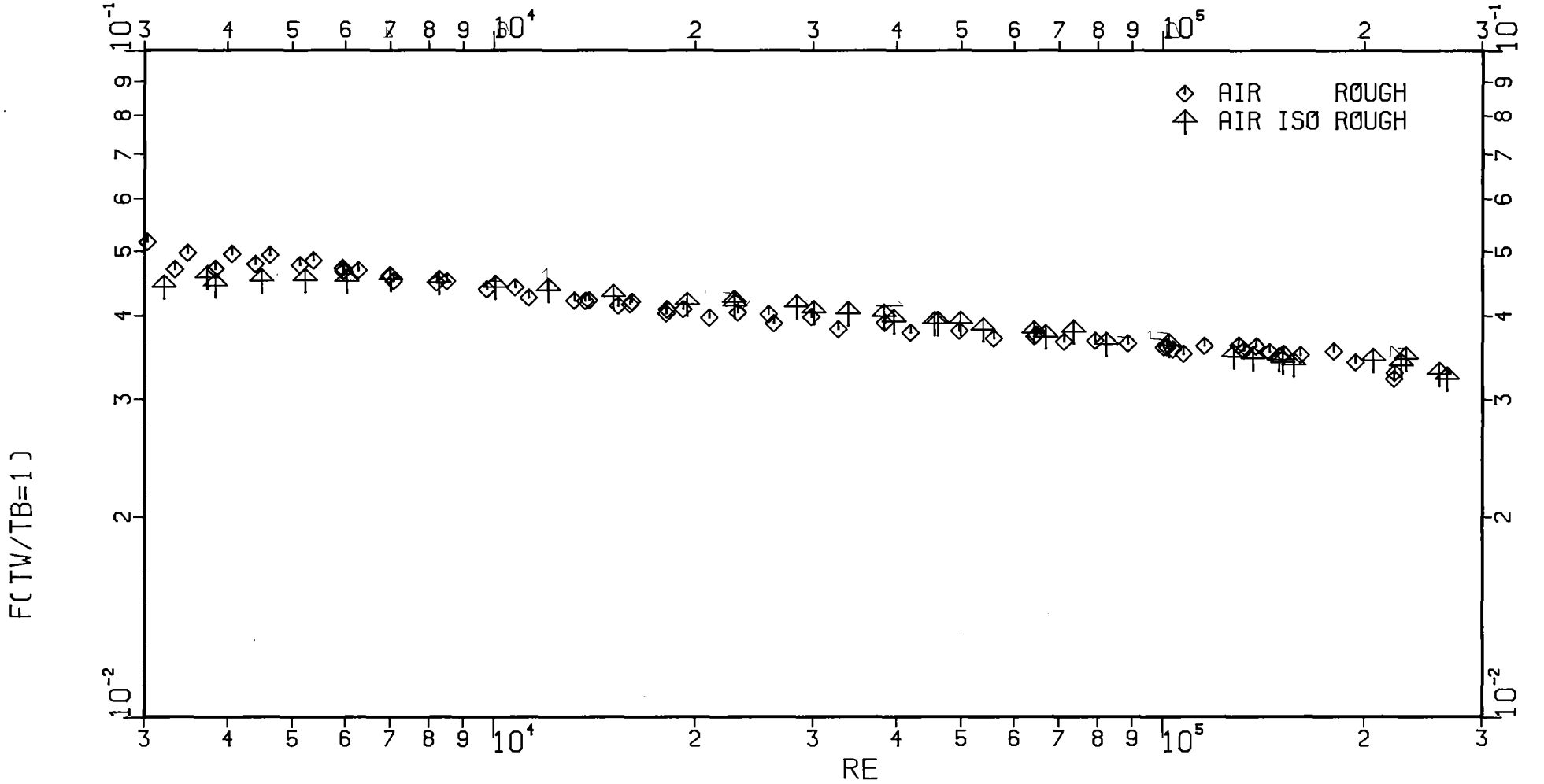

Fig.23: Measured friction factors corrected for the wall to bulk temperature ratio (air, KfK)

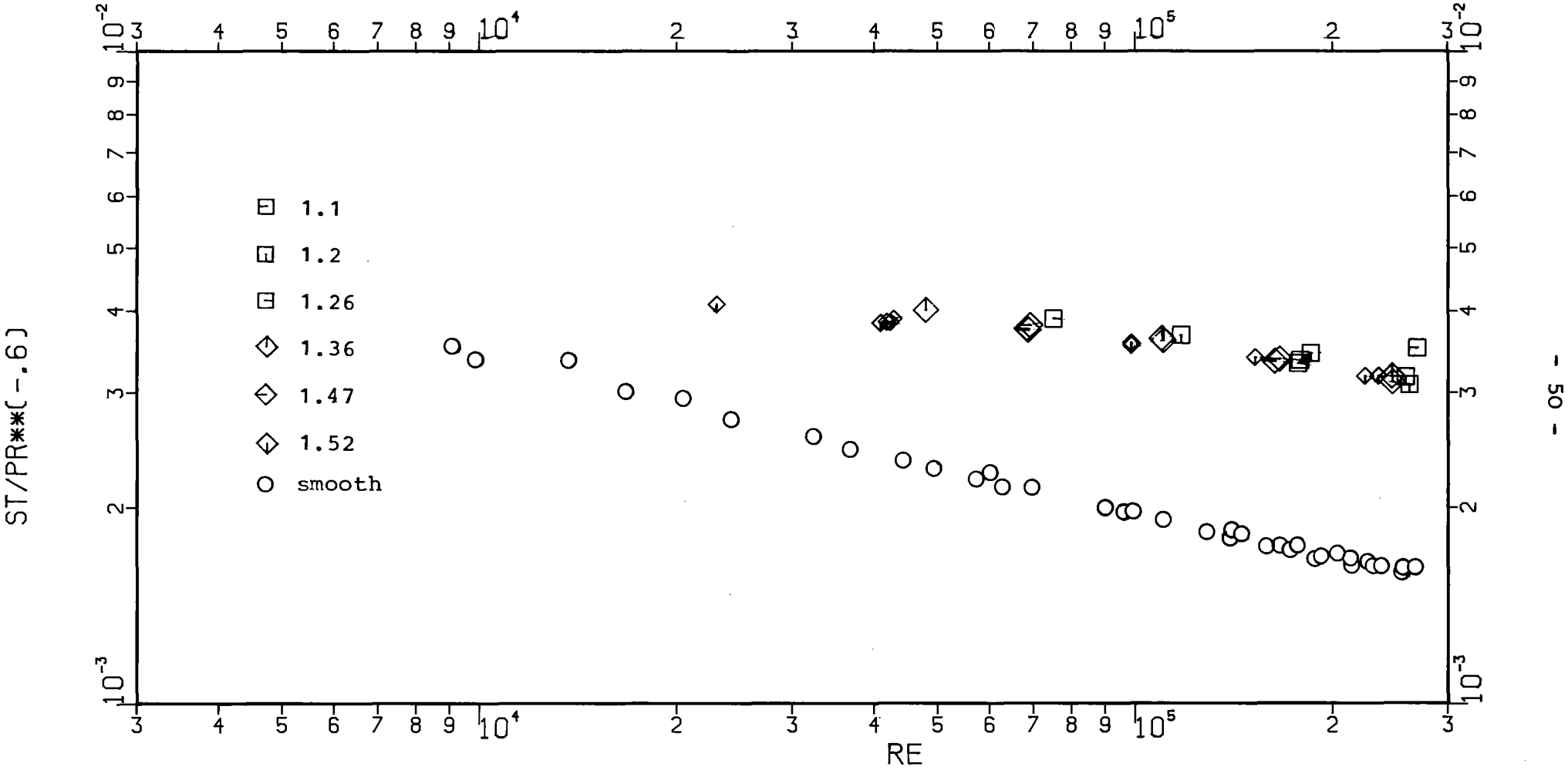

Fig.24: Measured Stanton numbers (CO_2, EIR)

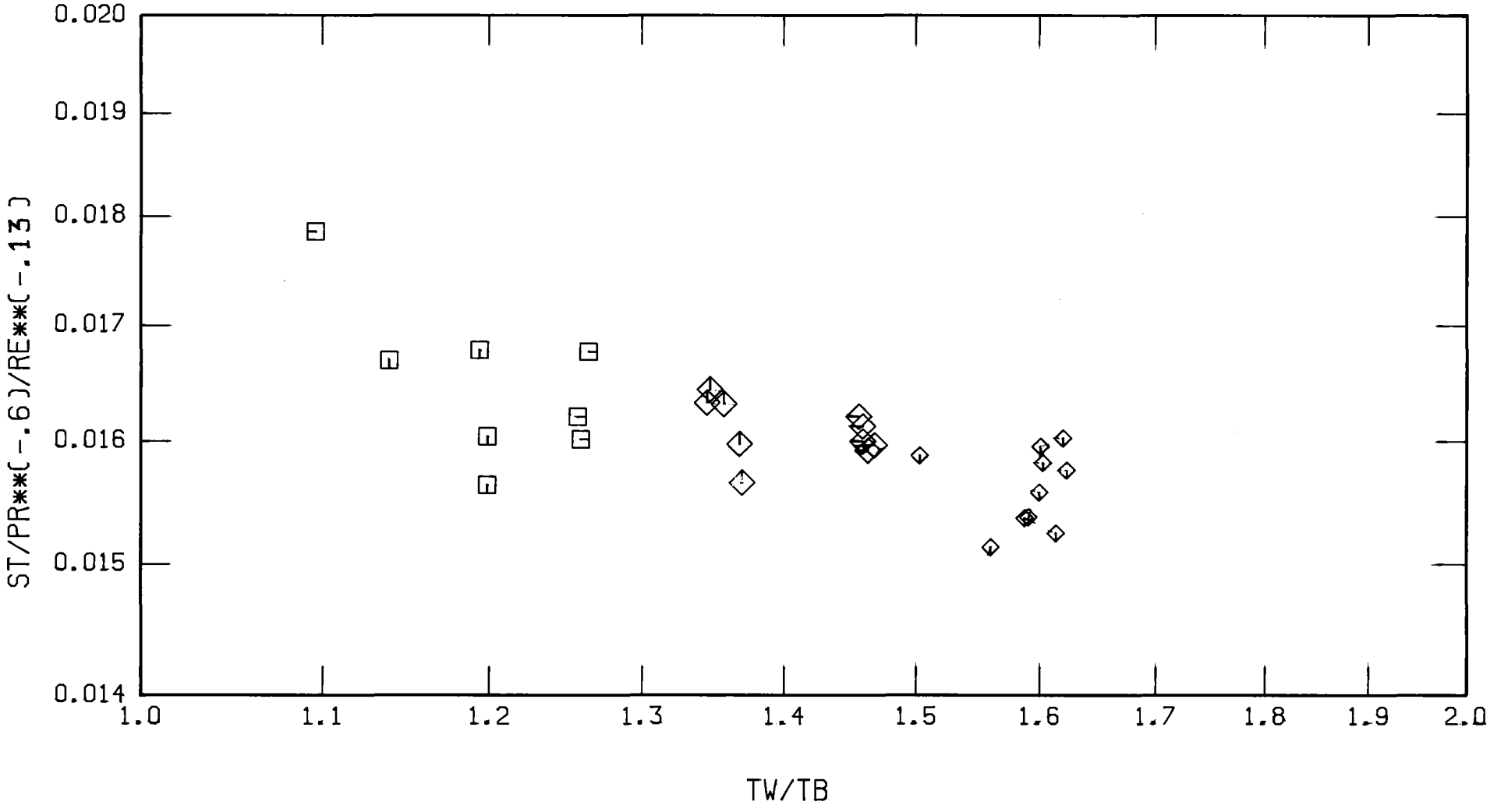

Fig.25: T_W/T_B-effect on Stanton number (CO_2, EIR)

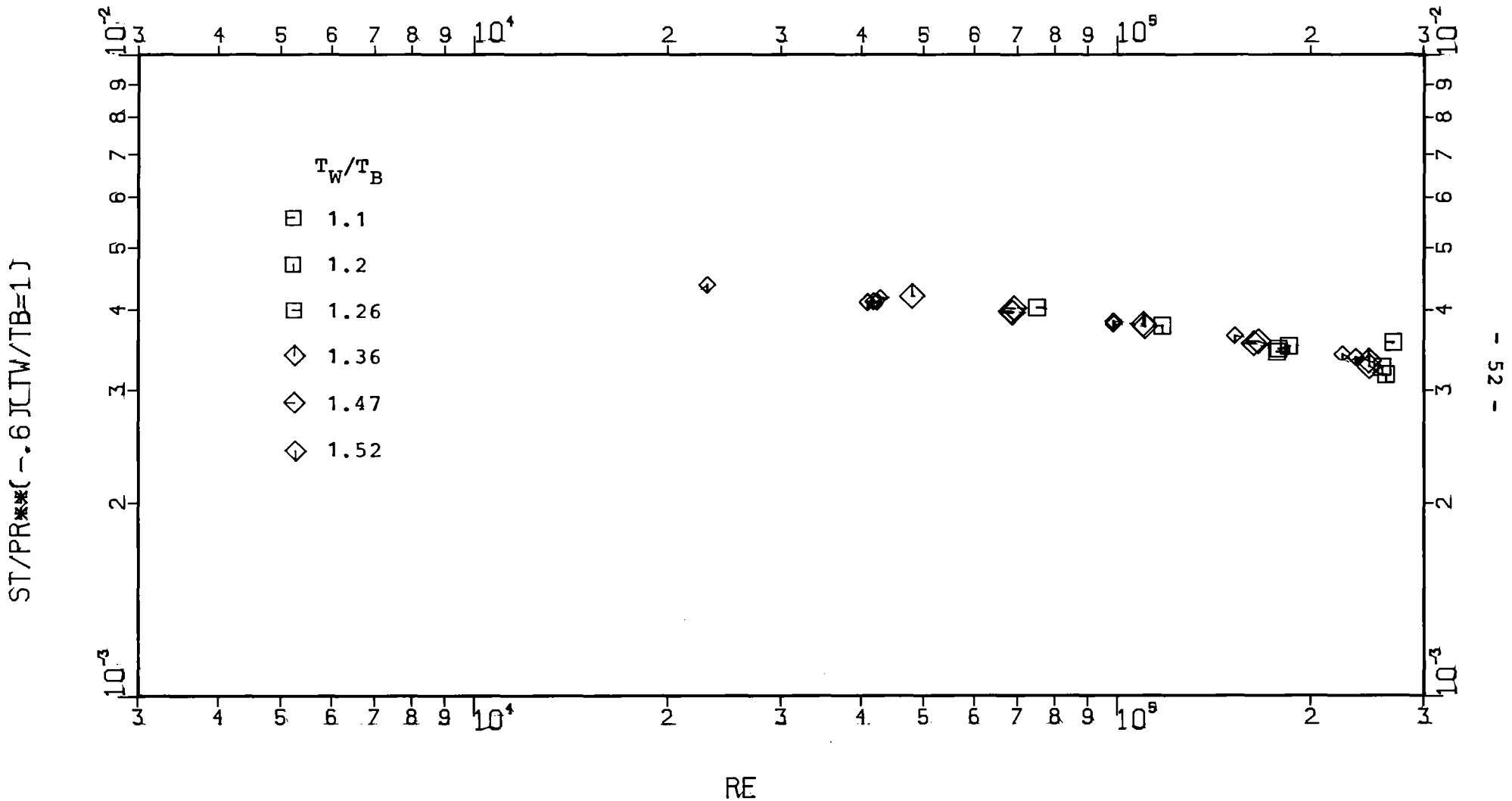

Fig.26: Measured Stanton numbers corrected for the wall to bulk temperature ratio (CO_2, EIR)

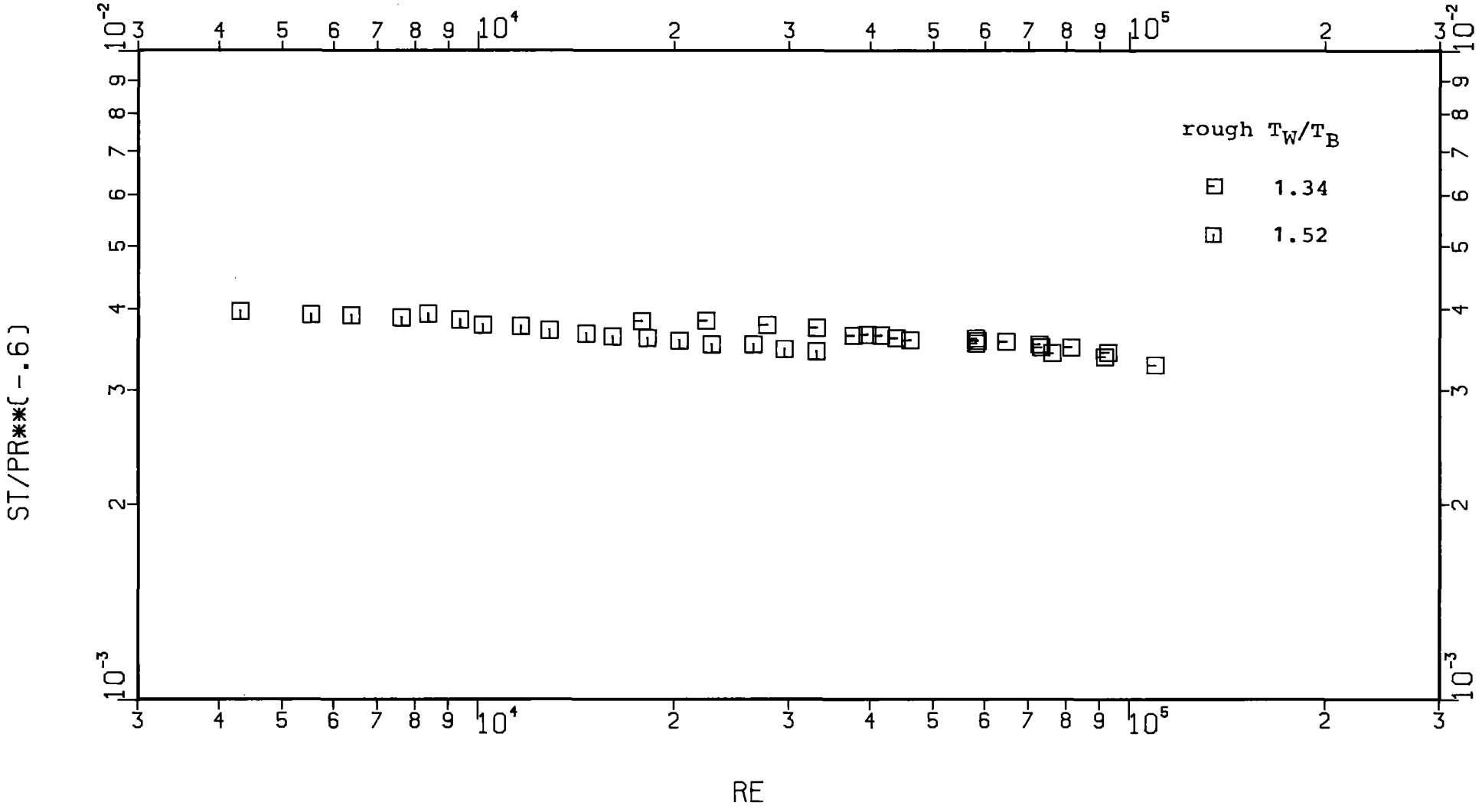

Fig.27: Measured Stanton numbers (He, KfK)

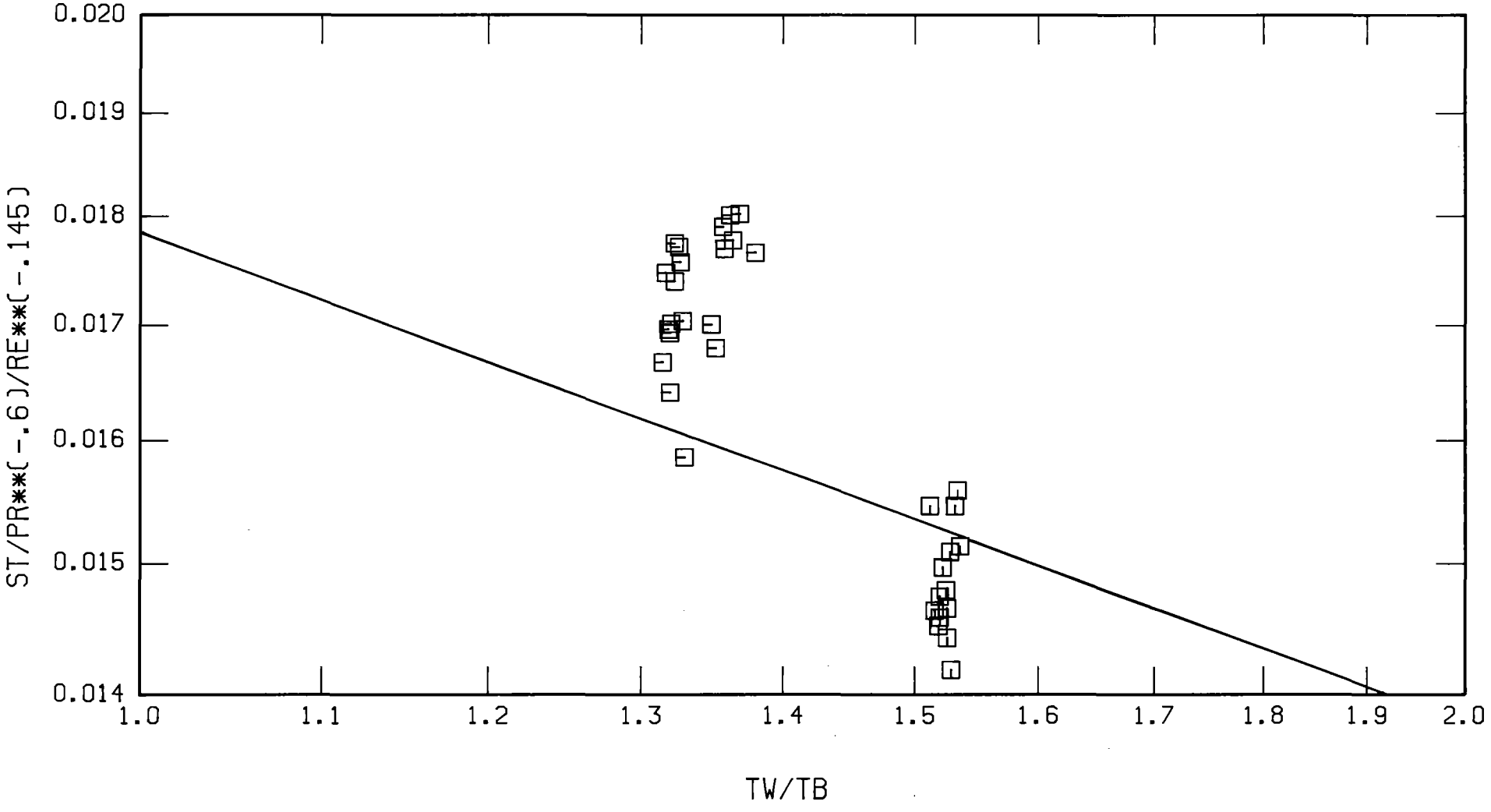

Fig.28: T_W/T_B-effect on Stanton number (He, KfK)

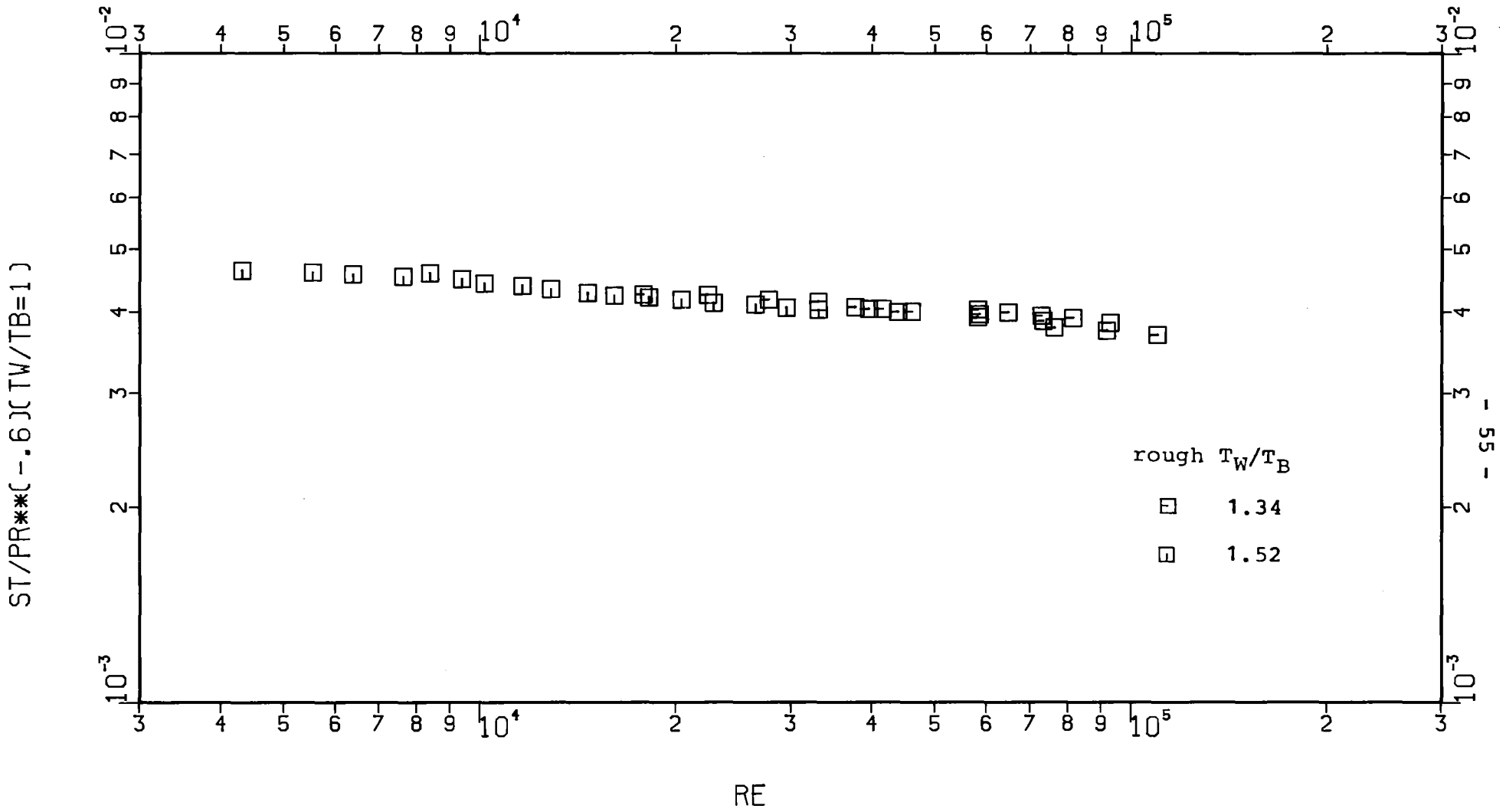

Fig.29: Measured Stanton numbers corrected for the wall to bulk temperature ratio (He, KfK)

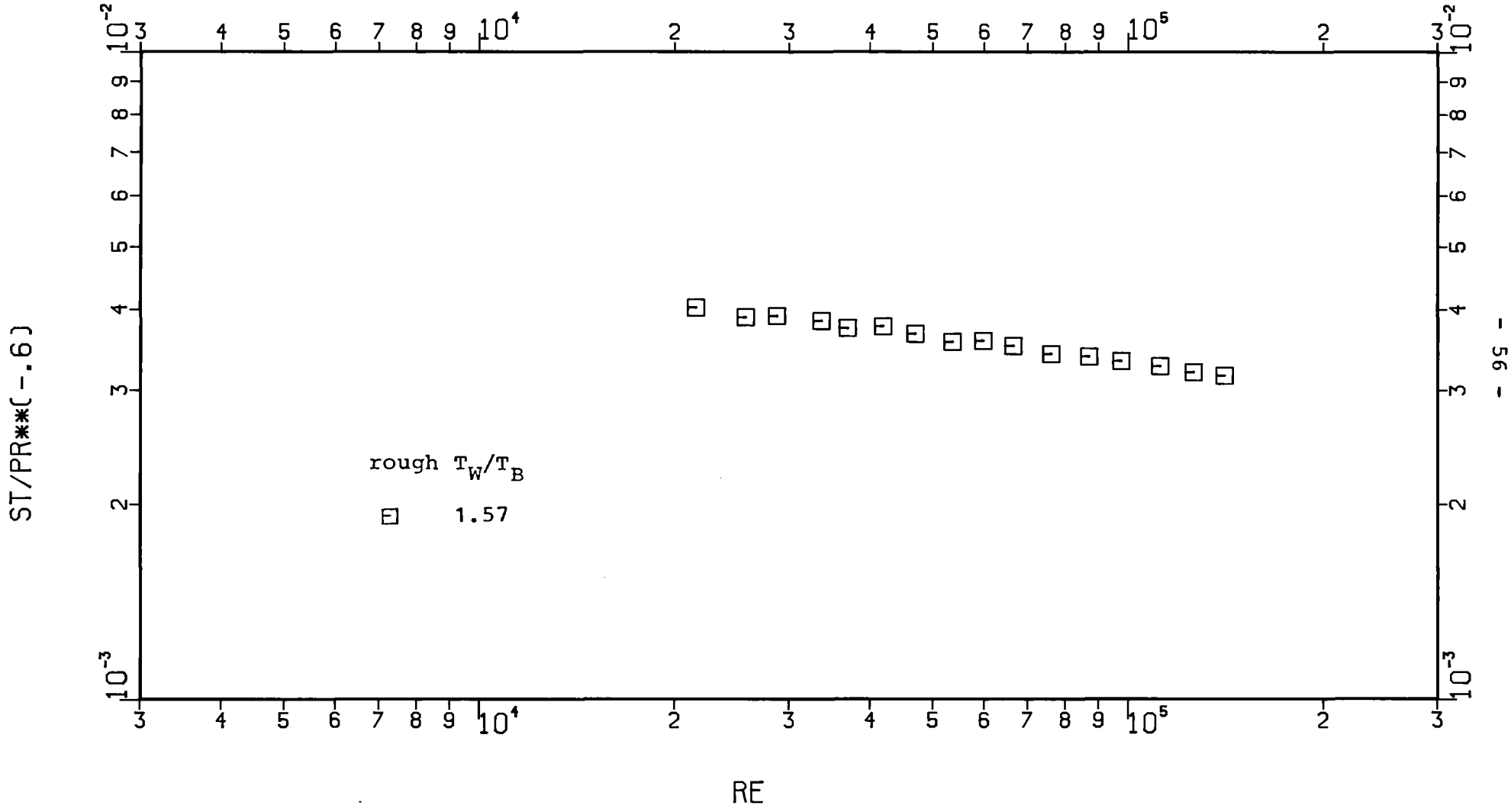

Fig.30: Measured Stanton numbers (N_2, KfK)

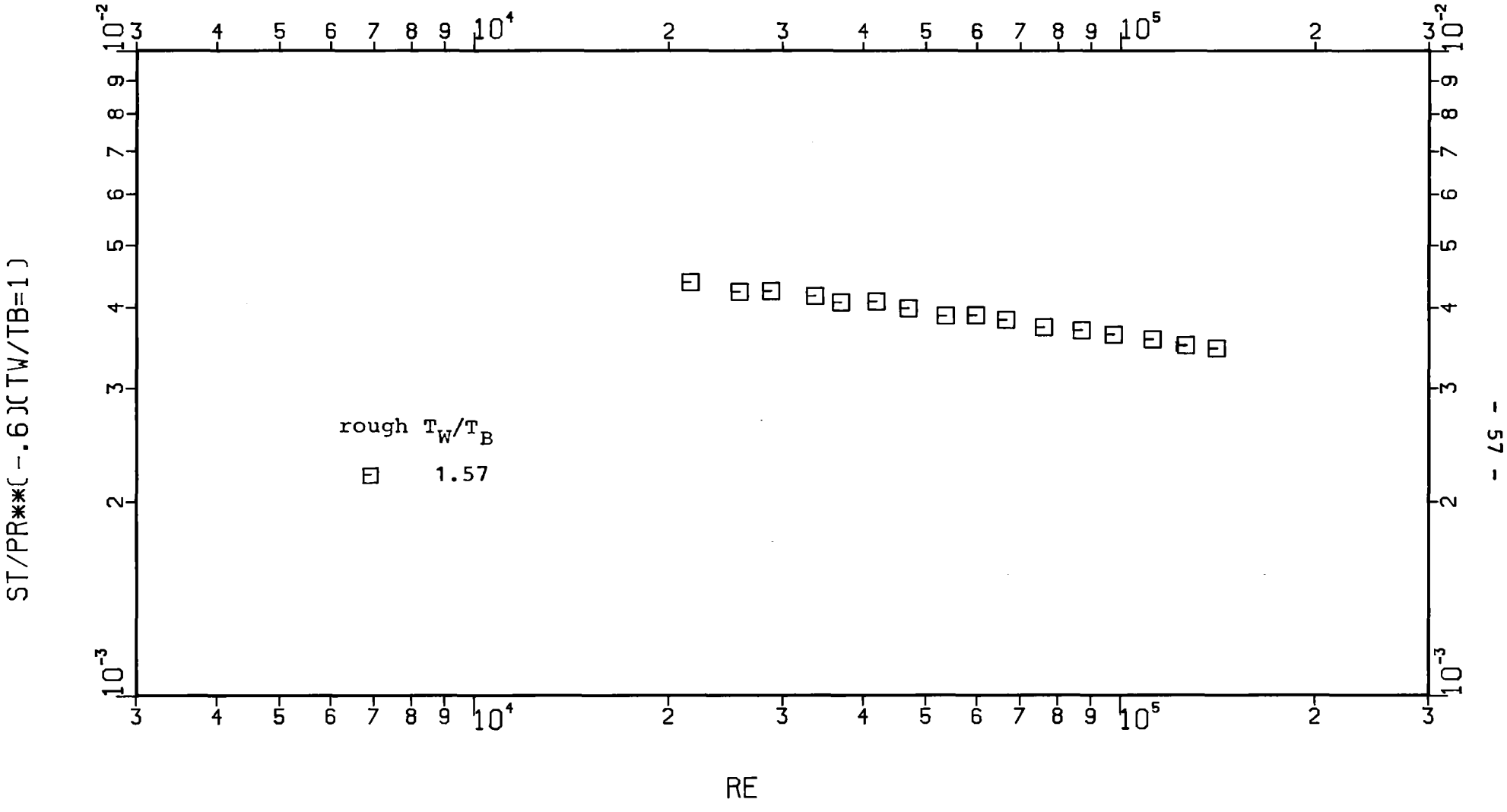

Fig.31: Measured Stanton numbers corrected for the wall to bulk temperature ratio (N_2, KfK)

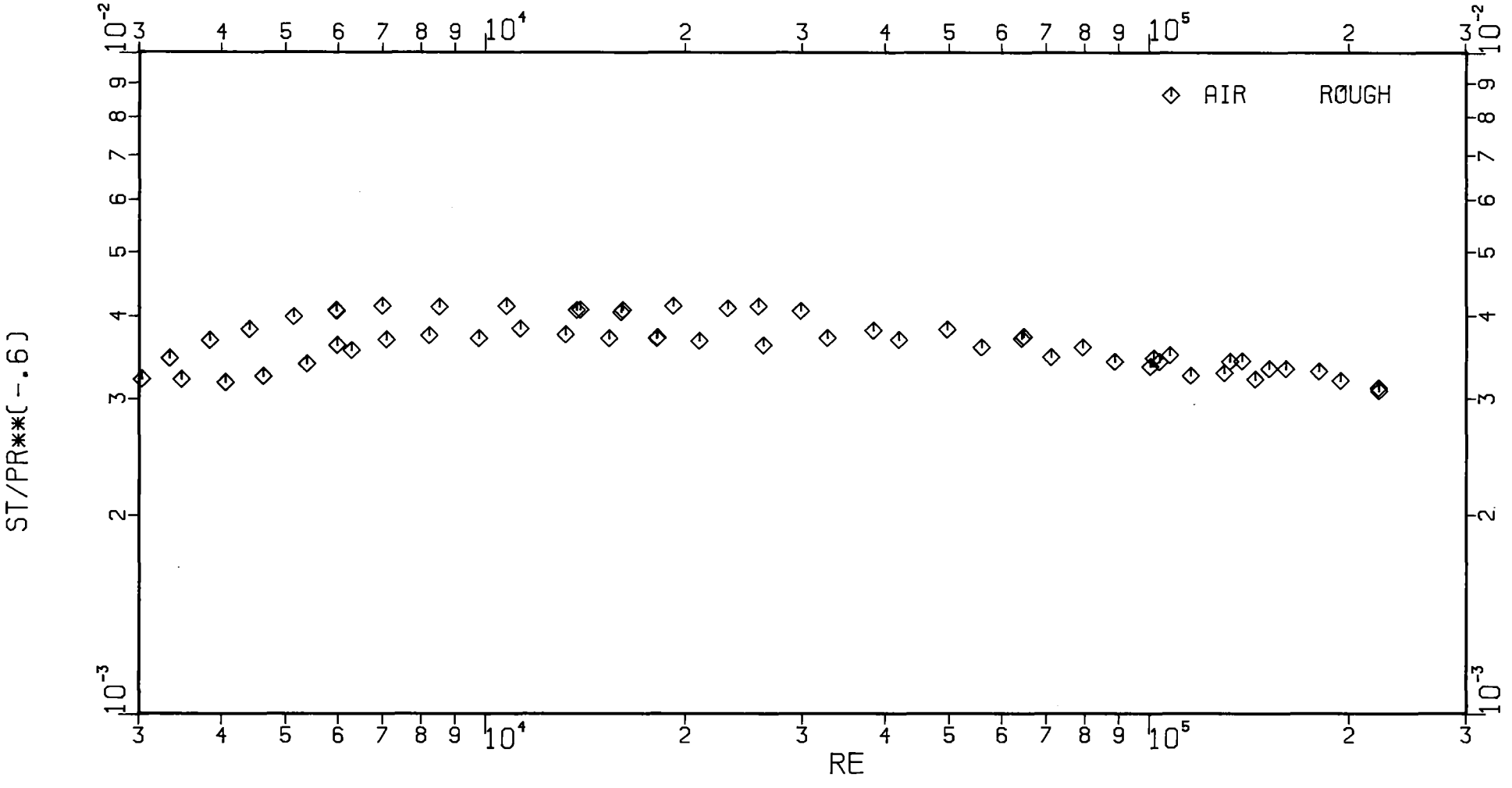

Fig.32: Measured Stanton numbers (air, KfK)

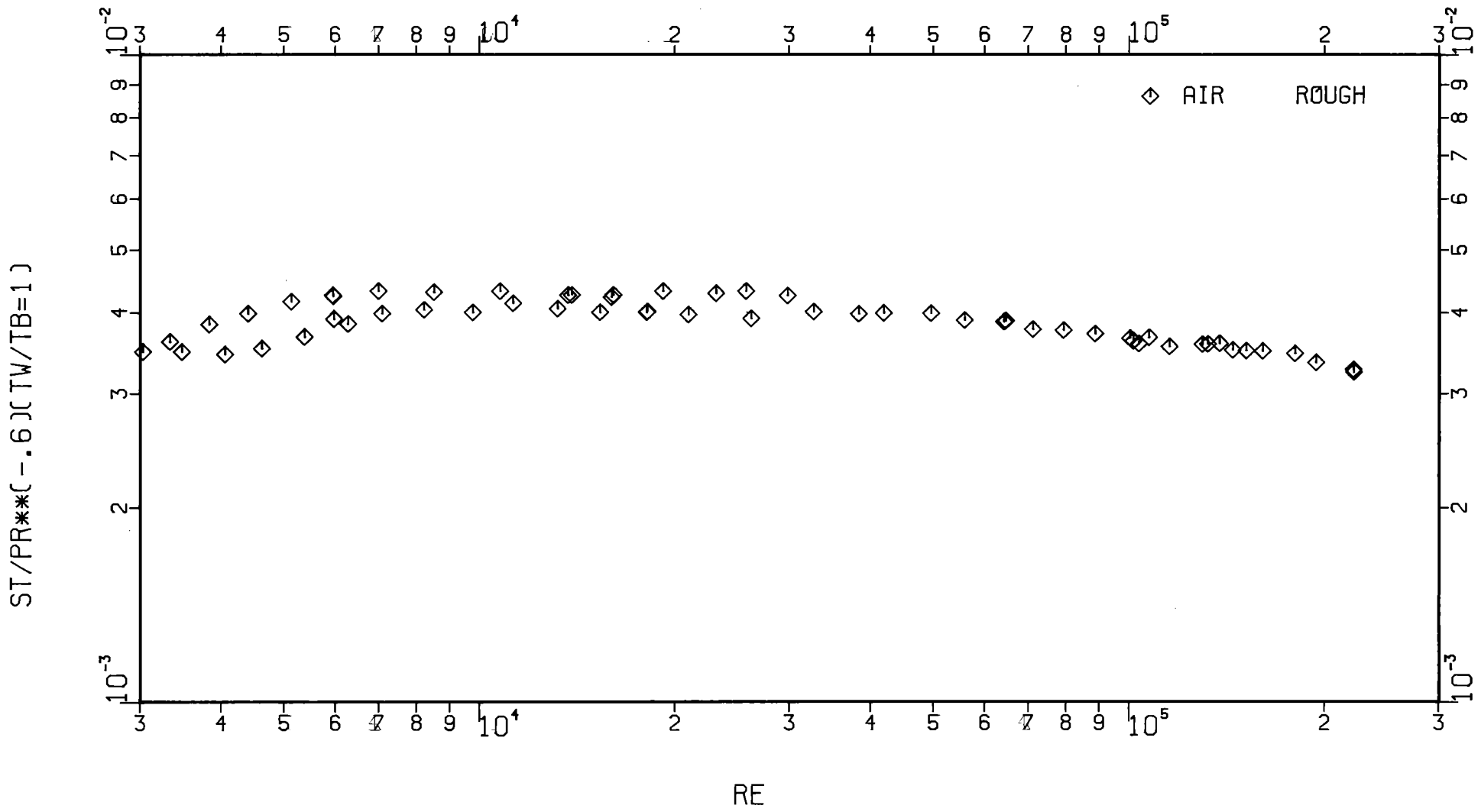

Fig.33: Measured Stanton numbers corrected for the wall to bulk temperature ratio (air, KfK)

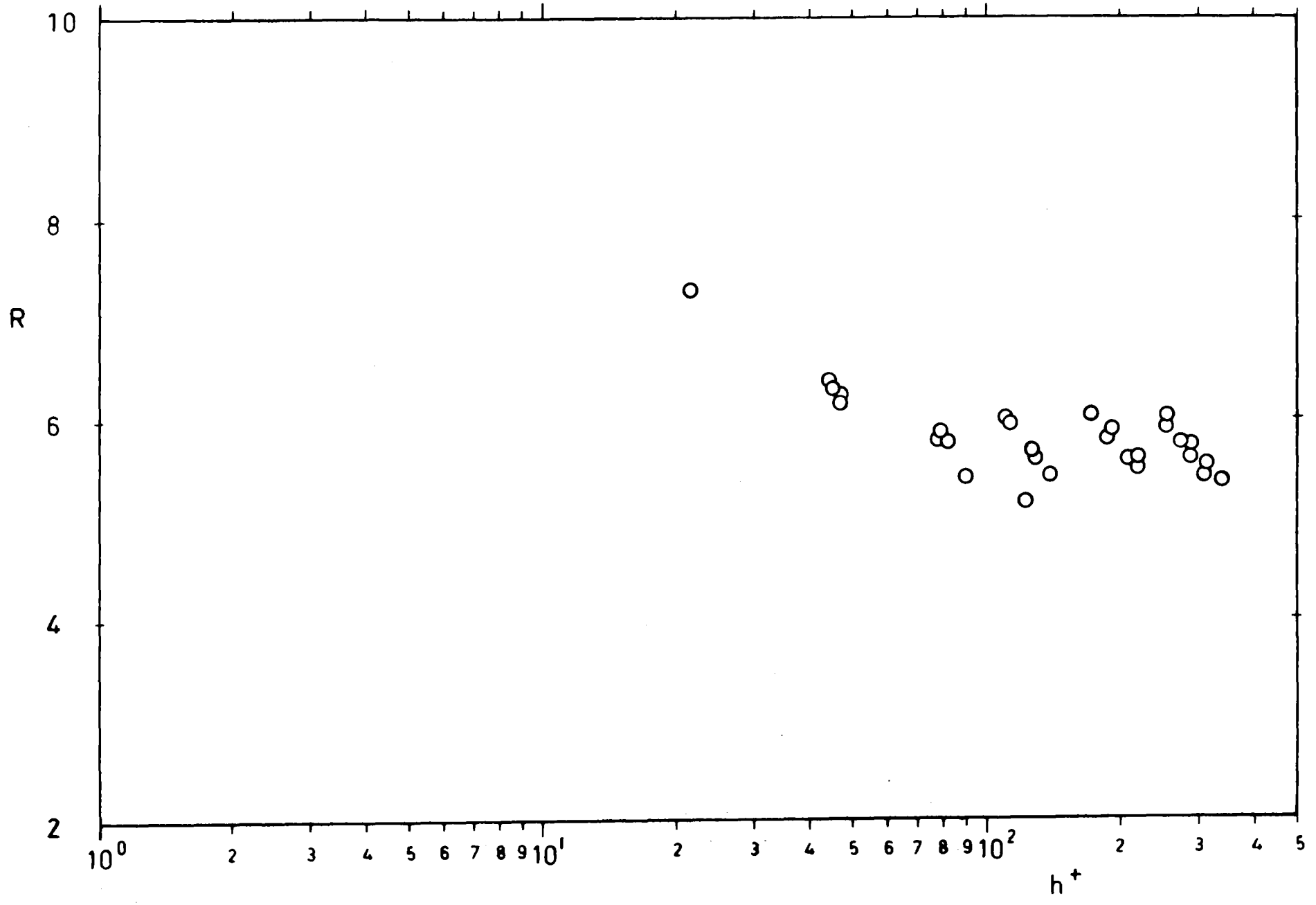

Fig.34: Roughness function R versus h^+ (CO_2, EIR)

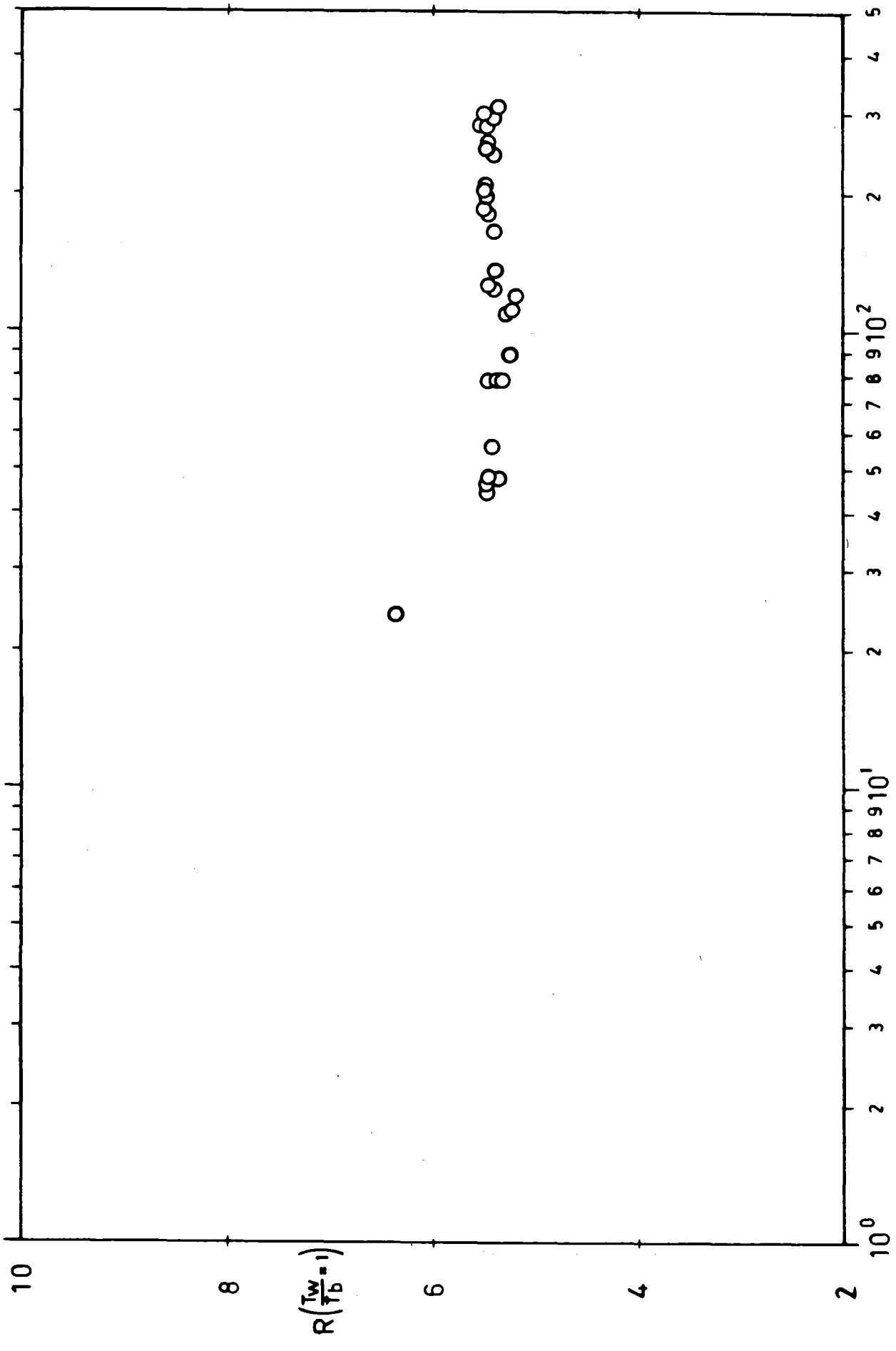

Fig.35: $R(T_W/T_B=1)$ versus h^+ (CO_2, EIR)

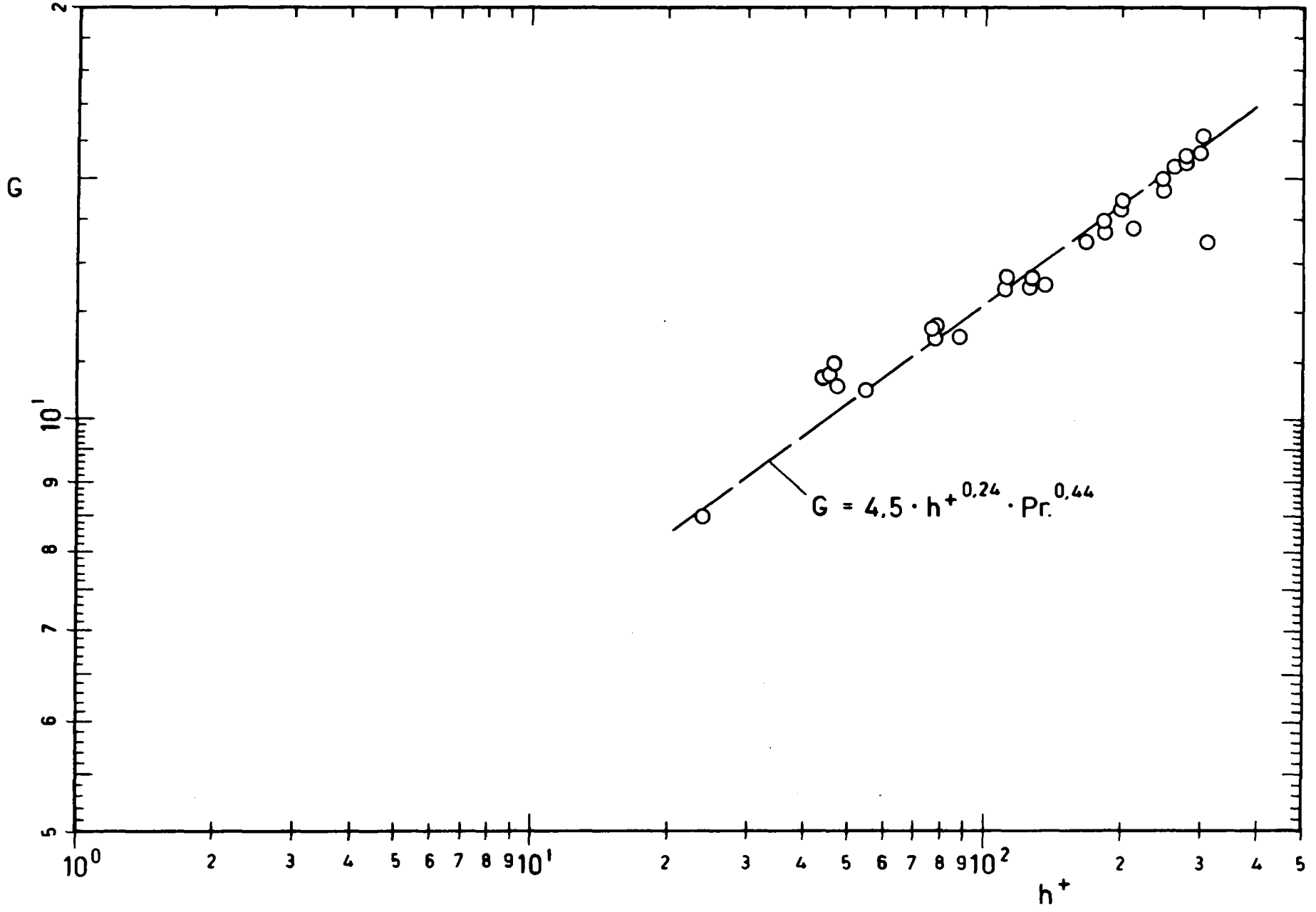

Fig.36: Roughness function G versus h^+ (CO_2, EIR)

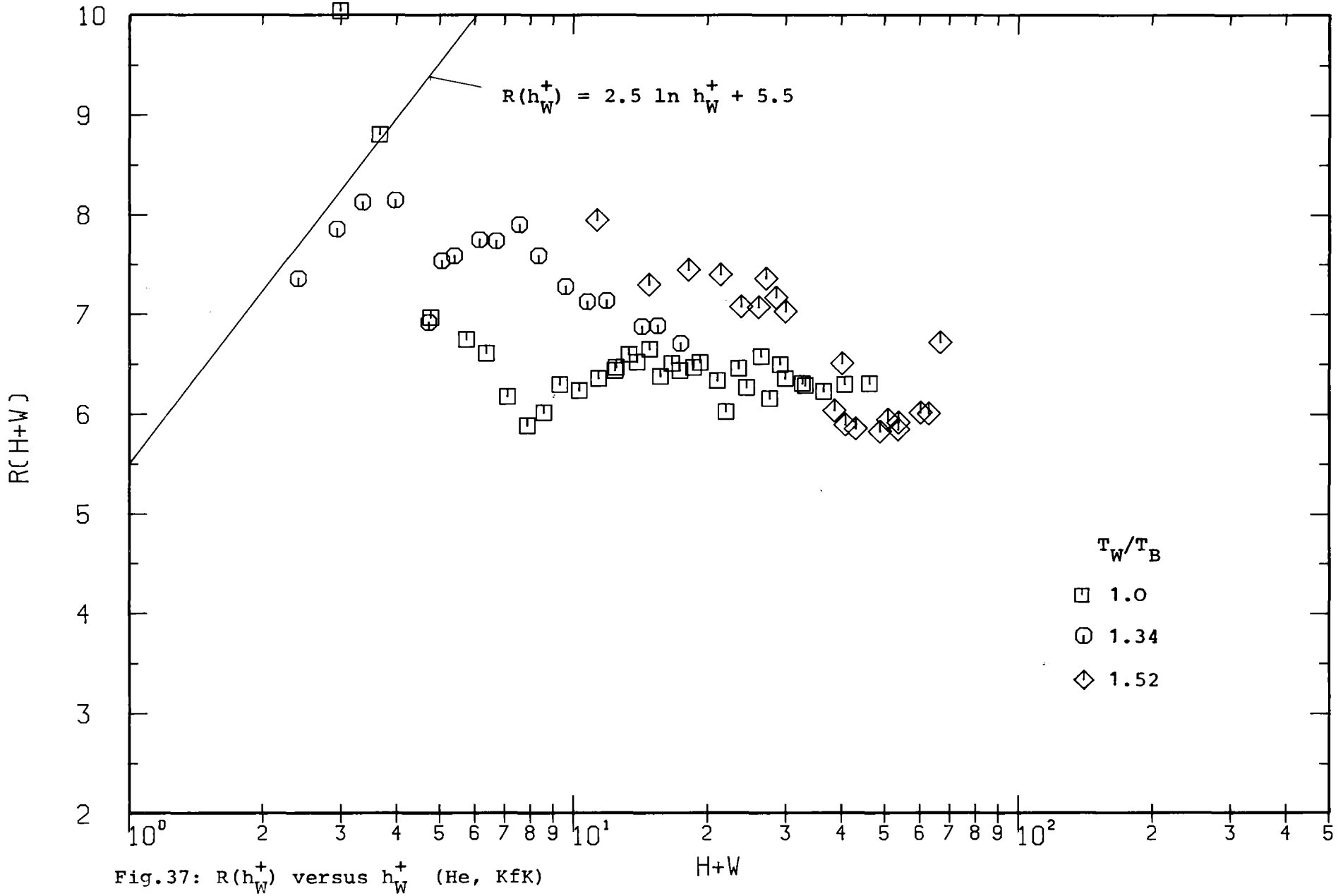

Fig.37: $R(h_W^+)$ versus h_W^+ (He, KfK)

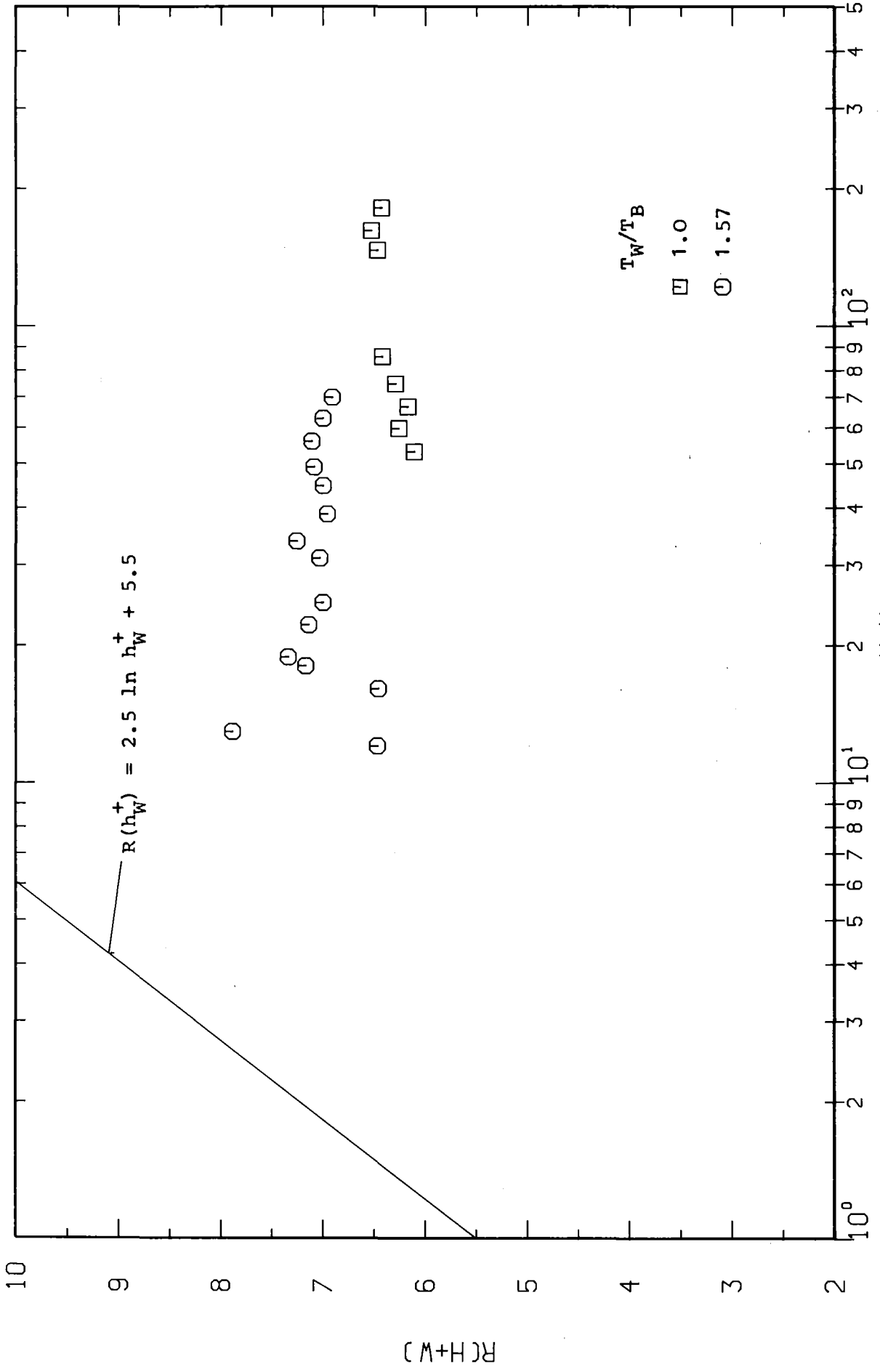

Fig.38: $R(h_W^+)$ versus h_W^+ (N_2, KfK)

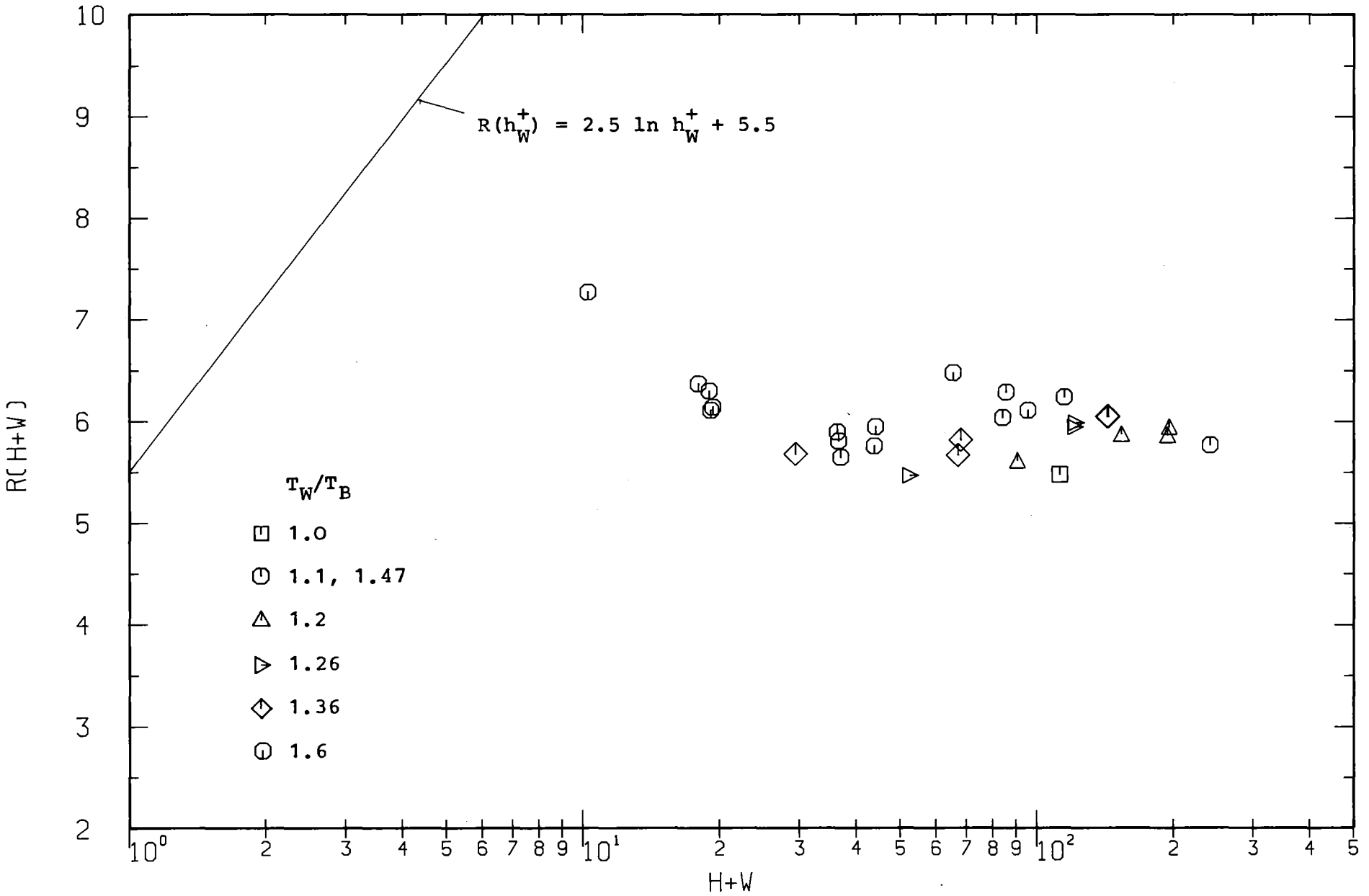

Fig.39: $R(h_W^+)$ versus h_W^+ (CO_2, EIR)

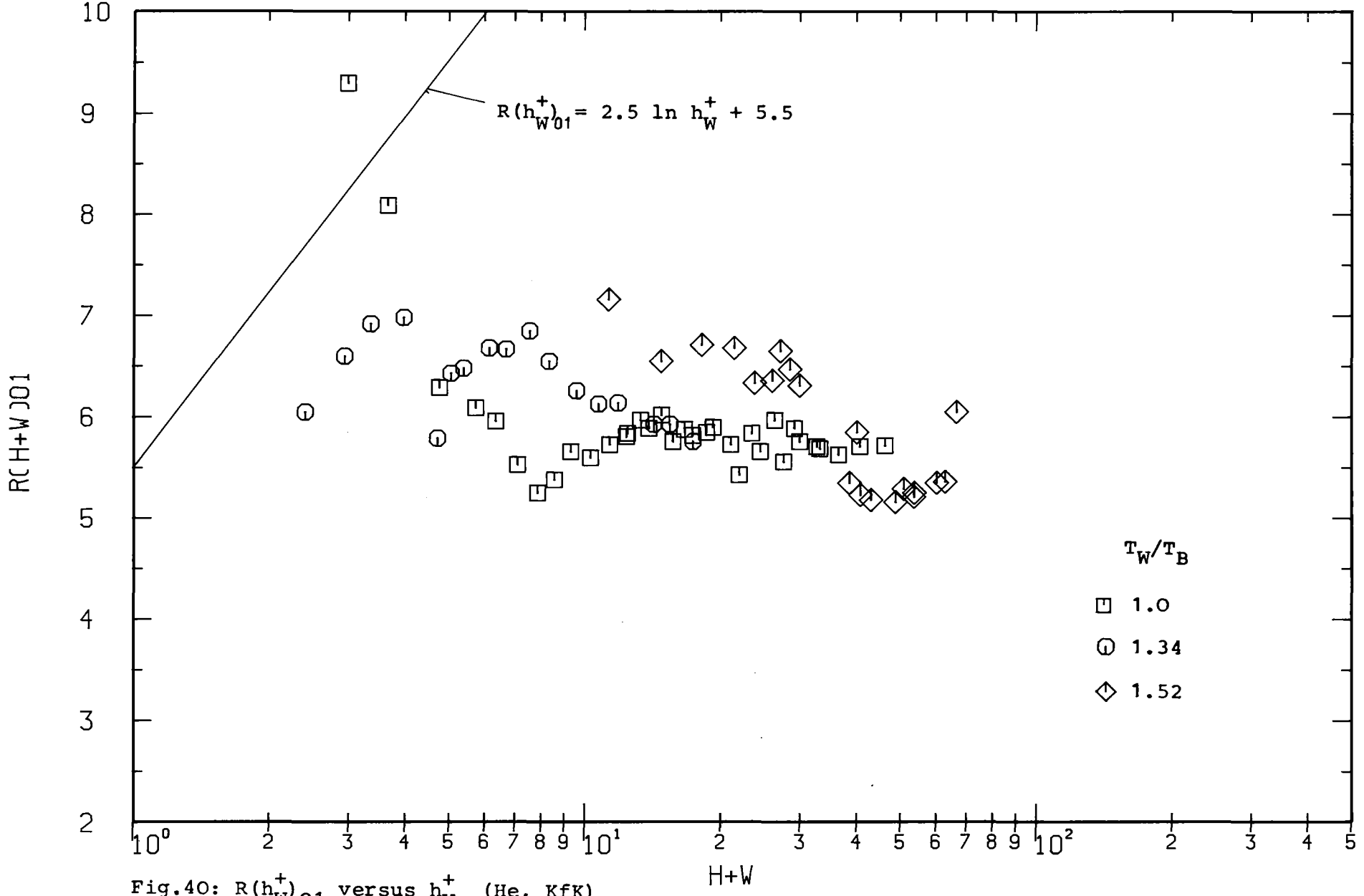

Fig.40: $R(h^+_W)_{01}$ versus h^+_W (He, KfK)

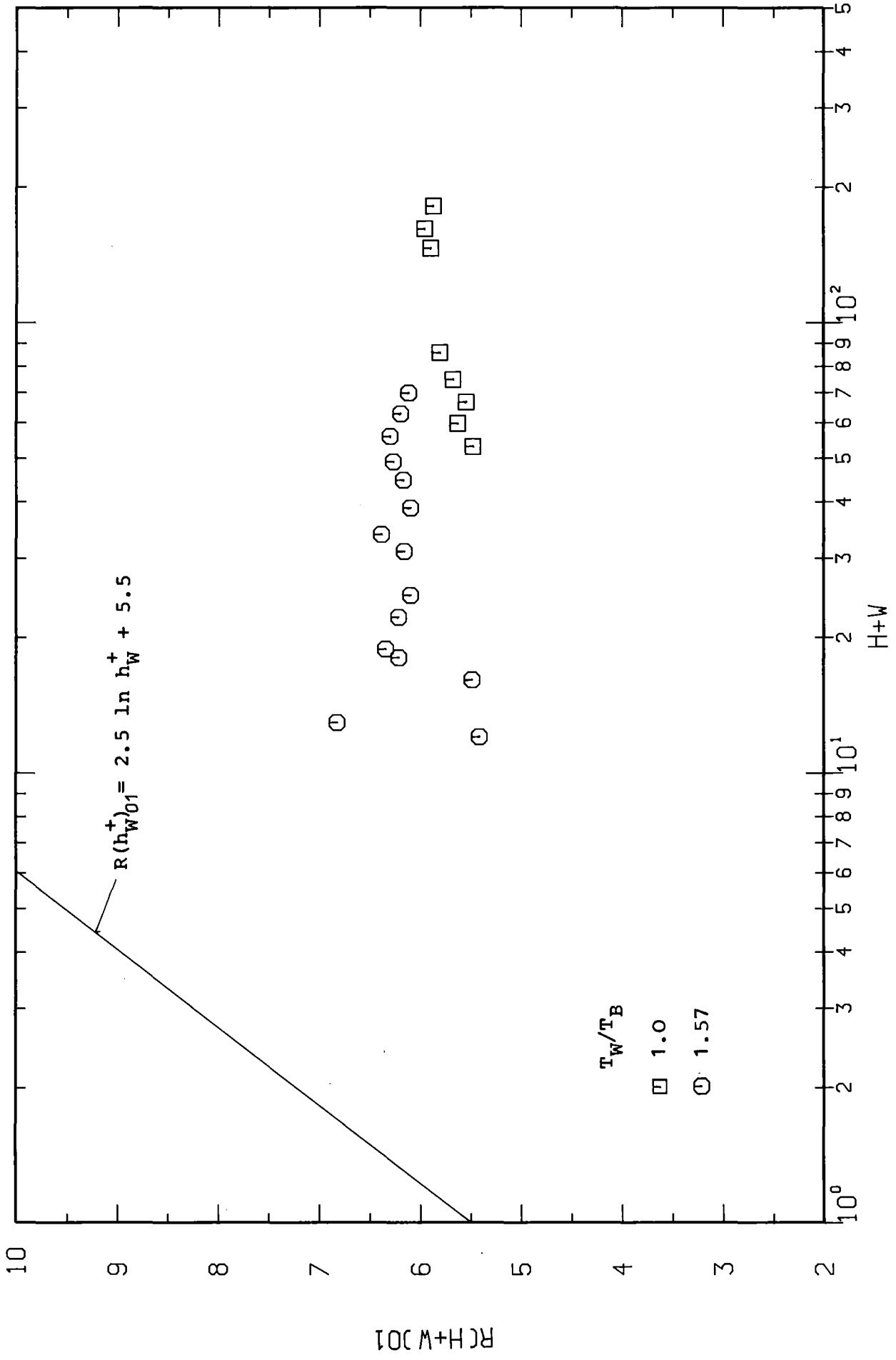

Fig.41: $R(h_W^+)_{01}$ versus h_W^+ (N_2, KfK)

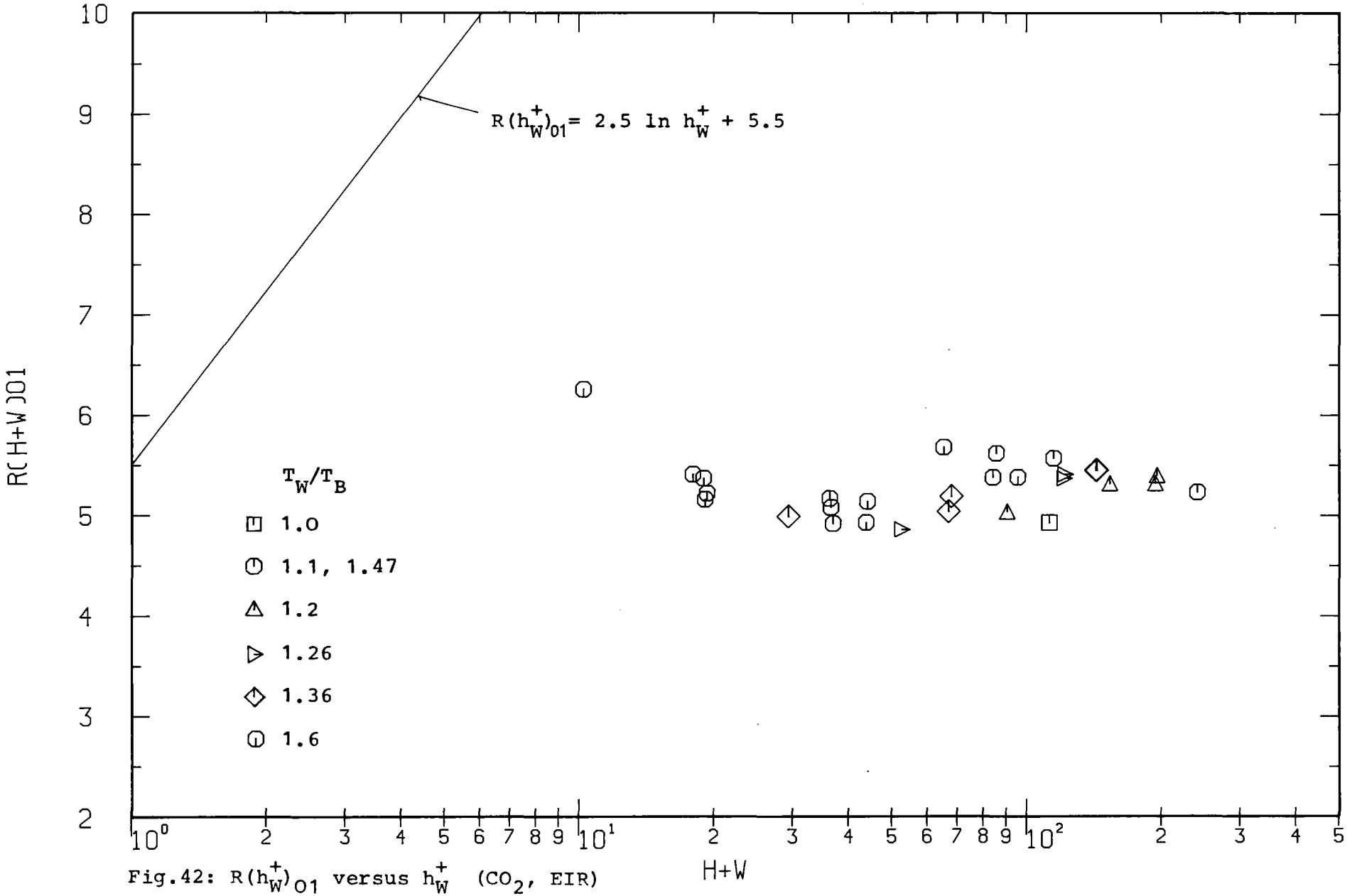

Fig.42: $R(h_{W}^{+})_{01}$ versus h_{W}^{+} (CO_2, EIR)

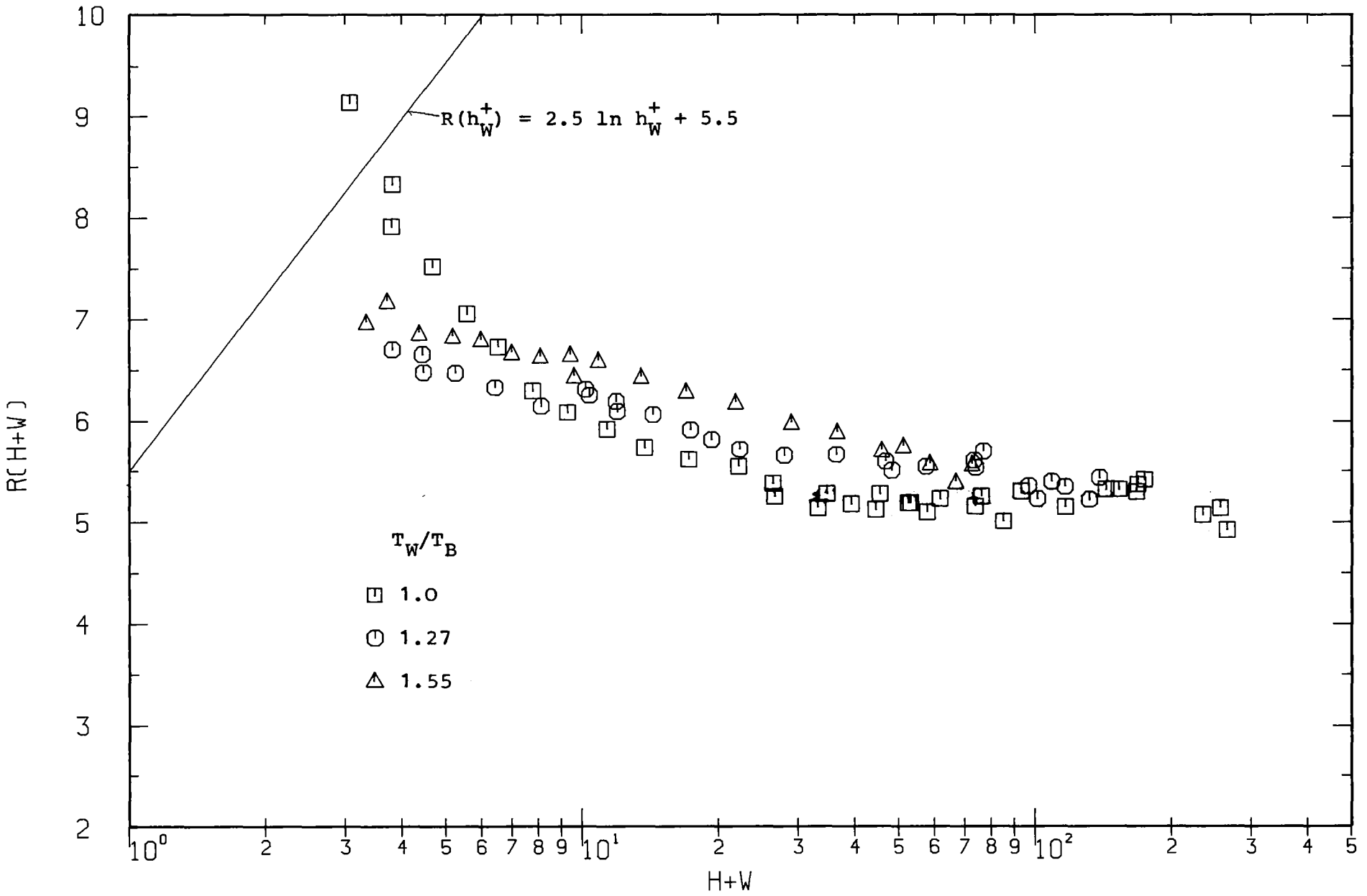

Fig.43: $R(h_W^+)$ versus h_W^+ (air, KfK)

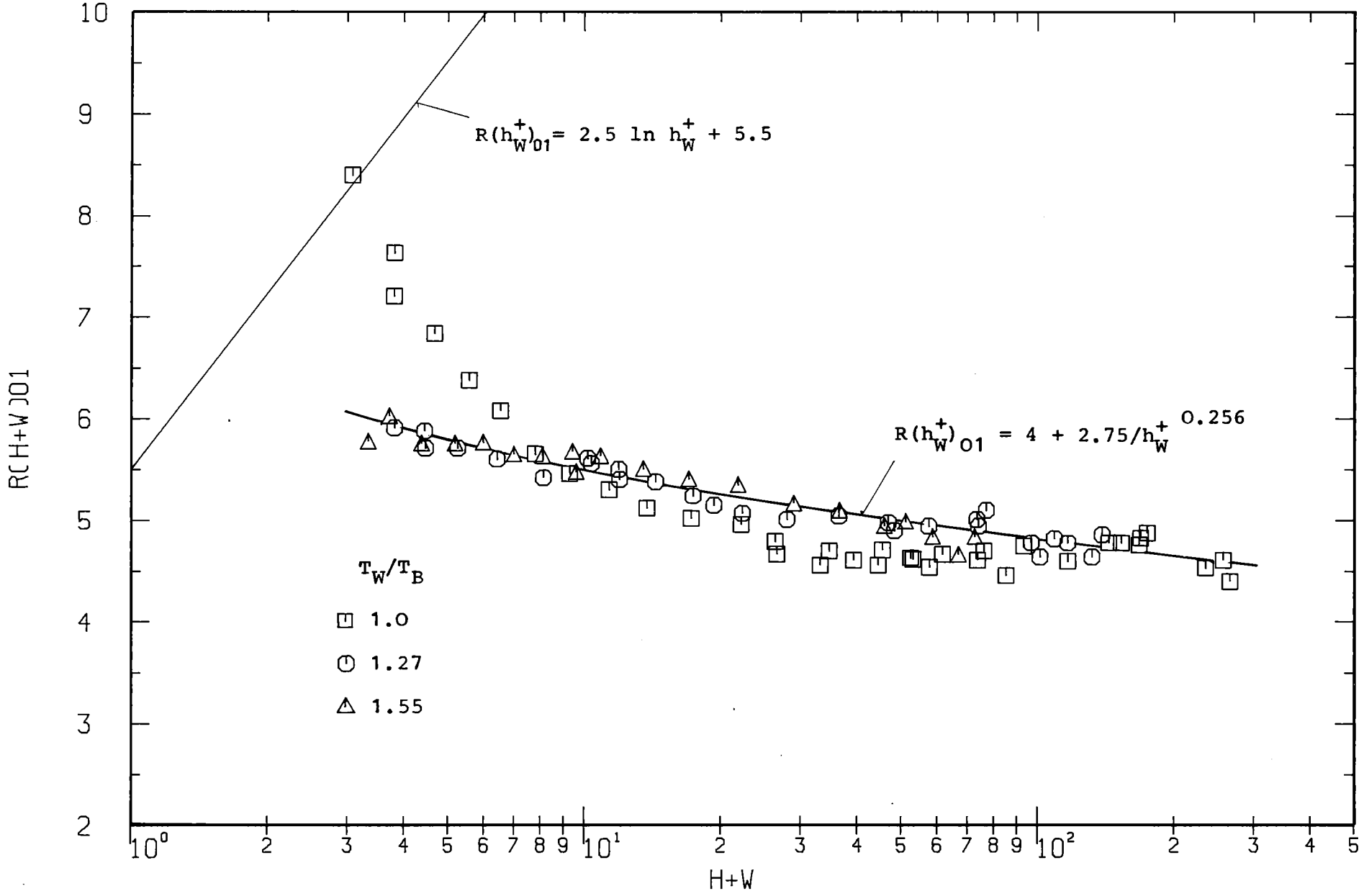

Fig.44: $R(h_W^+)_{01}$ versus h_W^+ (air, KfK)

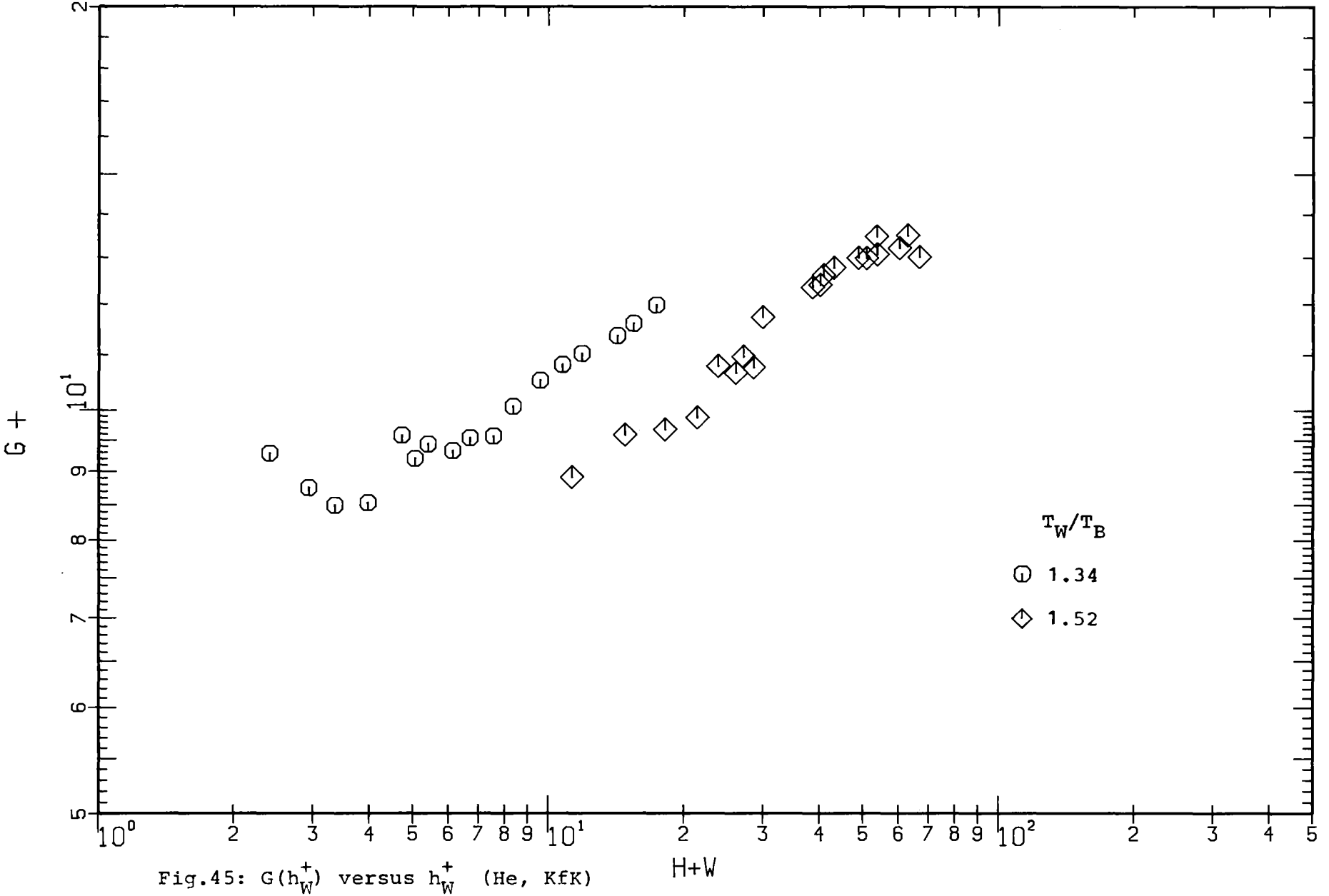

Fig.45: $G(h_W^+)$ versus h_W^+ (He, KfK)

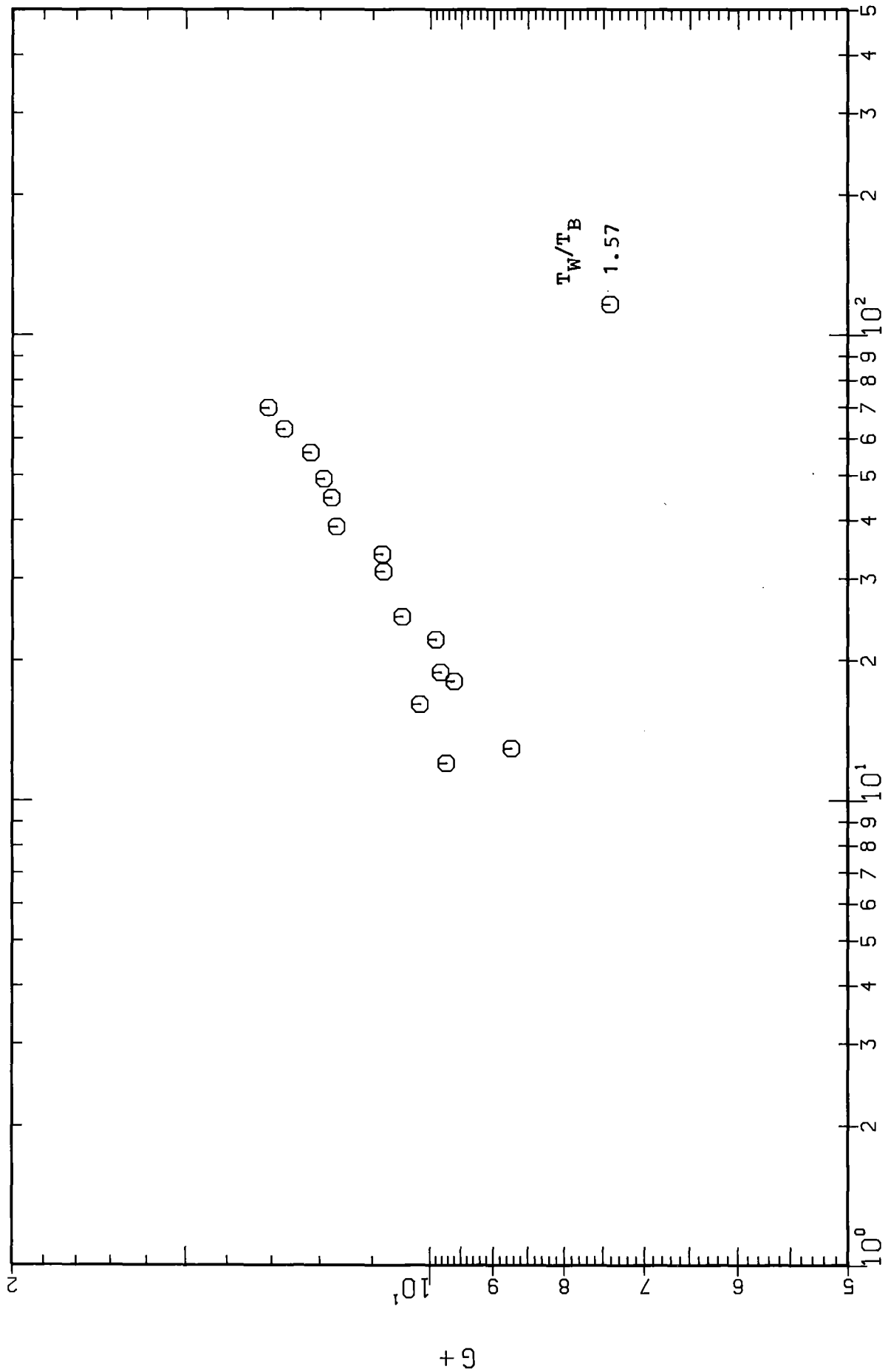

Fig.46: $G(h_W^+)$ versus h_W^+ (N_2, KfK)

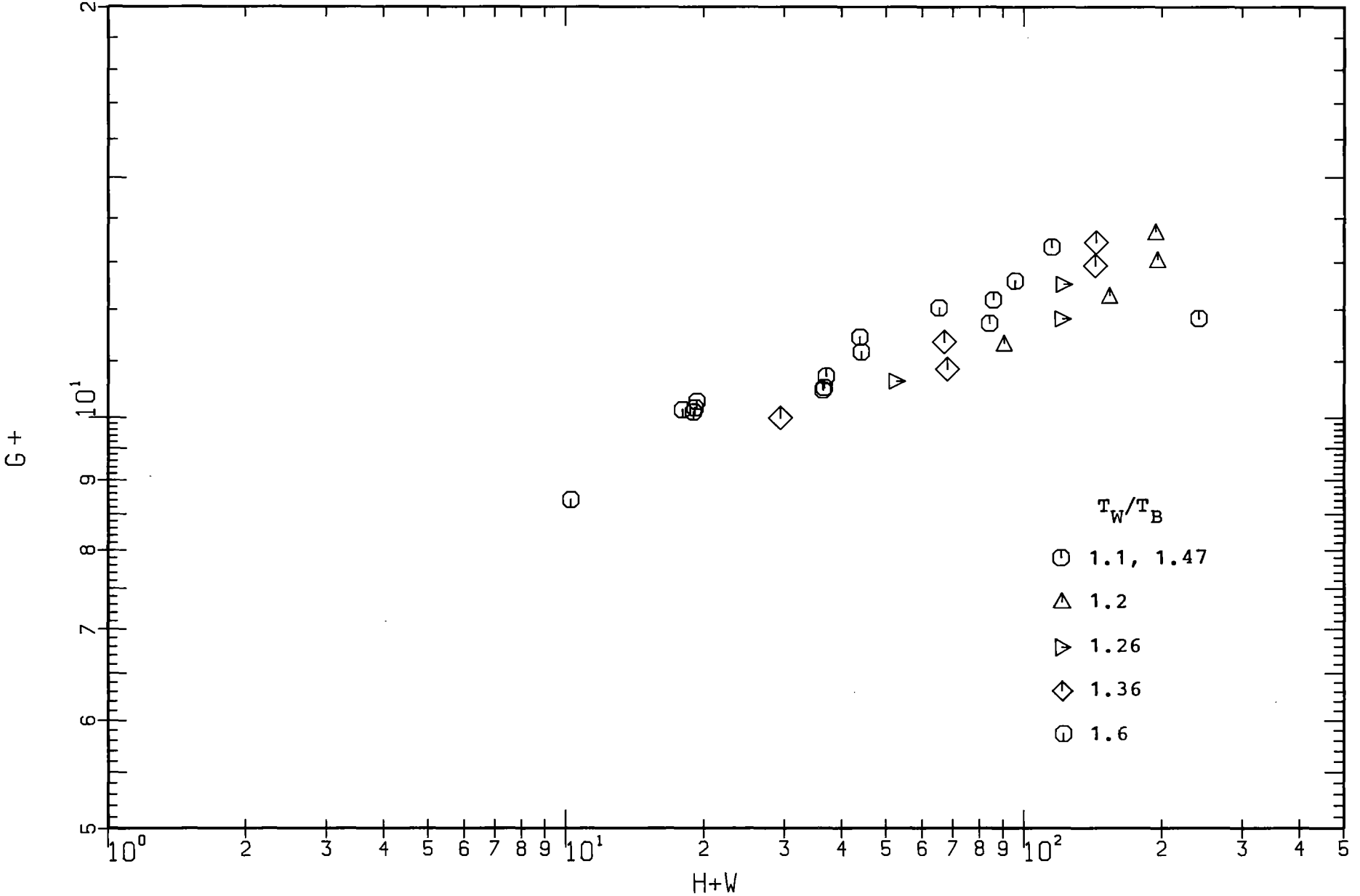

Fig.47: $G(h_W^+)$ versus h_W^+ (CO_2, EIR)

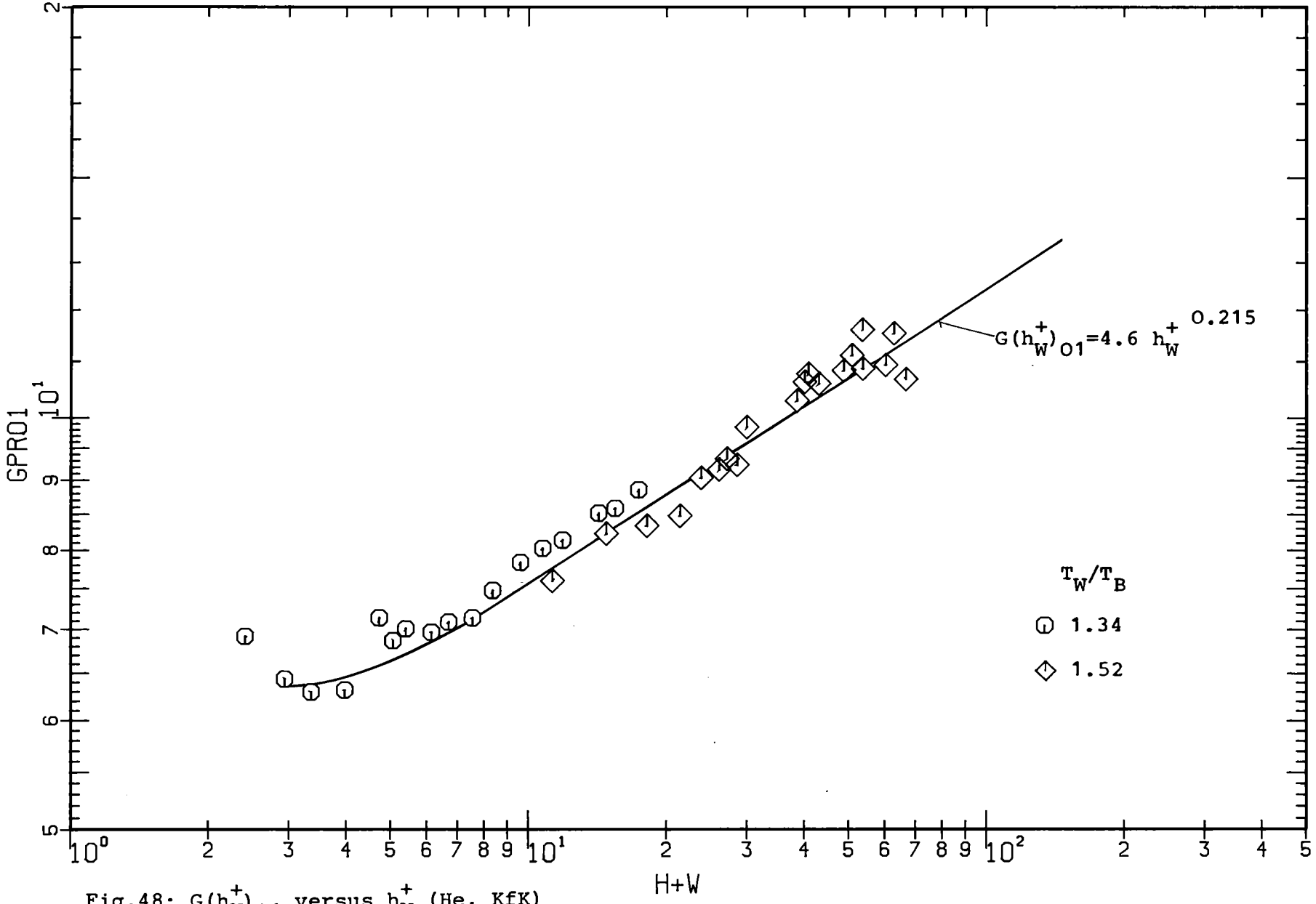

Fig.48: $G(h_W^+)_{01}$ versus h_W^+ (He, KfK)

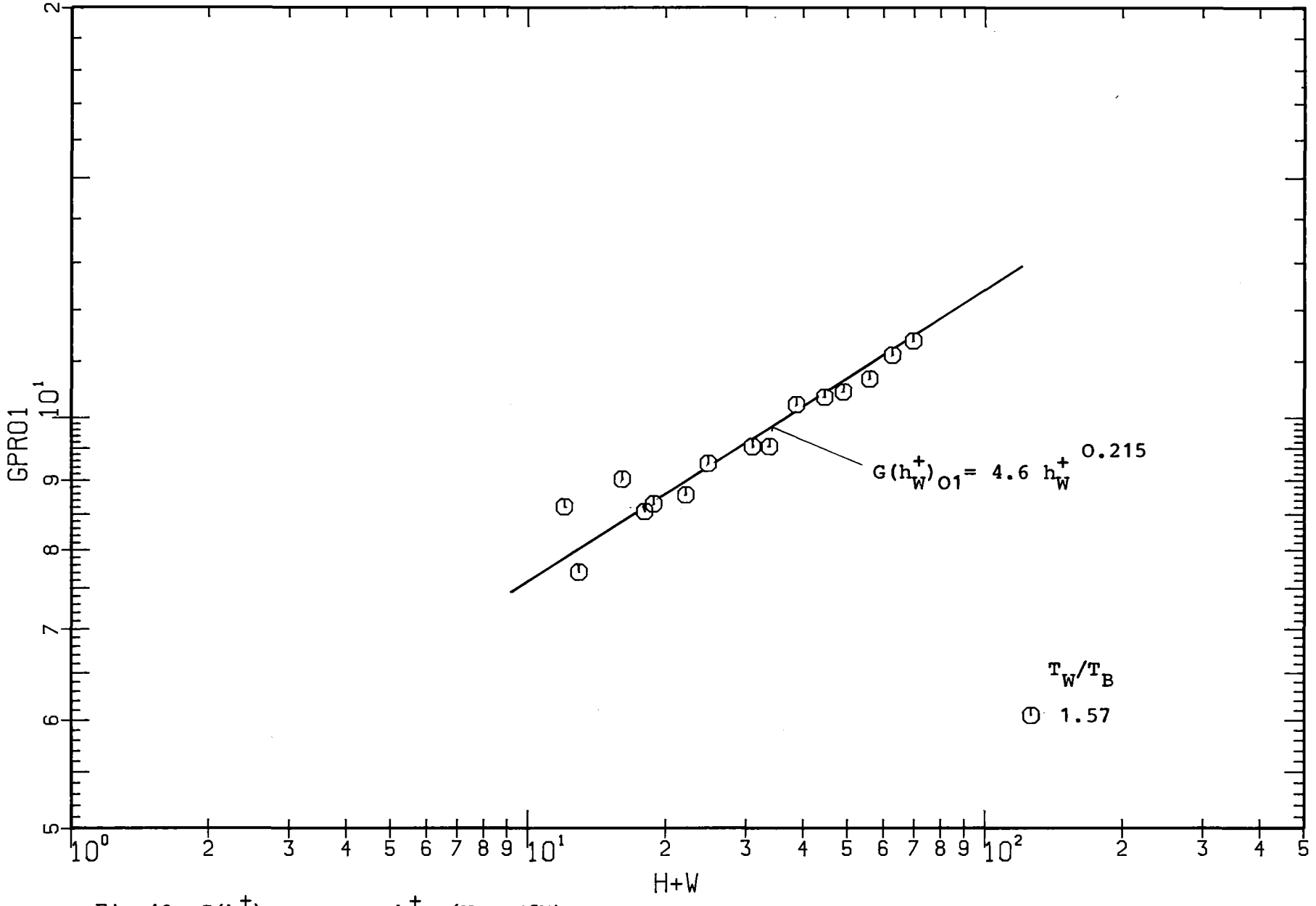

Fig.49: $G(h_W^+)_{O1}$ versus h_W^+ (N_2, KfK)

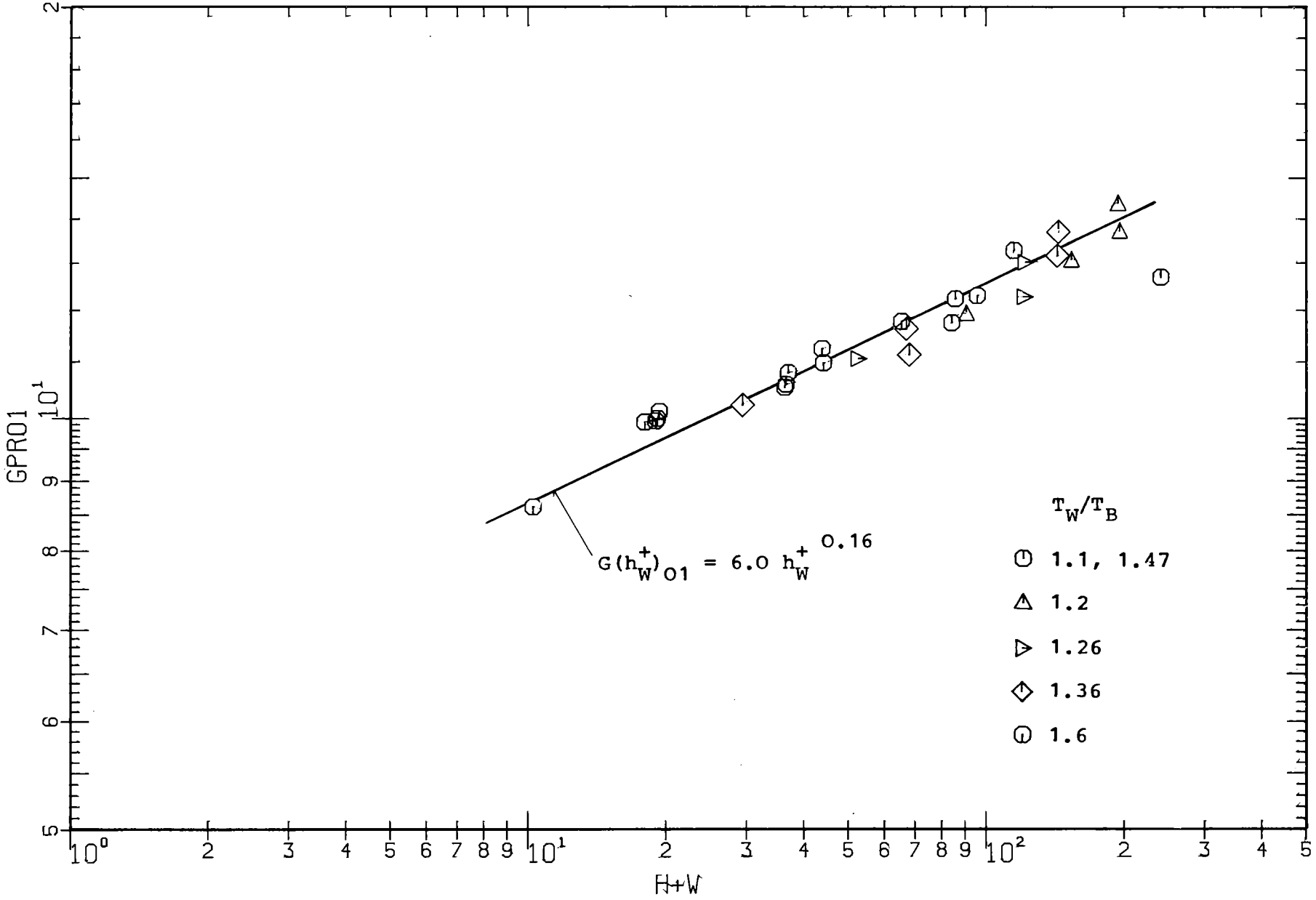

Fig.50: $G(h_W^+)_{O1}$ versus h_W^+ (CO_2, EIR)

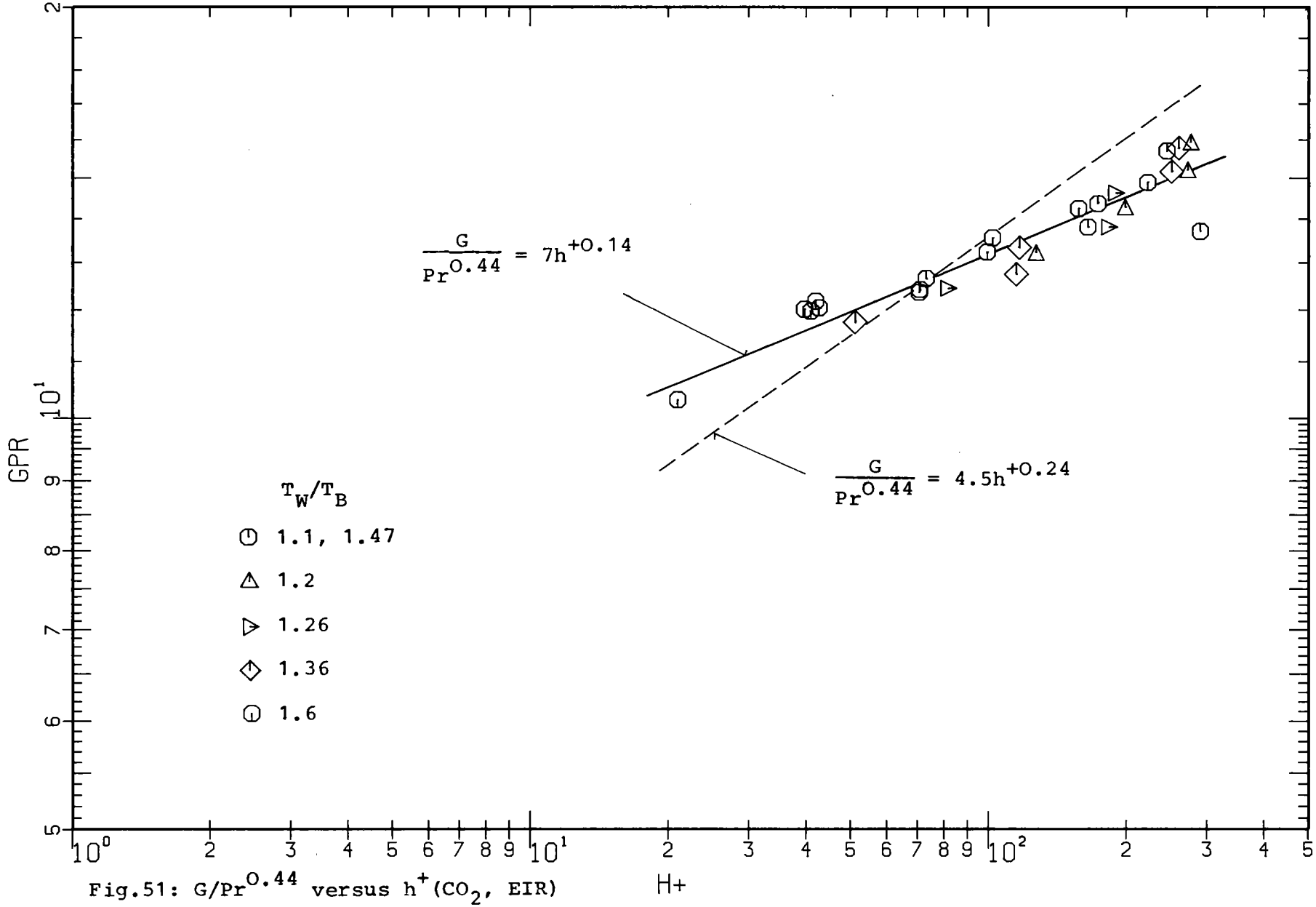

Fig.51: $G/Pr^{0.44}$ versus $h^+(CO_2, EIR)$

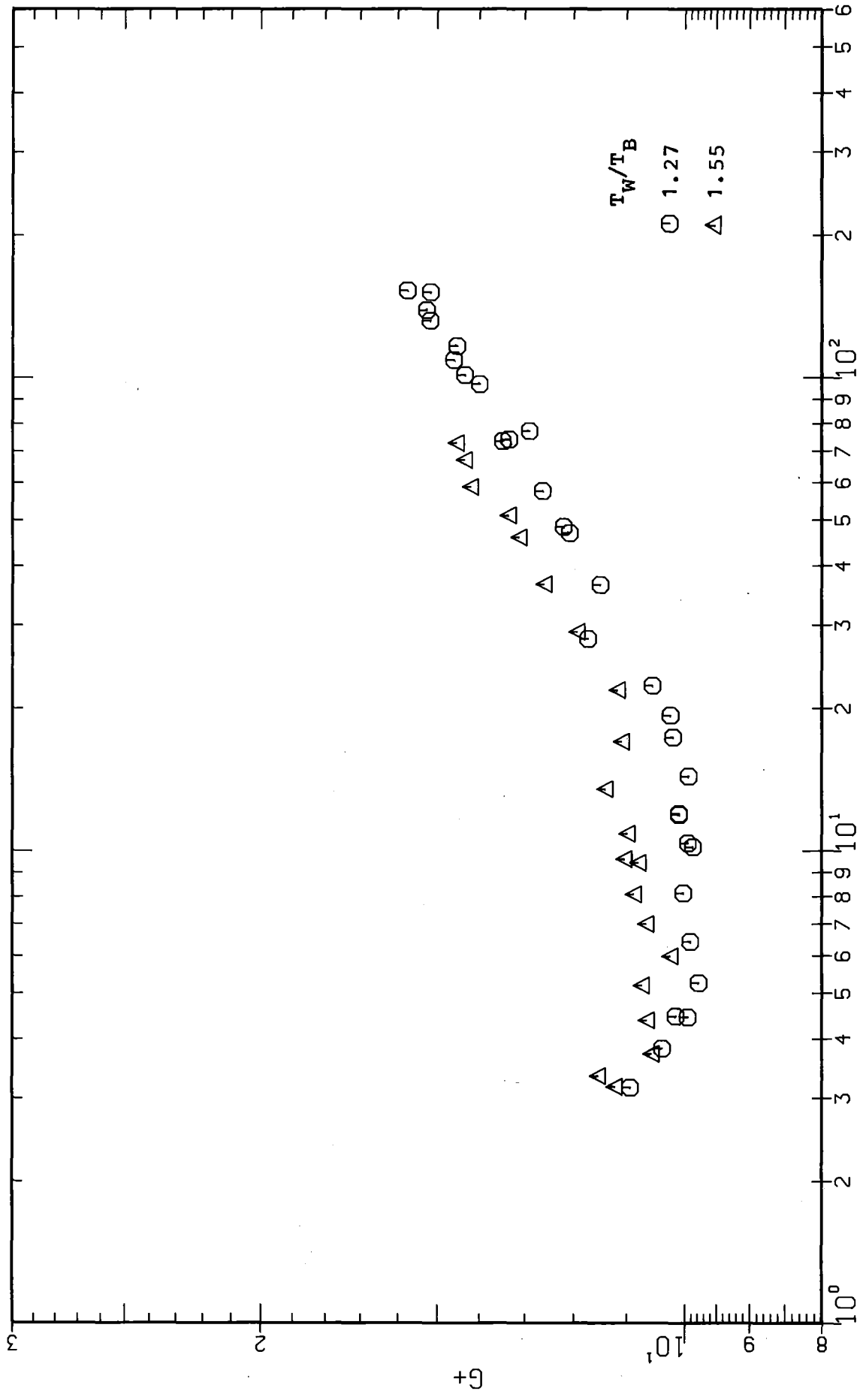

Fig.52: $G(h_W^+)$ versus h_W^+ (air, KfK)

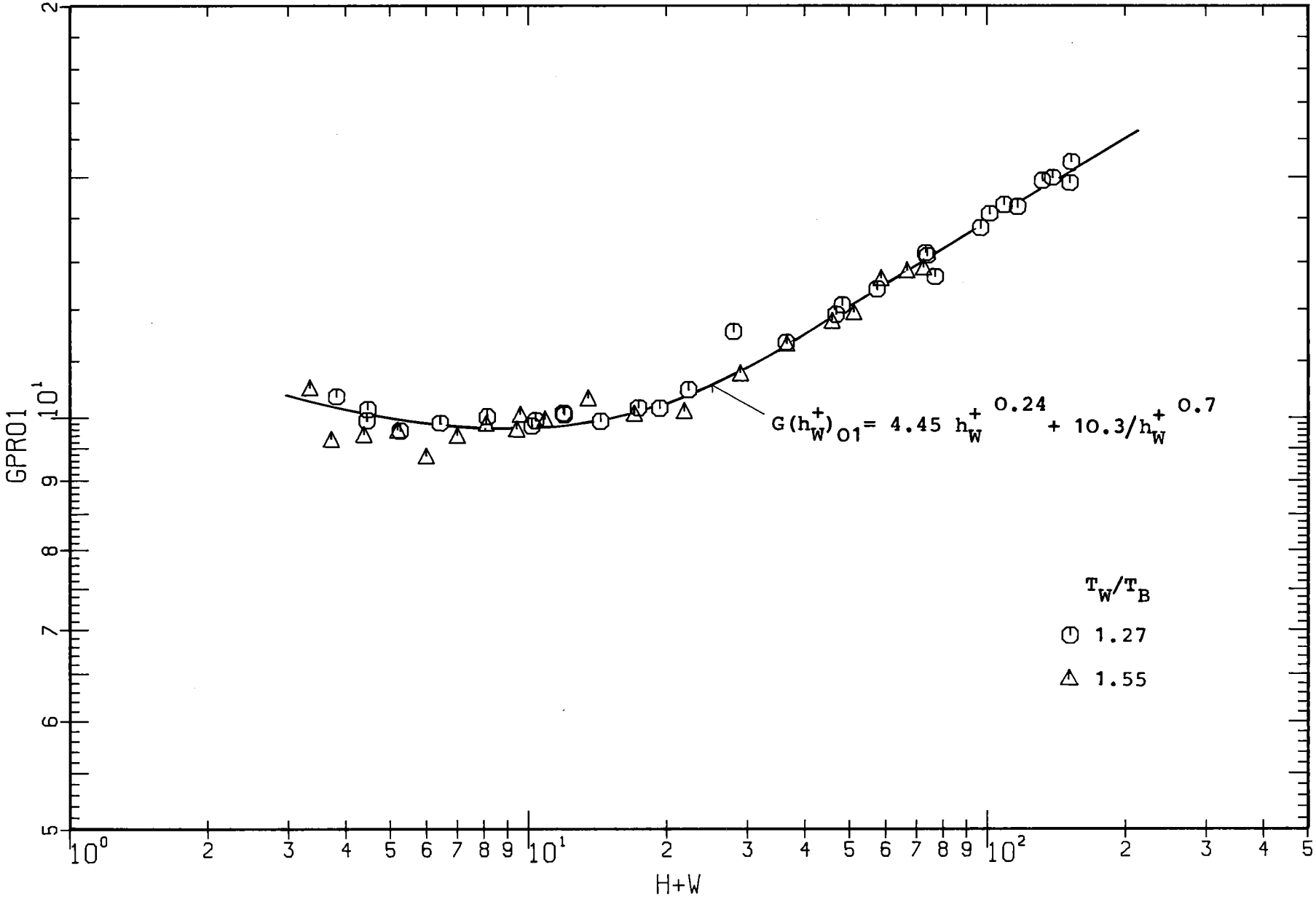

Fig.53: $G(h_W^+)_{O1}$ versus h_W^+ (air, KfK)

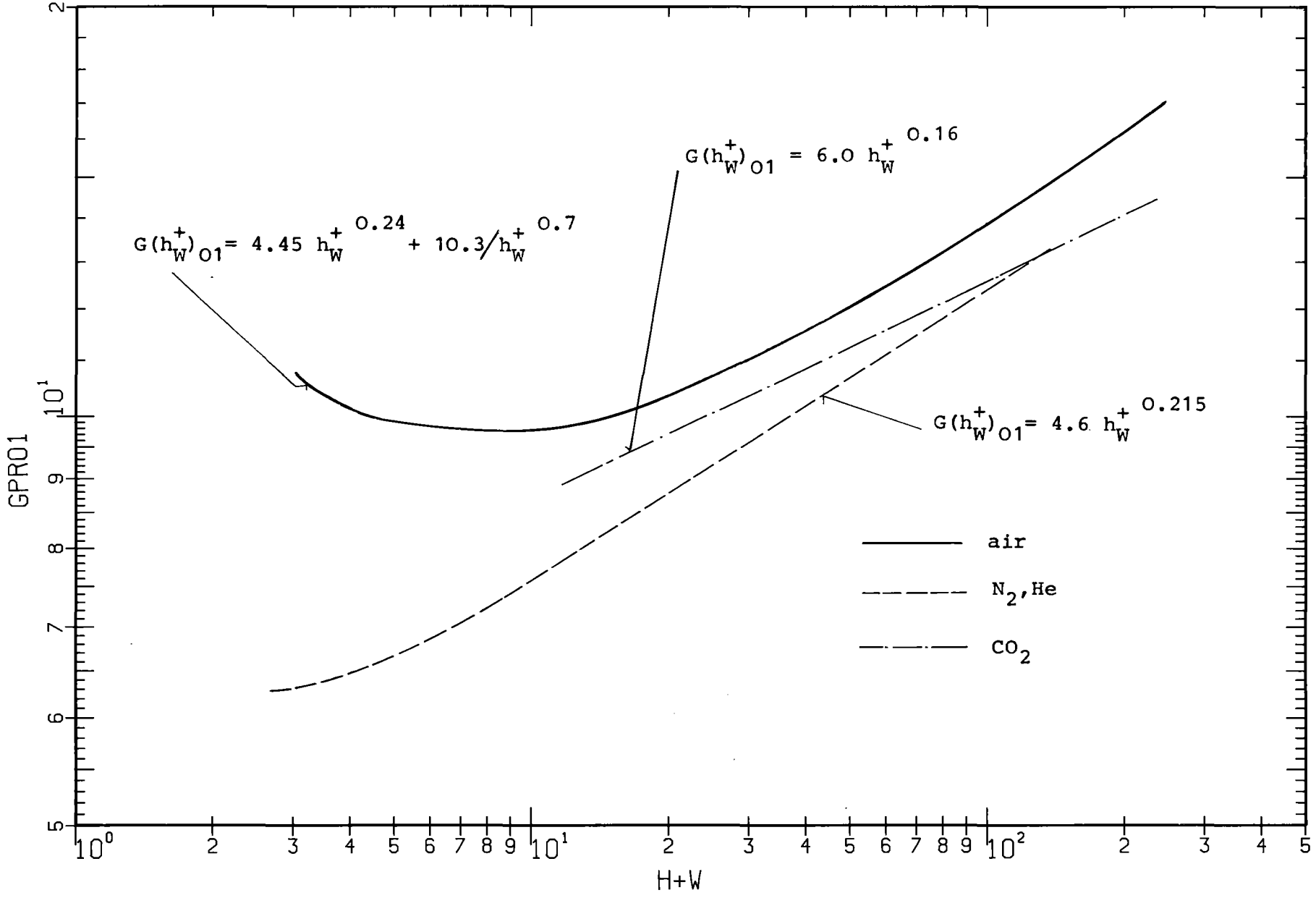

Fig.54: $G(h_W^+)_{01}$ versus h_W^+, comparison of results with various gases.

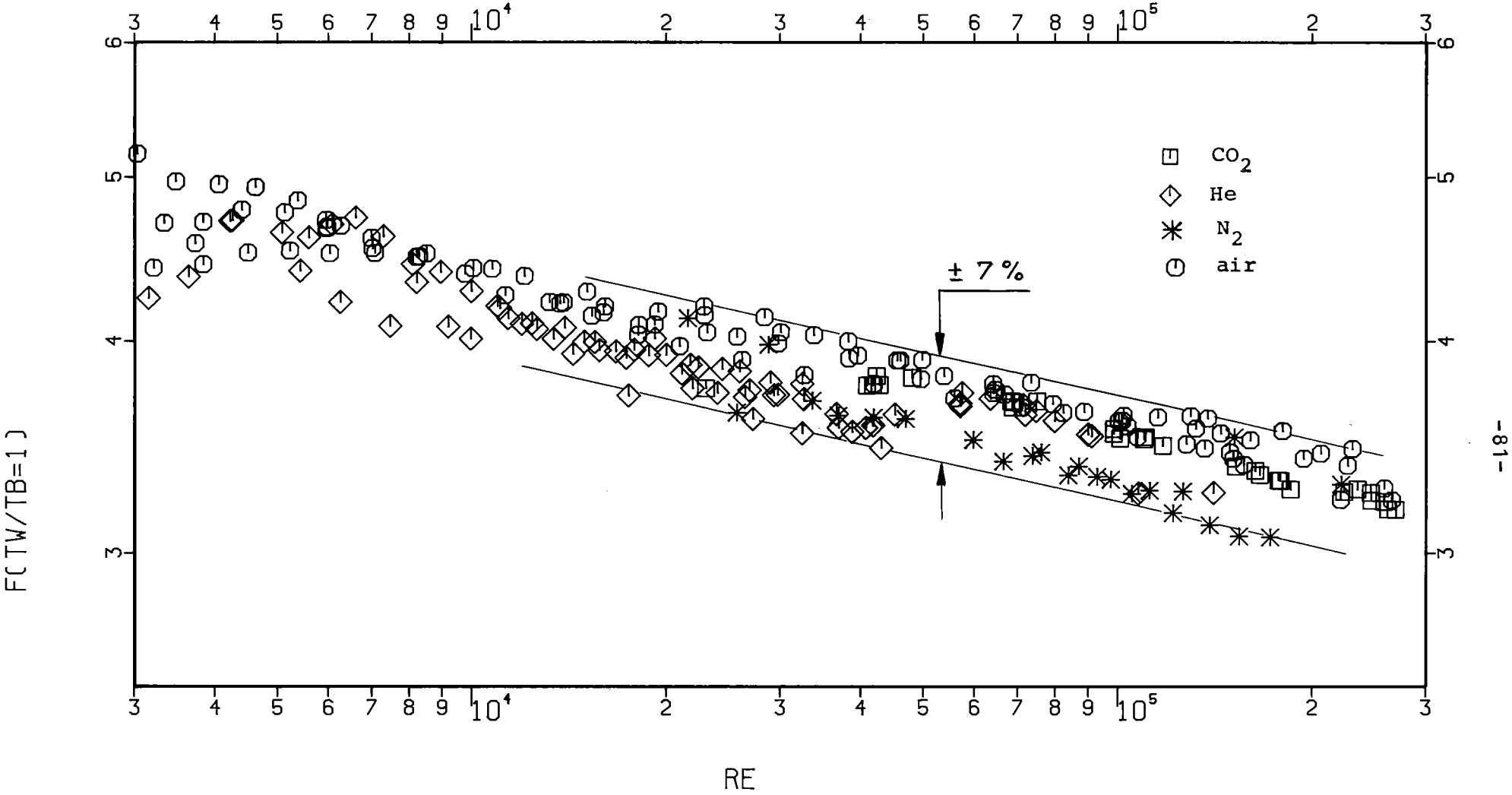

Fig.55: Comparison of measured global friction factors corrected for the wall to bulk temperature ratio.

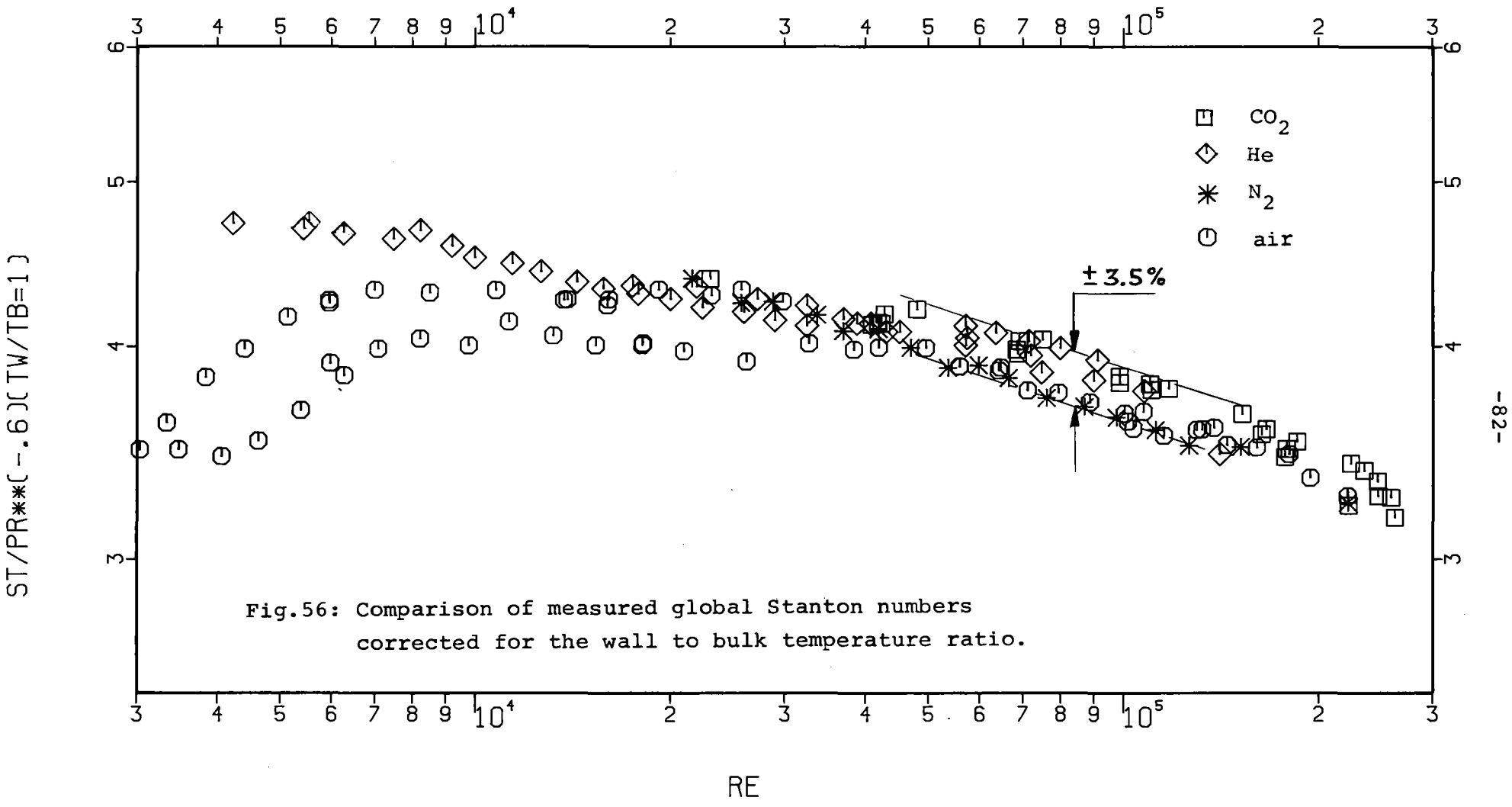

Fig.56: Comparison of measured global Stanton numbers corrected for the wall to bulk temperature ratio.